RESOLVING VARIABILITY IN SIZE STRUCTURE IN AN INDIVIDUAL-BASED MODEL FOR THE NORTH PACIFIC KRILL, *EUPHAUSIA PACIFICA*

By

Roxanne Robertson

A Thesis Presented to

The Faculty of Humboldt State University

In Partial Fulfillment of the Requirements for the Degree

Master of Science in Natural Resources: Fisheries

Committee Membership

Dr. Eric Bjorkstedt, Committee Chair

Dr. Andre Buchheister, Committee Member

Dr. Christine Cass, Committee Member

Dr. Erin Kelly, Program Graduate Coordinator

December 2021

ABSTRACT

RESOLVING VARIABILITY IN SIZE STRUCTURE IN AN INDIVIDUAL-BASED MODEL FOR THE NORTH PACIFIC KRILL, *EUPHAUSIA PACIFICA*

Roxanne Robertson

Individual-based models (IBMs) have emerged as a powerful tool for ecological research and are particularly well suited to studies of plankton ecology. In this thesis, I develop an IBM for the North Pacific krill, *Euphausia pacifica*, with the goal of replicating observed variability in size-structure in the northern California Current Ecosystem. Krill, and *E. pacifica* in particular, are central to the structure and function of the California Current Ecosystem. Their response to environmental forcing translates climate variability to higher trophic levels and underpins broader ecosystem responses. Recent observations indicate environmental and climate-related shifts in *E. pacifica* size distributions, which have important implications for understanding krill production dynamics and ecosystem interactions. I advance existing IBMs for *E. pacifica* by enabling temperature-dependent maturation and incorporating other observed relationships that were not captured in published models. I used a pattern-oriented modeling approach to develop a model capable of resolving realistic size and growth dynamics. Patterns in model output were compared to population size distributions from field-based observations off northern California. Modifications to the model were incorporated based on discrepancies between model output and field observations. The

resulting IBM represents a clear advancement toward obtaining accurate predictions of *E. pacifica* growth and size dynamics. The model captures seasonal and interannual patterns in growth and size across most life history stages. In addition to size dynamics, model-generated development, growth, and reproductive rates are generally consistent with field observations. Improved predictions of *E. pacifica* dynamics have implications across a broad range of issues, including estimates of forage biomass and research focused on life history strategies and population dynamics. The enhanced IBM I have developed strengthens the foundation for such models to serve as tools for broader examination of dynamics within the California Current Ecosystem.

ACKNOWLEDGEMENTS

This research was supported by the National Oceanic and Atmospheric Administration's Southwest Fisheries Science Center both directly and through the Cooperative Institute for Marine, Earth, and Atmospheric Sciences, in collaboration with Humboldt State University. Funding from the Malcom Oliphant Scholarship via Humboldt State University also contributed to this research. My thesis research would not have been possible without the Trinidad Head Line data set and the invaluable contributions of all who have participated in the program. I thank the captain and crew of the *R/V* Coral Sea and numerous technicians and volunteers who contributed to the Trinidad Head Line research program. I thank Dr. Jeffrey Dorman for graciously sharing code for the individual-based model he developed for *Euphausia pacifica*. I also thank my advisor, Dr. Eric Bjorkstedt, and my committee members, Dr. Andre Buchheister and Dr. Christine Cass for their encouragement, support, and thoughtful contributions to my thesis research.

TABLE OF CONTENTS

LIST OF TABLES

LIST OF FIGURES

LIST OF APPENDICES

INTRODUCTION

Individual-based models (IBMs) have emerged as a powerful tool for ecological research (DeAngelis and Mooji, 2005; DeAngelis and Grimm, 2014; DeAngelis, 2018). These models resolve dynamics at the level of an individual by tracking changes in an individual's state through the iterative application of (state-dependent) rules that govern how an individual responds to and is affected by its environment. By doing so, an IBM integrates the experience of an individual over time, explicitly capturing how the past conditions the present state of the individual and sets the stage for behaviors or responses going forward. Depending on the purpose for which an IBM is designed, processes may be described by detailed mechanistic submodels or represented as phenomenological patterns for which underlying mechanisms are not fully understood or are of limited relevance to the question at hand. The level of biological detail encompassed by IBMs varies, but, because they track the state of an individual, they are generally more complex than other mathematical models. The complexity of IBMs enables researchers to explore the effect of variability among individuals and the range of responses that can arise under varying internal and external conditions, including those that are not readily observed in nature (e.g., the characteristics of individuals that die) (Peck and Hufnagl, 2012). Because population, community, and ecosystem-level dynamics reflect the aggregated response of individuals to their environment, IBMs can also contribute to our understanding of larger-scale system-level properties (Railsback et al., 2002; Rademacher et al., 2004; Andrello et al., 2015; Blechschmidt et al., 2020).

IBMs are particularly well suited to studies of plankton ecology. They have been applied to research focused on understanding how environment and behavior affect the foraging success, predation risk, and transport of individuals (Leising, 2001; Batchelder et al., 2002; Ospina-Alvarez et al., 2012), how these processes scale up to population dynamics and species distributions (Meynecke, and Richards, 2014; Politikos et al., 2015) and shape the evolution of species' life histories (Van Winkle et al., 1993). In many cases, insights revealed by IBMs arise from integrating IBMs into circulation and ecosystem models. These studies also highlight the potential of IBMs as a powerful complement to biogeochemical ecosystem models (e.g., NEMURO; Kishi et al., 2007) that resolve plankton ecosystems in terms of flows of nutrients among coarsely structured ecosystem components (e.g., "phytoplankton", "small zooplankton"), but do not resolve the structure or dynamics of key species.

In this thesis, I develop an IBM for the North Pacific krill, *Euphausia pacifica*, with the goal of replicating observed variability in size-structure in the northern California Current Ecosystem (CCE). This work is motivated by the centrality of krill, and *E. pacifica* in particular, to the structure and function of the CCE. *Euphausia pacifica* are omnivorous and feed on phytoplankton, zooplankton, and marine snow (Ohman, 1984; Dilling et al., 1998). In turn, they are prey for numerous ecologically and economically important organisms and represent a key link between lower and higher trophic levels (Schoenherr, 1991; Brodeur and Pearcy, 1992; Hunt et al., 1999; Abraham and Sydeman, 2004; Becker et al., 2007; Miller and Brodeur, 2007; Miller et al. 2010).

The response of krill populations to environmental forcing translates climate variability to higher trophic levels and underpins broader ecosystem responses (Smiles and Pearcy, 1971; Gómez-Gutiérrez et al., 2005; Brinton and Townsend, 2003; Ruzicka et al., 2012; Jones et al., 2018).

Krill have a complex life cycle, with an ontogeny that spans several orders of magnitude in size. As such, resolution of size-structured dynamics, rather than only bulk biomass estimates, is important for obtaining accurate production estimates and understanding ecosystem interactions. The role of *E. pacifica* among lower trophic levels shifts with ontogeny. Early life history stages are potential prey for juvenile and forage fishes (Reilly et al., 1992; Brodeur et al., 2008; Bosley et al., 2014). As adults, *E. pacifica* become predators of smaller zooplankton, including the larval stages of fishes that once preyed upon their younger and smaller counterparts (Theilacker et al., 1986). The role of size in shaping ecological interactions underscores the importance of resolving structured dynamics of *E. pacifica*.

In the CCE, euphausiid dynamics are strongly linked to environmental forcing on seasonal and interannual scales (see 'Model System: California Current Ecosystem', below). Production tends to be greatest during spring and summer months coincident with upwelling conditions supportive of growth (Smiles and Pearcy, 1971; Tanasichuk, 1998; Shaw et al., 2010; Feinberg et al., 2010). Winter phytoplankton blooms can also trigger egg production (Feinberg et al., 2010). Variability in the onset and intensity of upwelling affects the abundance and biomass of krill species with cool-water, coastal

affinities, such as *E. pacifica* and *Thysanoessa spinifera* (Tanasichuk, 1998; Gómez-Gutiérrez et al., 2005; Sydeman et al., 2006). Larger-scale climate variability also has a pronounced effect on euphausiid assemblages and populations. For example, during El Niño events, abundance and biomass of cool-water species tends to decline in the CCE and warm-water species are encountered more frequently and in greater abundance (Brinton and Townsend, 2003; Smith, 1985; Marinovic et al., 2002; Peterson et al., 2017; Lilly and Ohman, 2018).

Environmental conditions also affect characteristics of individual krill. Detailed analysis of *E. pacifica* collected off northern California revealed a negative relationship between the size of *E. pacifica* adults and juveniles and temperature associated with seasonal and interannual variability (Robertson and Bjorkstedt, 2020). *Euphausia pacifica* adults, juveniles, and furcilia tend to be smaller during warmer (non-upwelling) seasons and larger during cooler (upwelling) seasons. At longer time scales, warm-water events (e.g., El Niño) disrupt seasonal growth patterns leading to persistent shifts in adult and juvenile size towards distributions dominated by smaller size classes. These patterns are consistent with the ability of juvenile and adult *E. pacifica* to shrink under warm conditions, even when food is not limiting (Marinovic and Mangel, 1999). Robertson and Bjorkstedt (2020) also found that early life history stages exhibited a contrasting response to that of adults and juveniles, in which interannual warming shifted the population towards larger size classes. The contrasting response between early life history stages and and juvenile and adult stages to interannual variability in temperature is consistent with

stage-dependent temperature-size relationships reported for diverse marine taxa, including crustaceans (Forster and Hirst, 2012). The warm-water event that occurred during 2014-16 had a particularly strong and abrupt effect on size distributions of *E. pacifica* off northern California; numerous adults collected during this event were smaller than size ranges reported in the literature and large adults were rare when the heatwave signal was strongest along the coast (Robertson and Bjorkstedt, 2020).

Two IBMs have previously been developed for *E. pacifica* (Lindsey et al., 2013; Dorman et al., 2015). These models have been applied to scientific inquiries focused on spatial distribution and production dynamics and revealed important insight into krill retention mechanisms and the link between euphausiid production dynamics and ecosystem variability (Dorman et al., 2011; Lindsey, 2013; Dorman et al., 2015). However, these models do not account for observed relationships in empirical data, including the tendency of juveniles and adults to shrink at higher temperatures (Marinovic and Mangel, 1999) and variability in size-at-maturity (Robertson and Bjorkstedt, 2020), that have the potential to influence growth and size distributions of *E. pacifica* (see, for example, implementation of Dorman et al. (2015) IBM below), which limits their utility for more detailed population and ecosystem modeling.

My research objective is to develop an IBM capable of resolving realistic variability in growth and size dynamics of *E. pacifica* off northern California. To do so, I adopt an approach grounded in pattern-oriented modeling (POM) (Grimm et al., 2005; Grimm and Railsback, 2013 and references therein), taking the time series of *E. pacifica*

size, temperature, and chlorophyll a data reported in Robertson and Bjorkstedt (2020) as the basis for evaluating model performance. Although statistical comparisons are often used to evaluate model agreement with data, POM is not grounded in formal statistics (e.g., estimating parameters via minimization of least-squares). Instead, POM is a modeling approach where patterns observed in the real system addressed by the model are used to inform model development and evaluation.

The application of POM leads to a structured and iterative approach to model development. I build on existing IBMs for *E. pacifica* (Lindsey, 2013; Dorman et al., 2015) to advance the model in two phases. The first phase is focused on revising submodels to better connect empirical estimates of vital rates to observed patterns in the field. I generate submodels to account for thermal sensitivity of ingestion at high temperatures and the effect of temperature on maturation. I also develop a submodel for assimilation that reflects dependence on temperature, body size, and prey density. The second phase of model development is focused on tuning the model to observed patterns through the design and implementation of phenomenological models that represent hypotheses focused on variability in energetics. I implemented POM as a sequential development; model versions were evaluated to test whether model output matched observed patterns and modifications were made to rectify discrepancies identified in preceding model versions. In other words, the methods determined results and results determined the next iteration of methods. As such, the traditional format which separates 'methods' from 'results' does not facilitate clear communication of model development. I

combine these sections below into 'Model Development' to describe how models were developed and justify modifications at each step.

THE MODEL SYSTEM

In this section I provide a more detailed review of the empirical data and its environmental context (the California Current Ecosystem) and the life cycle of *E. pacifica* that are to be integrated into or represented by the IBM. I also briefly introduce existing IBMs for *E. pacifica* (Lindsey, 2013; Dorman et al., 2015) with a focus on identifying key patterns and processes targeted for revision and improvement in this research.

The California Current Ecosystem

The CCE encompasses a biologically rich and highly productive environment along the West Coast of North America. Production and transport processes within the CCE are modulated by regional winds, vertical transport (upwelling), and bottom-up dynamics (Ware and Thomson, 2005; Kudela et al., 2008; Chavez and Messié, 2009; Checkley and Barth, 2009, and references therein). In the coastal environment, equatorward winds drive offshore transport of surface waters, which are replaced by cool and nutrient-rich waters upwelled from below. Coastal upwelling dynamics vary throughout the CCE, but are generally strongest during spring and summer months (Hickey and Banas, 2008; Bograd et al., 2009). Upwelling of nutrient-rich waters contributes to enhanced primary productivity which supports production in higher trophic levels. During El-Niño events, the onset of upwelling tends to be delayed, the duration of the upwelling season is often shortened, and upwelling intensity weakens (Bograd et al., 2009; Jacox et al., 2015). Since production in the CCE is closely related to upwelling

dynamics, shifts in upwelling phenology and intensity have the potential to alter ecosystem dynamics (Lenarz et al., 1995; Barth et al., 2007; Chenillat et al., 2012). Large-scale, climate-related shifts in horizontal transport (advection) also contribute to ecosystem variability via altered productivity, species composition, and spatial connectivity (Di Lorenzo et al., 2013). For example, anomalous transport of water masses hosting a diverse assemblage of zooplankton has the potential to impact nearshore ecosystem dynamics (Bi et al., 2011).

Field Data

The time series of *E. pacifica* body size, temperature, and chlorophyll a data used in our previous analysis provide a unique opportunity to evaluate an IBM's ability to resolve realistic dynamics in *E. pacifica* size distributions (Robertson and Bjorkstedt, 2020). These data are comprised of approximately monthly measurements from 2008 to 2020 obtained along the Trinidad Head Line, a transect off northern California (Figure 1; see Robertson and Bjorkstedt, 2020 for complete sampling methods). Length measurements of *E. pacifica* are stage-specific and span F1 – F7 furcilia (F4/5 furcilia are combined), juveniles, and adults. For this analysis, *E. pacifica* data were aggregated across stations TH03 – TH05. These stations were selected because most adult *E. pacifica* are distributed along and offshore of the shelf break and size distributions of immature and adult life history stages at these stations are representative of the entire transect (Robertson and Bjorkstedt, 2020).

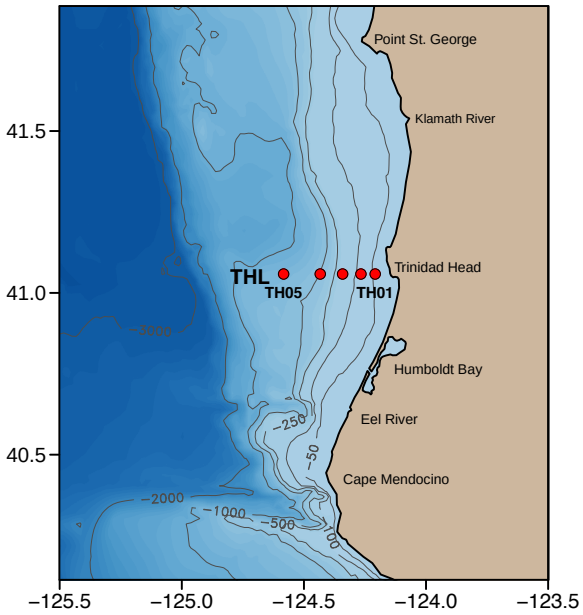

Figure 1. Bathymetric map of sampling location; Trinidad Head Line (THL; 41°03.50 N) off Trinidad, CA. Nearshore station (TH01) and offshore station (TH05) are labeled for reference. Bottom-depth is labeled in meters.

Hydrographic data collected at THL station TH04 (Figure 1; 41°03.50 N, 124°26.00 W; ~450 m water depth) were interpolated between (roughly) monthly cruises to provide daily values of environmental conditions at 1-meter bins from the surface to 200 m (Figure 2). In cases where hydrographic data were only available in the top 150 m, data were extrapolated from the last observed depth to 200 m (see Appendix A for methods).

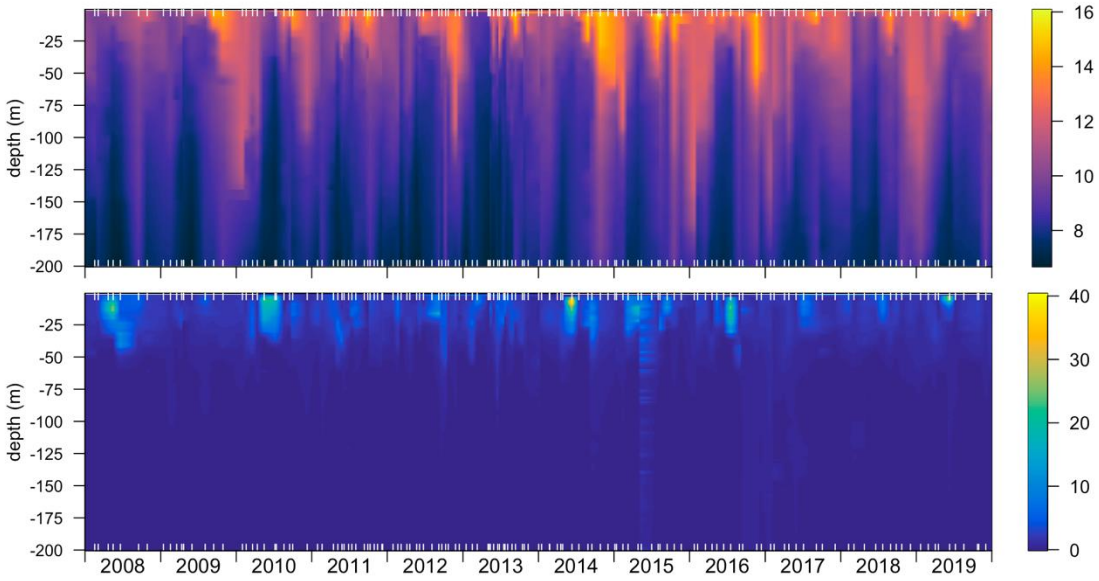

Figure 2. Time series (x-axis) of hydrographic data by depth (y-axis) at THL station TH04. top) Interpolated temperature (°C); bottom) Interpolated chlorophyll a concentration (mg L^{-1}). Rug indicates date of cruise and measurement.

E. pacifica Life Cycle and Ontogenetic Behavior

The *E. pacifica* life cycle includes 16 life history stages (Figure 3). After approximately 24 – 48 hours, an egg hatches into the first of two naupliar stages (Iguchi and Ikeda, 1994; Feinberg et al., 2006). Progression through nauplius N1, N2, and the metanauplius stage takes approximately six days. During this time, individuals do not feed. Next, individuals transition to the first of three calyptopis stages. At this point, feeding appendages are acquired and individuals are able to feed for the first time. Following progression through calyptopis C1 – C3, krill develop through up to seven furcilia stages. Development to the juvenile stage takes approximately 58 days. At this point, the individual closely resembles the adult form. Maturation occurs once individuals

obtain sexual characteristics (approximately 30-180 days after transition to the juvenile stage; Harvey et al., 2010; Shaw et al., 2021).

An IBM for *E. pacifica* must resolve behavior and physiology that determine environmental exposure and energetic dynamics. A key element of the life cycle is a transition in behavior represented by the initiation of diel vertical migration (DVM). Swimming legs are acquired in the F3 furcilia stage and individuals begin performing DVM (Vance et al., 2003; Feinberg et al., 2006). Vertical migration to shallower waters coincides with the onset of dusk and individuals return to deeper waters at dawn (Sato et al., 2013). The depth to which individuals migrate during daylight hours deepens with ontogeny (Vance et al., 2003; Liu and Sun, 2010; Im and Suh, 2016). Non-migrating individuals are exposed to a range of temperatures as they are moved throughout the water column, for example, as a sinking egg or when positioned in waters that are being vertically mixed.

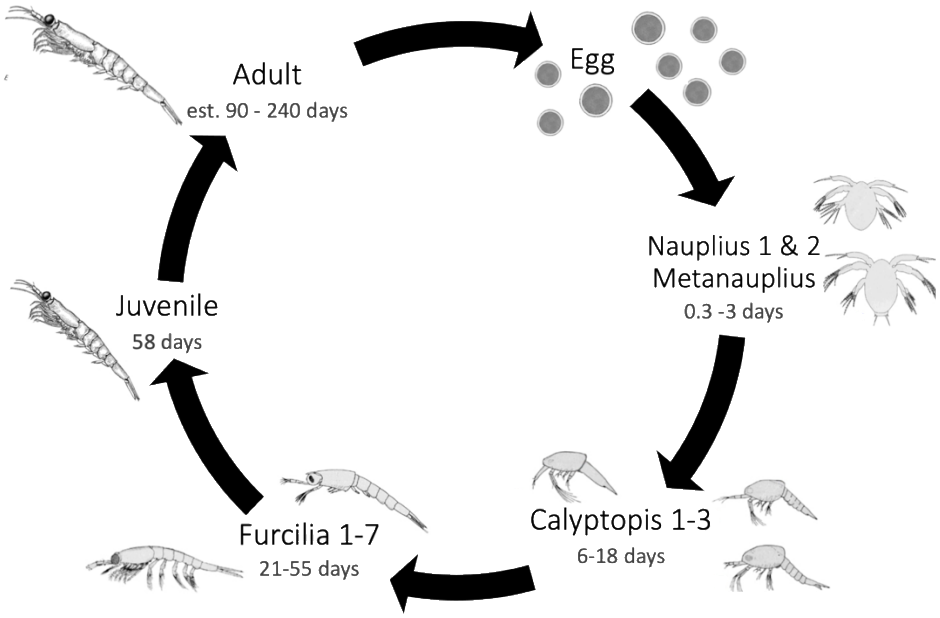

Figure 3. Life-history of *E. pacifica*. Development time (time to stage in days) for immature (Feinberg et al., 2006) and adult stages (Harvey et al., 2010 and Shaw et al., 2021).

Review of Existing IBMs and Motivation for Model Advancement

Existing IBMs implement growth and development with submodels that are based on laboratory observations and empirical data (Lindsey, 2013; Dorman et al., 2015). However, a few of the submodels fail to accurately characterize observed dynamics.

- Published IBMs do not allow for variability in size-at-maturity (as was observed in Robertson and Bjorkstedt, 2020) and instead implement maturation using invariant weight-based thresholds.

- Discrepancies between laboratory and field-based observations of growth with respect to temperature suggest published submodels do not capture realistic

dynamics. Submodels in Dorman et al. (2015) and Lindsey (2013) predict enhanced growth rates at higher temperatures (when sufficient food resources are available). This pattern directly contradicts lab-based observations that juvenile and adult *E. pacifica* growth rates above 14°C are negatively related to temperature, even when food is not limiting (Marinovic and Mangel, 1999). This rise-and-fall pattern in growth rate is observed across a wide range of taxa and can reflect a consumption-metabolism mismatch, whereby metabolic rates increase more than ingestion rates with respect to temperature (Rall et al., 2010; Lemoine and Burkepile, 2012 and references therein). Consequently, at higher temperatures, the amount of surplus energy available for growth decreases and growth rates exhibit a negative relationship with temperature (Brett, 1971; Rall et al., 2010; Lemoine and Burkepile, 2012).

- Ingestion rates have been shown to vary with temperature, body weight, and prey density (Ross, 1982a; Ohman, 1984). The ingestion submodel in Dorman et al. (2015) accounts for all of these factors. However, critical concentration, or the concentration of prey at which maximal growth is achieved, is resolved for discrete size groups, rather than implemented as a continuous function of size. Accurate estimates of critical concentration are important for obtaining the response of *E. pacifica* to prey density – which contribute to accurate estimates of ingestion. Rectifying the discrepancies between published submodels and *in-situ* dynamics will improve resolution of realistic growth

and size dynamics – crucial metrics for obtaining accurate production and biomass estimates and understanding ecosystem interactions.

Models presented herein include mechanistic and phenomenological approaches to modeling growth and development. The mechanistic approach to modeling growth calculates growth from the remainder of energy following allocation of assimilated material to respiration, molting, and (in the case of adults) reproduction (as in Lindsey, 2013). This approach enables modifications to specific energetic components (e.g., metabolic and ingestion rates) in the course of model development. In contrast, the phenomenological approach to modeling growth (as seen in Dorman et al., 2015) does not explicitly calculate energetic components. Instead, growth is scaled with temperature, body size, and food availability. In model versions presented here, development is modeled using a phenomenological approach. This approach uses either invariant weight-based thresholds (as in Dorman et al., 2015) or a temperature-dependent Bělehrádek development function (following Lindsey, 2013)

MODEL DEVELOPMENT

The model I developed is based on published IBMs for *E. pacifica* (Lindsey, 2013; Dorman et al., 2015). Like those models, the IBM versions developed herein build upon the POPCYCLE framework. POPCYCLE was initially developed to implement species-specific physiology and behavior at the individual-level for copepods (Batchelder and Miller, 1989). Bioenergetic rates (e.g., growth and assimilation rates) are calculated in carbon per unit of time (e.g., μg C d^{-1}) and are a function of life history stage, body size (μg C), and environmental exposure (temperature and food concentrations). Migration behavior (i.e., vertical position) is dependent upon life history stage and time of day. Model development, data analysis, and simulations were conducted in R (4.0.4; R Core Team, 2021).

Submodels within the IBMs fall along a spectrum that ranges from mechanistic, where a process is specified as a detailed function of factors affecting it, to phenomenological, where specification of the model may be grounded in hypotheses but underlying mechanisms are not modeled in detail. When empirical data linking processes to mechanisms are not available or do not resolve patterns observed in the real system, the phenomenological approach facilitates implementation of POM.

Generic Model Process

IBMs presented and developed herein follow a similar process schedule (Figure 4). Environmental conditions that drive the model are drawn from conditions along the

THL. At each timestep, vertical position, temperature, and food availability are determined. Energetic components (e.g., growth) are calculated based on environmental conditions and the state of the individual. If reproductive requirements have been met, adults reproduce. Following calculation of physiological rates, development is calculated. The individual is then evaluated for mortality, either due to starvation or end of lifespan.

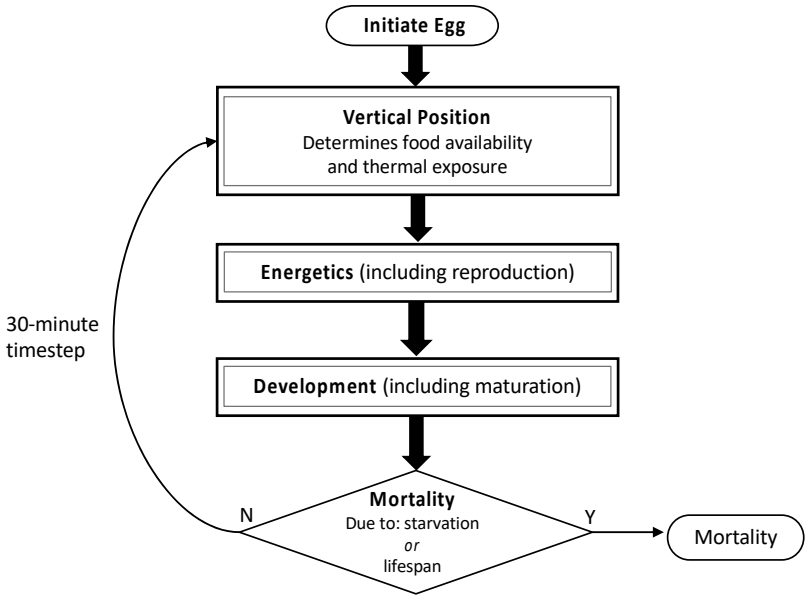

Figure 4. Flow diagram of process schedule in individual-based models. Following initiation of an egg, for each 30-minute timestep vertical position, energetics (e.g., assimilation and metabolism), development, and mortality (due to starvation or end of lifespan) are determined.

Application of Pattern-Oriented Modeling

I implemented POM to develop a series of models that sequentially address discrepancies between model predictions and observed patterns. At each iterative step in model development, model size distributions were compared to field-based observations.

Discrepancies between model output and observations were identified and used to inform modifications of submodels. The modified submodels were then incorporated into the IBM and the new model version was evaluated by comparison of model output and observations. This process was repeated until I arrived at a model that produced realistic patterns in size distributions and reduced discrepancies between model output and observations.

To assess IBM predictions of seasonal patterns in growth and size dynamics, I generated a seasonal climatology of temperature, chlorophyll a concentration, and median size of *E. pacifica* by stage. Krill size data were screened for outliers; for each life history stage, measurements outside the 5 and 95% quantile range were removed. Climatological values were estimated by fitting generalized additive models (GAMs; 'mgcv' version 1.8-33; Wood, 2017) to each response variable as a function of day-of-year. GAMs were based on cubic cyclic splines to ensure continuity across transitions between years. To resolve seasonal variability throughout the water column, a GAM was fit to each of 200 one-meter bins of temperature and chlorophyll a concentration and the results were concatenated to recover a time-by-depth matrix (Figure 5).

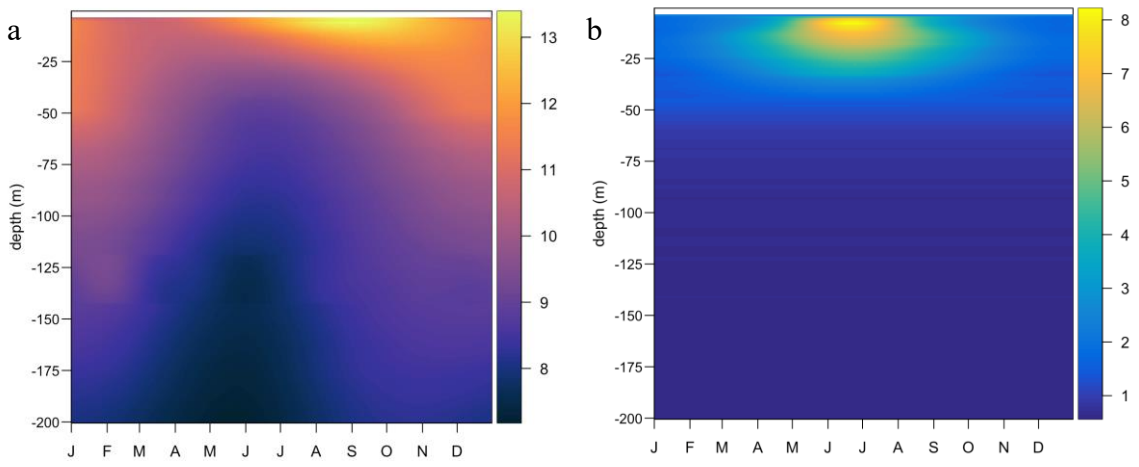

Figure 5. Seasonal climatology of hydrography along the THL. a) Temperature (C°) and b) chlorophyll a concentration (mg L^{-1}) versus month (x-axis) at THL station TH04 from 2007 – 2020.

Initially, pattern matching was focused on seasonal dynamics from climatological results. Seasonal patterns were qualitatively analyzed and modifications were made based on discrepancies between the shape of model output and field-based observations. Following analysis of seasonal patterns, time series scenarios were qualitatively and quantitatively analyzed (see details below). Like seasonal pattern-matching, modifications were made based on discrepancies between model output and field observations. I focused on matching patterns during years that were oceanographically consistent, as opposed to years characterized by sharp oceanographic transitions, such as the arrival of the Warm Blob and onset of the 2015-16 El Niño (Chao et al., 2017). Documented shifts of water masses and zooplankton assemblages during these periods indicate the potential for sampling transient krill populations with diverse size

distributions (Wells et al., 2017; Peterson et al., 2017; Bjorkstedt and Robertson, unpublished data).

Quantitative metrics of model performance included the root-mean square error (RMSE; 'rmse' in 'Metrics'; version 0.1.4; Hamner and Frasco, 2018) and direct correlation ('cor' in 'stats'; version 4.0.4; R Core Team, 2021) between THL observations and IBM predictions of median size (body length) for F1 furcilia – adult life history stages. Time series scenarios started on 1 January 2008 and were run through 31 December 2019. To allow for spin-up (i.e., development time) quantitative analyses were confined to a period starting on 1 March 2008 (furcilia stages) or 1 January 2010 (juvenile and adult stages). A lower RMSE and higher correlation between IBM predictions and THL observations indicated model improvement relative to other model versions. I emphasized the ability to replicate adult size distribution, because adult size is a strong determinant of overall biomass and production estimates (due to relatively large body size and longer stage duration).

Model development included numerous iterations and model versions. A few select versions that represent key modifications are presented here. These versions range from an initial ('Phase I') model that incorporates reformulated submodels that better reflect realistic temperature-dependent growth, development, and assimilation dynamics to versions that build on these mechanistic improvements by incorporating phenomenological modifications to improve resolution of discrepancies in seasonal and interannual patterns.

Body Size

Published IBMs and those developed here express individual state in units of carbon weight (W; µg C). However, our field-based observations of *E. pacifica* body size and published information on growth rates (e.g., Shaw et al., 2010) record body size as a length measurement. To facilitate comparisons between model output and field observations, body weight (*W*) was converted to dry weight (*DW*; mg), total length (*TL*; mm), and body length (*BL*; mm) per the following equations (1-3):

$$DW = \frac{\frac{W+1.985}{0.401}}{1000} \quad (1)$$

$$TL = \frac{DW}{0.795}^{1/3.239} \quad (2)$$

$$BL = \frac{TL-0.2807}{1.218} \quad (3)$$

following (Shaw et al., 2010; Feinberg et al., 2007, and Ross, 1982a).

Body length represents the distance from the back of the eye to the base of the telson (Shaw et al., 2010) and is used for comparison to length measurements along the THL. Total length represents the distance from the back of the eye to the tip of the telson (Gómez-Gutiérrez et al., 2006) and is used for comparison to published growth rates, which are typically expressed in mm TL d^{-1} (e.g., Shaw et al., 2010).

Preliminary versions of the model revealed biased estimates for F1 and F2 furcilia. Rather than modify energetics, which would impact growth and body size of subsequent life history stages, I modified the weight-to-length conversion for F1 and F2 furcilia as follows (equations 4 and 5):

$$F1\ Furcilia\ TL = DW^{1/3.239} \quad (4)$$

$$F2\ Furcilia\ TL = \frac{DW}{0.900}^{1/3.239} \quad (5)$$

This modification is justified by the difference in body form between F1 and F2 furcilia and later life history stages, especially the broader telson and wider carapace. This modification has no impact on weight-based processes in the model and is consistent with the POM approach.

Demographics

IBMs developed here are not implemented to simulate population dynamics, they track a single individual representative of a cohort. However, field observations are a composite of individual growth trajectories (size-at-age) that arise from variable egg production over time and mortality. Therefore, it is necessary to weight the contribution of each simulated cohort (i.e., size-age trajectory) to the size distribution existing on each day for fair comparison to field observations. To do so, I weight the initial value of each

cohort by climatological egg production and apply cumulative size-dependent mortality over the course of that cohort's lifetime. Production and size-based mortality rates are applied to model output post-simulation. Note that other sources of mortality (i.e., starvation or end of lifespan) are implemented in the IBM (see 'Generic Model Process' above and 'Mortality' below).

Egg production (eggs d^{-1}) was estimated by fitting a GAM to *E. pacifica* egg density (from THL vertical ring-net data collected at station TH02 from 2009 – 2016) as a function of day-of-year (Figure 6). Observations of egg densities greater than two standard deviations from the mean were removed prior to fitting the model. The GAM was based on a cubic-cyclic spline to ensure continuity across the start and end of the seasonal cycle. Effective degrees of freedom were fixed (edf = 8) to resolve early and late seasonal peaks in egg production. To implement egg production as a discrete value, egg densities predicted by the GAM were scaled to a maximum of 1000 eggs d^{-1} and rounded to the nearest integer for weighting of IBM output data.

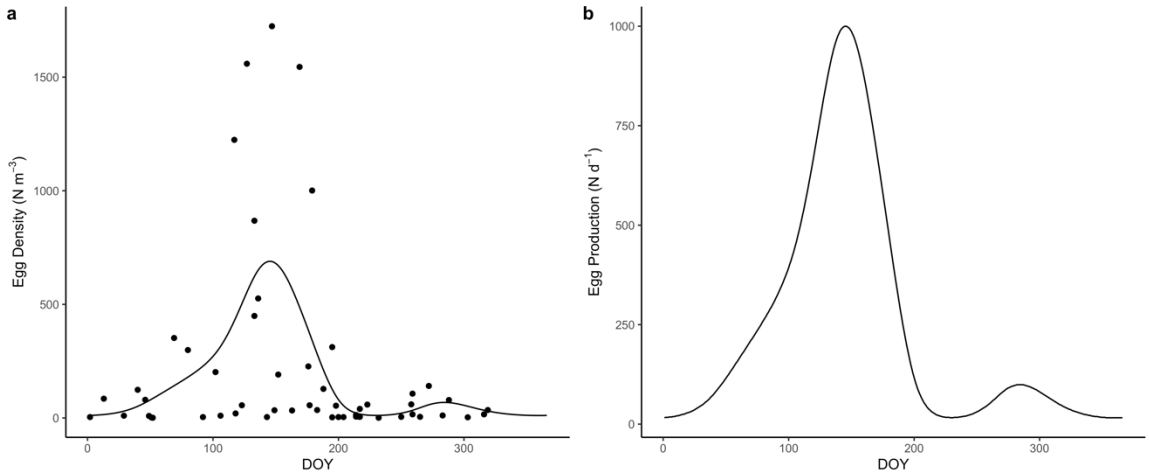

Figure 6. Observed and predicted egg density. a) GAM (line) fit to THL observations (points) of egg density by day-of-year (x-axis) at THL station TH02 from 2009 – 2016; b) Scaled egg production values by day-of-year.

Size-based (predation) mortality was calculated following Peterson-Wroblewski (1984) who estimated weight-based instantaneous mortality as (equation 6):

$$Mortality = (5.26 * 10^{-3}) * DW^{-0.25} \quad (6)$$

where $Mortality$ is instantaneous mortality (day^{-1}) and DW is dry weight (g). Body weight (µg C) was converted to dry weight (g) following equation 1. The size-specific instantaneous mortality rate was applied to the daily mean size of the individual.

The resulting densities for each cohort by date and stage were used to generate population size distributions (e.g., median body length) over time. Stage-specific

minimum (10^{th} quantile), median (50^{th} quantile), and maximum (90^{th} quantile) size was calculated for life history stages for which THL observations exist (F1 furcilia – adults).

Base IBM: Based on Dorman et al. (2015)

A published IBM for *E. pacifica* resolves the important life-history behavior and structure described above (Dorman et al., 2015). Growth is scaled directly as a function of body size, temperature, and food availability. This model includes 13 life history stages: egg, metanauplius, calyptopis C1 – C3, furcilia 1 -7 (furcilia 4/5 are combined), juvenile, and adult. Nauplius 1 and 2 are subsumed in the non-feeding egg stage. Development (i.e., transition to the next life history stage) of non-feeding and feeding stages is implemented using degree day and invariant weight thresholds, respectively (Table 1). Initial egg weight is 2.58 µg C. Starvation occurs when an individual's weight drops below 70% of the maximum weight achieved by the individual over the course of its life.

Table 1. Thresholds used to implement development of *E. pacifica* to the next life history stage in the Dorman et al., (2015) IBM. Degree-day thresholds were used for egg and metanauplius stages. All other stage transitions are determined by invariant weight thresholds (µg C).

Life History Stage	Threshold	Threshold Units
Egg	17.06	degree-days
Metanauplius	38.28	degree-days
Calyptopis C1	2.33	µg C
Calyptopis C2	3.52	µg C
Calyptopis C3	6.52	µg C
Furcilia F1	11.76	µg C
Furcilia F2	17.7	µg C
Furcilia F3	32.44	µg C
Furcilia F4/5	55.77	µg C
Furcilia F6	70.56	µg C
Furcilia F7	78.02	µg C
Juvenile	84.9	µg C
Mature Adult	1500	µg C

I ported the Dorman et al. (2015) bioenergetics code from Fortran to R (Figure B1) to serve as 1) a base against which to demonstrate model improvements and 2) as a structural template into which submodels would be integrated, thus ensuring compatibility of outputs. Vertical migration behavior followed rules described below (see

'Vertical Position and Migration Behavior'). To evaluate patterns in seasonal and interannual size distributions, this 'Base' model was forced with environmental conditions from climatological and time series data. For each simulation, an egg was initiated every ten days. A 30-minute timestep was used to calculate growth in size and development from one life history stage to the next. The length of this timestep enables realistic implementation of vertical migration and provides frequent updates to individual stage variables (e.g., size). Date, depth, environmental conditions, energetic components, and individual characteristics (e.g., size, stage, age, and mortality status) were recorded every six hours. Output (body size) from climatological and time series simulations was compared with field-based observations.

Vertical Position and Migration Behavior

In IBMs presented here, daytime depth is stage-dependent and based on *in-situ* observations (Vance et al., 2003; Im and Suh, 2016; Table 2). To simulate mixing of non-migrating krill, egg – F2 furcilia stages are exposed to the mean of temperature and chlorophyll a concentration over a stage-specific depth range. Vertical migration is implemented once krill reach the F3 furcilia stage, the first stage at which swimming legs are fully developed (Boden, 1950). At the onset of dusk, individuals are moved from their stage-specific daytime depth to the depth (below 10 m) at which maximum chlorophyll concentration occurs. Individuals return to their corresponding daytime depth with the onset of dawn. Civil twilight, the time at which the sun is 6° below the horizon, is used to mark the onset of dawn and dusk, which translates to a minimum of 7.75 (summer) and maximum of 13.75 (winter) hours spent in shallower waters. The timing of civil twilight

is date-specific and determined using 'crepuscule' in 'maptools' (Bivand and Lewin-Koh; version 1.1-1).

Table 2. Diel vertical migration (DVM) behavior of krill in IBMs. Non-migrating stages (Egg – F2 furcilia) are exposed to the mean temperature and chlorophyll a concentration across the noted depth range (e.g.,10 to 100 m). Krill performing DVM migrate at night to the depth at which maximum chlorophyll occurs and return to their stage-specific day depth during daylight hours.

Stage	DVM	Day Depth (m)	Night Depth (m)
Egg	No	10 to 100	10 to 100
Nauplius N1	No	10 to 100	10 to 100
Nauplius N2	No	10 to 100	10 to 100
Metanauplius	No	10 to 50	10 to 50
Calyptopis C1	No	10 to 50	10 to 50
Calyptopis C2	No	10 to 50	10 to 50
Calyptopis C3	No	10 to 50	10 to 50
Furcilia F1	No	10 to 50	10 to 50
Furcilia F2	No	10 to 50	10 to 50
Furcilia F3	Yes	25	Maximum Chlorophyll Depth
Furcilia F4/5	Yes	35	Maximum Chlorophyll Depth
Furcilia F6	Yes	45	Maximum Chlorophyll Depth
Furcilia F7	Yes	50	Maximum Chlorophyll Depth
Juvenile	Yes	150	Maximum Chlorophyll Depth
Adult	Yes	200	Maximum Chlorophyll Depth

Base IBM: Diagnosis

The Base IBM performed poorly in resolving realistic patterns in size distributions (Figure 7). Predicted size distributions for furcilia stages were relatively constant and did not exhibit seasonal or interannual variability (Figure 7a and b). Model predictions for older life history stages were almost completely out of phase with observed trends in size at seasonal scales. Juvenile size was overestimated in winter and underestimated in spring and summer and did not match well with field observations in the time series scenario. Likewise, simulated size distributions of adults contrasted sharply with field-observations; model adults were larger in winter and smaller in spring (Figure 7a). Like other life history stages, interannual variability in adult size was not well resolved (Figure 7b and c). Across all life history stages, correlations indicated a poor match between field observations and IBM predictions (Figure 7d).

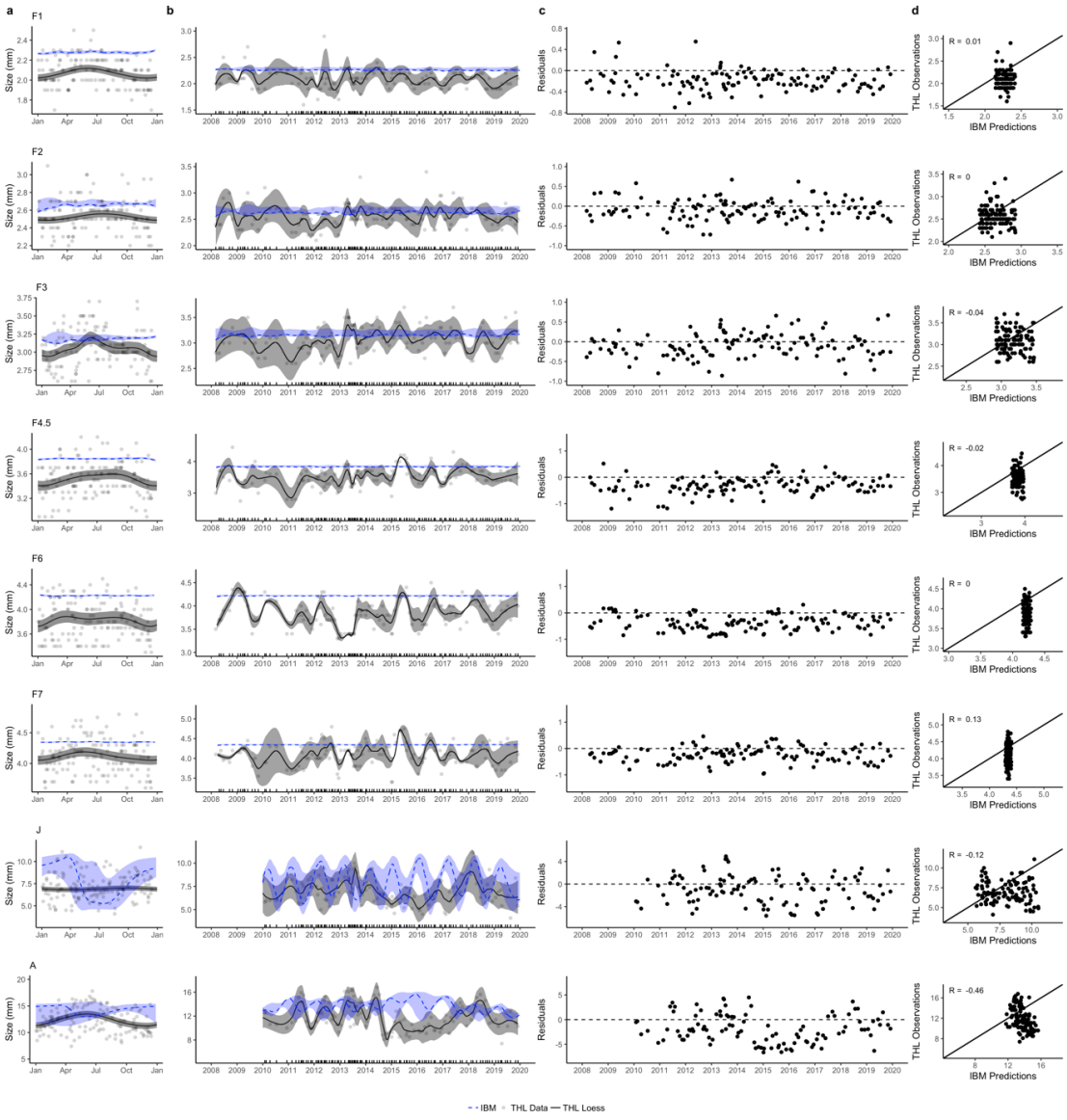

Figure 7. Stage-specific size (BL in mm; y-axis) distributions from the Base IBM (energetic submodels from Dorman et al., 2015) forced with a) climatologies and b) time series of temperature and chlorophyll a concentration along the THL. IBM results (blue dashed-line indicates median size; blue ribbon spans loess smooth of minimum (10^{th} quantile) and maximum (90^{th} quantile) body length) and THL data (gray points indicate median size by cruise date; solid black line represents loess smooth of median size, gray ribbon spans ± 1 SD). c) Residuals from THL observations and IBM predictions of median size. Horizontal dashed-line at zero for reference. d) Correlation between median size of THL observations and IBM predictions. Title in top left corner of first column indicates life history stage (F1 – F7 furcilia, J = Juvenile, A = Adult) by rows.

Phase I IBM: Reanalysis and Reality

The Phase I IBM retains the process schedule and vertical migration rules from the Base model. However, I took a more mechanistic approach to modeling growth. Growth is calculated from the carbon remaining following allocation of assimilated carbon to respiration, molting, and reproduction (as in Lindsey, 2013). This approach enables modifications to specific energetic components (e.g., ingestion rate). A detailed description of submodels follows, but in general I constructed submodels to better account for thermal sensitivity of ingestion at high temperatures and the effect of temperature on maturation. I also constructed a submodel for assimilation that reflects dependence on temperature, body size, and prey density. Like the Dorman et al. (2015) IBM, development is implemented using a phenomenological approach. However, rather than using invariant weight thresholds to determine stage transitions, the Phase I model uses a temperature-dependent Bělehrádek development function (following Lindsey, 2013; see 'Development' below for details).

Life history stages are parsed more finely in the Phase I IBM than the Base IBM. The Phase I IBM includes 15 life history stages: egg, nauplius 1 and 2, metanauplius, calyptopis C1 - C3, furcilia F1 - F7 (furcilia F4/5 are combined), juvenile, and adult. Life history stage determines behavior (e.g., feeding, vertical position) as well as whether growth is modelled directly as a function of temperature, food availability, and body weight, or mechanistically as the remainder of energy following allocation of assimilated energy to somatic maintenance and reproduction (Table 3).

Table 3. Feeding behavior and type of growth submodel for *E. pacifica* life history stages in the Phase I IBM. 'Direct' growth model indicates growth is calculated by scaling expressions that relate growth rate to body size and temperature. In contrast 'Mechanistic' growth model indicates growth is calculated from the remainder of assimilated carbon following allocation to metabolism, molting, and in the case of adults, reproduction.

Stage #	Stage	Feeding	Growth Model
1	Egg	No	Direct
2	Nauplius N1	No	Direct
3	Nauplius N2	No	Direct
4	Metanauplius	No	Direct
5	Calyptopis C1	Yes	Direct
6	Calyptopis C2	Yes	Direct
7	Calyptopis C3	Yes	Direct
8	Furcilia F1	Yes	Mechanistic: (Assimilation – Costs)
9	Furcilia F2	Yes	Mechanistic: (Assimilation – Costs)
10	Furcilia F3	Yes	Mechanistic: (Assimilation – Costs)
11	Furcilia F4/5	Yes	Mechanistic: (Assimilation – Costs)
12	Furcilia F6	Yes	Mechanistic: (Assimilation – Costs)
13	Furcilia F7	Yes	Mechanistic: (Assimilation – Costs)
14	Juvenile	Yes	Mechanistic: (Assimilation – Costs)
15	Adult	Yes	Mechanistic: (Assimilation – Costs)

Energetic Submodels

Energetic submodels (physiological rates) are defined in text as daily rates of carbon allocation (µg C d^{-1}). In the IBM, daily rates are scaled to 1/48 of the daily rate to reflect the 30-minute time step at which they are applied.

Growth

Growth dynamics over the life history of *E. pacifica* are described in detail below, but share a common characteristic of being dependent on temperature. To capture this dependence, Q_{10} relationships were used to scale physiological rates by temperature using equation 7:

$$Rate_2 = Rate_1 * Q_{10}^{(T_2 - T_1)/10°C} \quad (7)$$

where $Rate_2$ is the projected physiological rate at temperature T_2 (expressed in °C), $Rate_1$ is a known physiological rate at temperature T_1, and Q_{10} is the factor by which the physiological rate increases per 10°C rise in temperature. In this study, Q_{10} coefficients were established for each physiological process (i.e., ingestion, metabolism, molting, and reproduction) based on information in Ross (1979). Q_{10} values were calculated using the complete expression relating each physiological rate to weight at 8 and 12°C (Table 4). This method differs from that utilized by Ross (1982a) by including the intercept and

weight-specific coefficient regardless of whether they were significantly different at 8 and 12°C.

Table 4. Expressions for physiological rates from Ross (1979 and 1982a) and from my re-analysis of Ross's data. Intercept (a) and weight-specific coefficients (b) for allometric equations describing the relationship between physiological rate (µg C d^{-1}) and body weight (µg C), where physiological rate = $a * W^b$. A = Adults, J = Juveniles, F = furcilia, FJA = furcilia, juvenile, and adults. Note that growth of early life history feeding stages (ELHF) follows a linear equation where growth = $a + W * b$. Q_{10} coefficients in this study are calculated using complete allometric expressions (versus only using intercepts if weight specific coefficients were not significantly different, as in Ross, 1979 and 1982a).

Source	Physiological rate (Stage)	Q_{10}	T (°C)	*a*	*b*
Ross (1979, 1982a)	Ingestion (FJA)	3.35	8	0.249	0.910
			12	0.404	0.910
Ross (1979, 1982a)	Metabolism (A)	1.9	8	0.154	0.810
			12	0.200	0.810
Ross (1979, 1982a)	Metabolism (J)	1.9	8	0.154	0.810
			12	0.200	0.810
Ross (1979, 1982a)	Metabolism (F)	2	8	0.171	0.839
			12	0.266	0.839
Ross (1979, 1982a)	Reproduction (A)	3.6	8	0.006	1.035
			12	0.010	1.035
Ross (1979, 1982a)	Molting (FJA)	2.46[a]	8	0.011	0.853
			12	0.021	0.805
Ross (1979, 1982a)	Growth (ELHF)		8	-0.057	0.124
			12	-0.315	0.198
This study	$Ingestion_{Max}$ (FJA)	3.35	8	0.249	0.910

Source	Physiological rate (Stage)	Q_{10}	T (°C)	*a*	*b*
			12	0.404	0.910
This study	Metabolism (A)	3.37	8	0.139	0.930
			12	0.224	0.932
This study	Metabolism (J)	3.35	8	0.121	0.964
			12	0.192	0.968
This study	Metabolism (F)	3.25	8	0.103	0.996
			12	0.162	1.001
This study	Reproduction (A)	3.61	8	0.006	1.035
			12	0.010	1.035
This study	Molting (FJA)	$5.08*weight^{-0.12}$	8	0.011	0.853
			12	0.021	0.805
This study	Growth (ELHF)	1.74	8	-0.057	0.124
			12	-0.315	0.198

a: Average Q_{10} for all weights, range is 3.37 (30 ug C) to 1.93 (3,000 ug C).

Growth of non-feeding stages

Following Lindsey (2013), initial egg weight is set at 3.2 µg C (versus 2.58 in the Dorman et al. (2015) IBM), based on observations of *E. pacifica* egg size off Oregon (Gómez-Gutiérrez et al., 2003).

By definition, non-feeding stages lose weight. Estimates from Ross (1979) indicate greater rates of weight loss in non-feeding stages at 8°C compared to 12°C. This pattern contradicts general rate-temperature relationships, in which metabolic rate tends to increase with temperature, at least over range of temperatures typically experienced by

an organism (Cossins and Bowler, 1987). Since alternative rates for non-feeding stages were not available, I selected a rate to implement weight loss (-0.145 µg C d^{-1}) within the range of Ross's observations that generated realistic sizes of early life history stages. The rate of weight loss in non-feeding stages was scaled with temperature using a generic Q_{10} of 2.0.

Growth of feeding stages

Growth of feeding stages (calyptopis C1 through adult) is dependent upon temperature and food concentration. Food concentration in µg C is estimated from chlorophyll a concentration following a 1 µg chlorophyll a: 60 µg C conversion (as in Dorman et al., 2015).

Growth rates of furcilia, juvenile, and adult stages are calculated as a function of explicit input and output variables following the expression for a carbon-only crustacean energy budget (equation 8; Dagg 1976):

$$Growth = Assimilation - Metabolism - Molting - Reproduction \quad (8)$$

Specific definitions are developed below, but components of this equation can generally be described in the following terms. Assimilation is calculated as the product of ingestion and assimilation efficiency, the amount of carbon ingested that is retained and available

for energetic processes. Metabolism represents the energy required for catabolic and anabolic processes. As in Ross (1982a) metabolic rate estimates account for leakage, or the amount of dissolved organic carbon released from the individual. Molt rate is calculated as the loss of carbon at each ecdysis (molt event) divided by the molt interval in days. Allocation to reproduction was estimated by Ross (1982a) and is based on the total amount of carbon allocated to broods over an individual's lifetime following maturation.

Growth rates of early life history feeding stages (ELHF; calyptopis C1 – C3) are modeled directly using the empirical relationship between growth rate (µg C d^{-1}) and body weight (W, µg C) (Ross, 1982a; equation 9).

$$Growth \text{ (derived at } 12°\text{C)} = -0.315 + 0.198\,W \quad (9)$$

Growth of ELHF stages is scaled with temperature using a Q_{10} of 1.74 (Table 4).

The ELHF growth expression (equation 9) was derived under maximal food resources. As such, it represents maximum growth rate for ELHF stages. To account for variability in food resources, growth rates of ELHF stages were scaled by the ratio of available food concentration to critical concentration, the food concentration at which

maximal growth is achieved (see 'Assimilation' below for how critical concentration is calculated).

Growth: Assimilation

Ingestion is dependent on size, temperature (Ross, 1982a), and food concentration (Ohman, 1984; Kiørboe, 2008). Q_{10} coefficients are used to scale ingestion rates with temperature. To account for the effects of body weight and food concentration, I developed an ingestion rate function of the Type III form identified by Ohman (1984; equation 10):

$$Ingestion\ Rate_{Food\ Concentration} = \frac{a_{FoodConc.} * Food\ Concentration^2}{1 + a_{FoodConc.} * T_h * Food\ Concentration^2} \quad (10)$$

where $a_{FoodConc.}$ is the capture efficiency or attack rate and T_h is the handling time and scale this equation with body weight.

To determine weight-dependent critical concentration, which is defined as the food concentration at which maximal growth is achieved, I fit an allometric model to critical concentration and body weight data from Ross (1979) and Ohman (1984; Table 5 and Figure 8a; *critical concentration = 16.48*W*$^{0.35}$). An allometric model was preferred over an asymptotic model on the basis of greater biological relevance; as body size increases, the amount food required to maintain a larger size and grow is expected to

increase, not to plateau, thus requiring more food to achieve maximum growth. Ingestion rates were then predicted as a function of weight and food density using a Type III functional response model scaled so that ingestion is 90% of maximum ingestion ($Ingestion_{Max}$; Table 4) at critical concentration across all sizes (Figure 8b). Ingestion is capped so that it does not exceed ingestion at critical concentration (as in Dorman et al., 2015).

Table 5. Critical concentration (CC; µg C l^{-1}) for various sizes of *E. pacifica* krill at 8 and 12°C. Data from Ross (1979) and Ohman (1984). NA indicates field does not apply to data source.

Source	Size class (µg C)	Avg. weight in size class	CC at 8°C	CC at 12°C
Ross (1979)	< 750	273	100	125
Ross (1979)	750-1650	1205	190	225
Ross (1979)	1650	2564	320	375
Ohman (1984)	NA	4700	290	NA

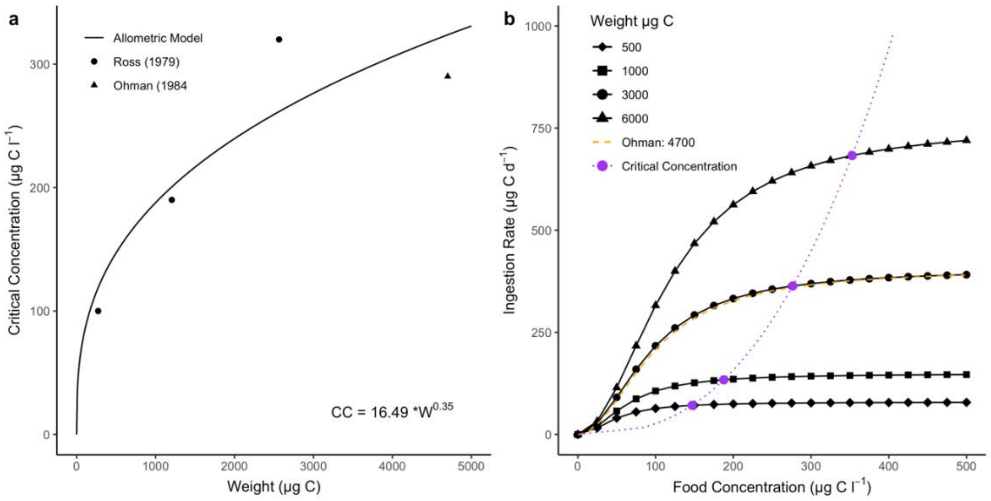

Figure 8. a) Allometric model (line) fit to critical concentration (CC; µg C l^{-1}; y-axis) and weight data (x-axis) at 8°C from Ross (1979; points) and Ohman (1984; triangle); b) Predicted ingestion rates for various sizes of krill using weight- and food concentration-dependent function (at 8°C to match experimental temperature in Ohman, 1984). Closed purple circles and purple dotted-line indicate critical concentration at various body sizes (see legend). Orange dashed-line represents the Type III functional response for the average krill size (4700 µg C) in Ohman's (1984) study.

Existing IBMs scale energetics using Q_{10} values determined by Ross (1979). In the Dorman et al. (2015) IBM, growth rate is scaled directly with the Q_{10} for growth. In the Lindsey (2013) IBM, ingestion and respiration are scaled with corresponding Q_{10} values from Ross (1979), who calculated a greater Q_{10} for ingestion than metabolism (i.e., ingestion increases faster than metabolism as temperature increases). The result in both IBMs is that growth rate exhibits a positive relationship with temperature and is not constrained at higher temperatures. A monotonic increase in growth with temperature, however, contradicts observations that juvenile and adult *E. pacifica* growth rates are negatively related to temperature above 14°C, even when food is not limiting (Marinovic

and Mangel, 1999). Furthermore, a rise-and-fall pattern in growth rate with respect to temperature is observed across a wide range of taxa and can reflect a consumption-metabolism mismatch, whereby energetic costs exceed assimilation (Rall et al., 2010; Lemoine and Burkepile, 2012 and references therein; Alcaraz et al., 2014; Grote et al., 2015).

To resolve disparities between growth predictions from existing IBMs and observations, I refined the energetics component of the IBM to allow for shrinking as reported in Marinovic and Mangel (1999) by modifying the Q_{10} value used for scaling of ingestion rates in juvenile and adult stages. This modification is supported by observations that indicate Q_{10} values tend to decrease with increasing temperature (Ege and Krogh, 1914; Alcaraz et al., 2014). At intermediate and high temperatures, the relationship between ingestion rate and temperature is strongly correlated with that of growth rate and temperature, more so than the thermal sensitivity of other energetic components (Kingsolver and Woods, 1997). Based on the strong correlation between thermal sensitivity of ingestion and growth, I chose to modify ingestion (as opposed to other energetic components).

In my IBM, transition to a temperature-dependent Q_{10} begins once an individual reaches the juvenile stage. Dependency on the temperature-dependent Q_{10} scales linearly with juvenile weight, such that for krill exceeding 266 µg C (~8 mm TL, the minimum size of krill in Marinovic and Mangel, 1999), the Q_{10} is defined by a sigmoidal relationship with temperature (Figure 9). The sigmoidal model was anchored by the Q_{10}

value for ingestion (3.35) estimated by Ross (1982a) at temperatures between 8 and 12 °C and tuned by manipulation of Q_{10} values at higher temperatures to generate negative growth rates consistent with rates reported by Marinovic and Mangel (1999). The resulting Q_{10} values are within a typical range for biological rates (Cossins and Bowler, 1987).

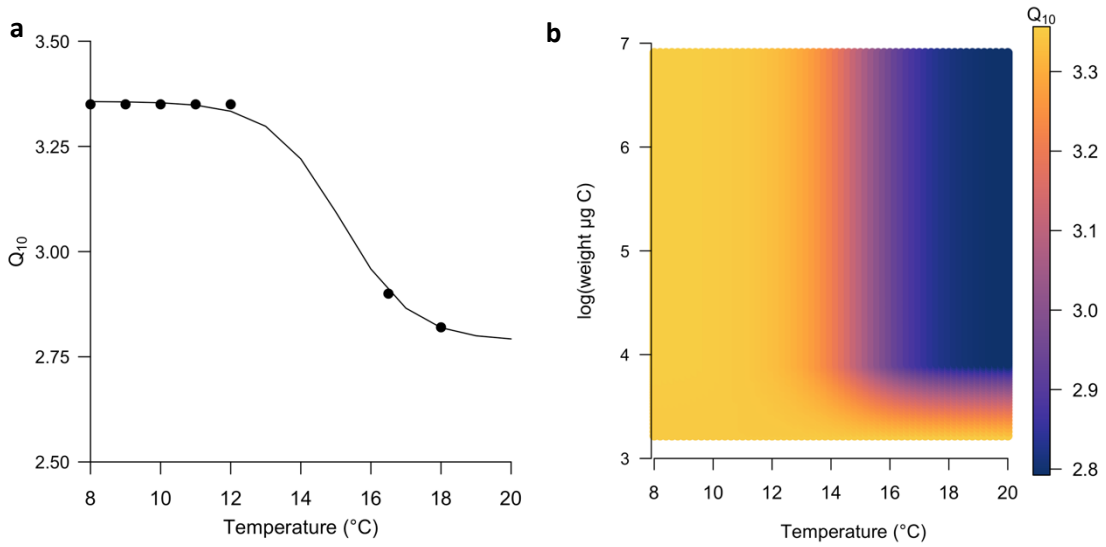

Figure 9. Q_{10} values for ingestion. a) Predicted Q_{10} values for ingestion generated from sigmoidal model (black line) fit to empirical (upper asymptote) and simulated (lower asymptote) Q_{10} data; b) Q_{10} ingestion values (see color legend) for various log-scaled weights of krill (y-axis) and temperatures (x-axis).

Preliminary IBM simulations with realistic environmental conditions indicated that individuals in stages with substantial vertical migrations (i.e., juvenile and adult) frequently exhibit negative growth during the daytime when they are deeper in the water column. The magnitude of negative growth generated unrealistic growth dynamics as a consequence of inadequate food resources at depth. The IBM accounts only for phytoplankton food. However, krill are also capable of feeding on alternate food sources

(e.g., marine snow and zooplankton) that are more broadly distributed and available at depth (Dilling et al., 1998; Nakagawa et al., 2003; Park et al., 2011; Im and Suh, 2016). To account for food at depth, I modified the environment so food concentration for juvenile and adult stages is 30% of what was available at the daily maximum chlorophyll depth. This modification is only implemented if food at depth is below 30% of what was available at the maximum chlorophyll depth. This modification is supported by evidence indicating *E. pacifica* feed on alternate prey sources (e.g., tintinnids and copepods) while at depth during the daytime (Nakagawa et al., 2003). I also decreased metabolic demand during daylight hours by 30% for adults and 20% for juveniles. This modification reflects observations that indicate decreased feeding activity during the day at depth (Nakagawa et al., 2003).

Growth: Metabolism

Ross's direct measurement of growth was greater than the difference between assimilation and energetic costs. Ross attributed the discrepancy in the energy budget to possible measurement errors (Ross 1982b). Metabolic rate was suspected to have been underestimated, possibly as a consequence of suppressed activity due to confinement of krill in a small vial during respiration experiments and errors in leakage estimates.

Under the assumption that empirical estimates of metabolism were the sole source of imbalance in Ross's (1982a) energy budget, I re-calculated metabolic rates for furcilia, juvenile, and adult stages using Ross's data and expressions for assimilation, growth,

molting, and reproduction. I rearranged equation 8 to generate a new estimate of metabolic rate (equation 11, Figure 10, and Table 4):

$$Metabolism = Assimilation - Growth - Molting - Reproduction \quad (11)$$

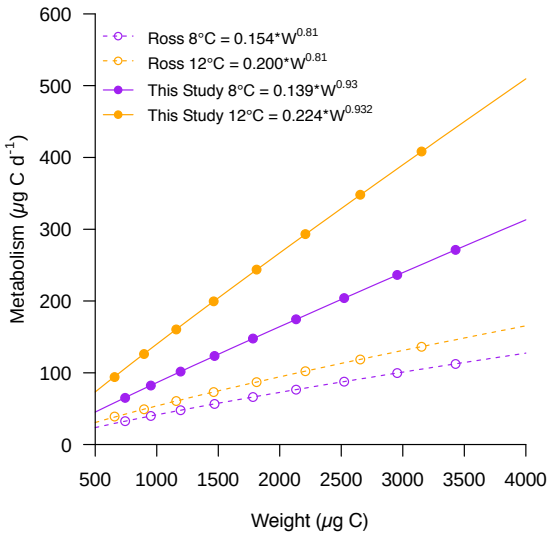

Figure 10. Adult metabolic rate at 8 (purple) and 12°C (orange) versus body weight. Expressions are from Ross (1982a; dashed-lines) and this study (solid-lines). Open circles represent original data from Ross (1979), filled circles represent metabolic rates calculated in this study. New allometric equation for metabolic rate assumes underestimation in original estimate by Ross (1982a).

Growth: Molting

I retained the allometric equation for molt rate determined by Ross (1982a; Table 4). The Q_{10} for molt rate exhibits a clear inverse relationship with body weight (Ross, 1979). To account for this pattern, I fit an allometric model to data from Ross (1979). The resulting model expresses the temperature sensitivity of molt rate ($Q_{10\ Molt}$; equation 12) as a function of body weight (W; Figure 11) and is defined as:

$$Q_{10\,Molt} = 5.08 * W^{-0.12} \quad (12)$$

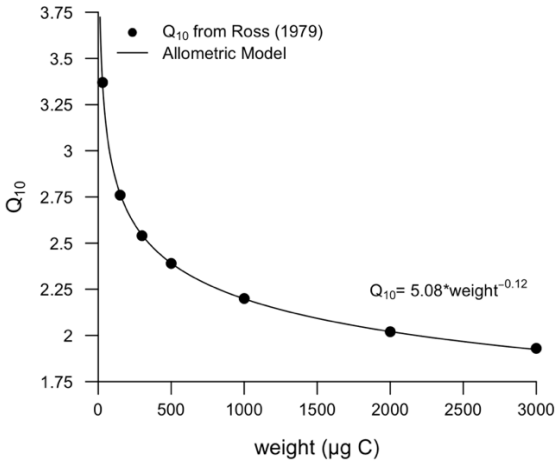

Figure 11. Allometric model (line) fit to Q_{10} values (points) for molt production and weight data from Ross (1979).

Growth: Reproduction

Allocation of energy to reproduction commences once an individual reaches maturity. Allocation to reproduction follows the relationship defined in Ross (1979; equation 13):

$$Reproductive\ Weight\ Allocation\ (RWA) = 0.010(W + 1.98)^{1.035} \quad (13)$$

where allocation to stored reproductive weight (RWA; µg C) at each timestep is predicted as a function of body weight (W; µg C). Allocation of energy to reproductive stores is

independent of whether there is sufficient food to maintain costs of living. This allows an individual to shrink but still reproduce, as has been observed in the field and laboratory (e.g., Shaw et al., 2010).

Release of eggs is based on rules from the Dorman et al. (2015) IBM. Release of eggs occurs only at night and is dependent upon interbrood period (the time between release of eggs) and the ratio of stored reproductive weight (RW) to body weight (BW). Interbrood period is set to 10 days. Individuals release eggs every 10 days if RW:BW is between 2.5 and 7.5%. If the RW:BW ratio is greater than 7.5%, eggs are released independent of interbrood period. The number of eggs released is equal to the reproductive weight divided by egg weight (3.2 µg C). If any reproductive weight is leftover after egg release, it is conserved as reproductive weight for subsequent timesteps.

Application of Mechanistic Submodels for Growth

Results from the Phase I model indicate that growth rates for furcilia stages are similar to those predicted by the Base IBM (Figure 12a). Growth rates for juvenile and adult stages closely match growth rates from the Base IBM up to 12°C, at which point they reflect the modification that generates negative growth above 17.28°C (Figure 12b - e).

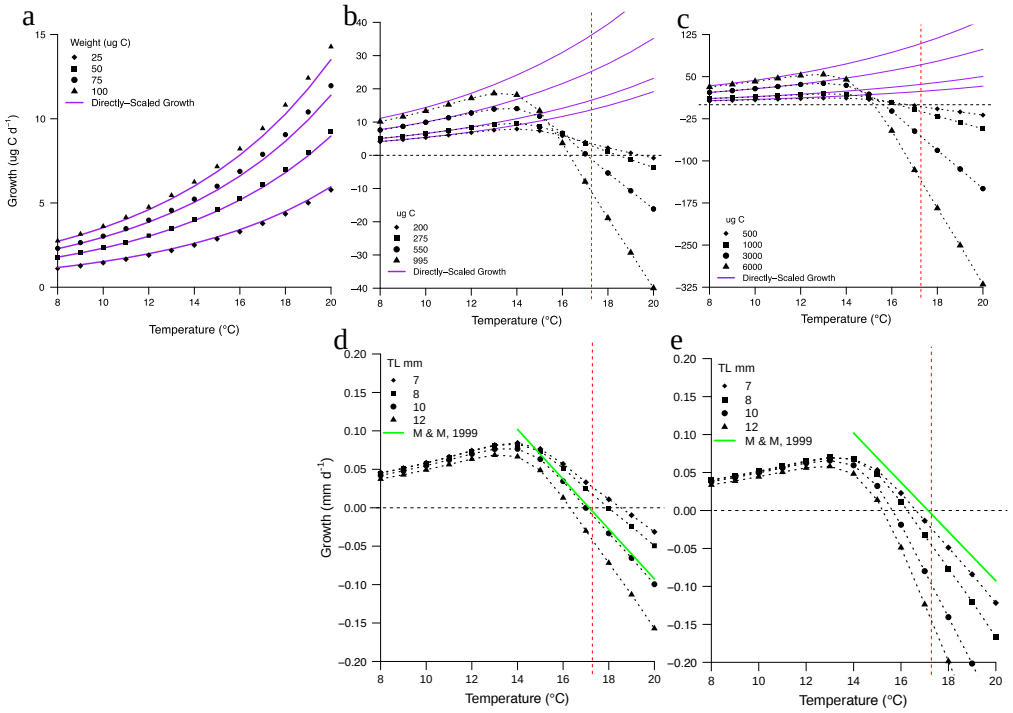

Figure 12. Growth rates (top row: µg C d^{-1}; bottom row: mm d^{-1} TL) for various sizes (see legend) of a) furcilia, b and d) juvenile, and c and e) adult life history stages based on the Base IBM (purple lines in top row) and Phase I IBM (black dashed-lines with symbols; see legend). Purple lines in top row represent empirically estimated growth rates based on measurements of growth at 8 and 12°C (Ross, 1982b; Dorman et al., 2015). Solid green line in bottom row represents estimate of negative growth rates for the average size krill (10 mm) used in Marinovic and Mangel, 1999. Vertical red-dashed line indicates observed transition to negative growth at 17.28°C (Marinovic and Mangel, 1999). Horizontal dashed-line at zero for reference.

Development

Immature stages

Development of immature stages is defined by a Bělehrádek function developed by Lindsey (2013) for *E. pacifica*. The Bělehrádek model predicts stage duration as a function of temperature (Bělehrádek, 1930). The Bělehrádek model Lindsey (2013) developed is based on empirical data of *E. pacifica* development rates from Ross (1981)

and Feinberg et al. (2006) (Figure 13). Progression to the subsequent life history stage is determined by equation 14:

$$Duration_i = a_{Dur,i}(T + B)^{c_{Dur}} \quad (14)$$

where $Duration_i$ is the duration of stage i in days, $a_{Dur,i}$ is an empirically determined stage-specific constant which defines the initial functional slope (day °C^{-1}; Table C1), T is temperature in °C, B is a stage-independent temperature shift specific to *E. pacifica* (15.052 °C), and c_{Dur} is an empirically derived constant that determines curvature (here, c_{Dur} = -2.05).

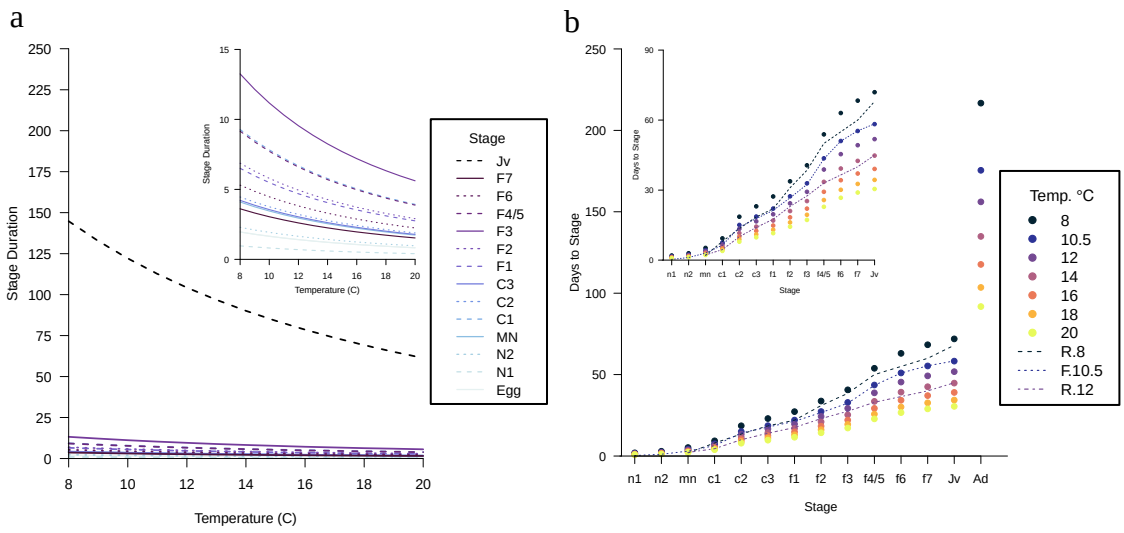

Figure 13. Bělehrádek function for development of *E. pacifica* (development to juvenile stage was reproduced using Lindsey's (2013) Bělehrádek function). a) Stage duration (days) versus temperature. Stage indicated by color (see legend). Inset depicts stage duration of eggs through F7 furcilia. b) Days to stage (development time) versus stage at various temperatures (see legend). R.8 and R.12 indicate empirical observations at 8 and 12°C, respectively (Ross, 1981; Ross, 1982b). F.10.5 indicates empirical observation at 10.5°C (Feinberg et al., 2006). Inset depicts development time for the N1 nauplius through juvenile stage.

Maturation

Both Lindsey (2013) and Dorman et al. (2015) implement maturation using invariant weight-based maturation rules (e.g., maturity occurs once an individual reaches 1500 µg C). To accommodate variability in size-at-maturation (as was observed in Robertson and Bjorkstedt, 2020), I defined a schedule of maturation by extending the Bělehrádek function developed by Lindsey (2013). To include an estimate for juvenile stage duration, and thus a temperature-dependent schedule for maturation, I estimated juvenile stage duration from data in Ross (1982b) and field observations (Harvey et al., 2010; Shaw et al., 2021). I retained the value for the curvature coefficient used by

Lindsey (2013) but generated new estimates for $B_{juvenile}$ and $a_{Dur,}$juvenile. The coefficients for juvenile stage duration ($a_{Dur,juvenile}$ = 9.0*10^4, $B_{juvenile}$ = 8, c = -2.05) generate a schedule of development within the range of estimates from laboratory and field-based experiments (Figure 13; Ross; 1982b; Harvey et al., 2010; Shaw et al., 2021).

Maximum Size

Rather than implement an invariant weight limit on maximum adult size (as in Dorman et al., 2015), maximum weight of adults was constrained using a linear model that predicted maximum size as a function of minimum size-at-maturity. A linear model was fit to minimum size-at-maturity (10^{th} quantile) data from THL samples collected at station TH03 – TH05 from 2008 to 2020 (Figure 14; for comprehensive sampling and processing methods see Robertson and Bjorkstedt, 2020). Model individuals were allowed to exceed the predicted size by 50% up to a maximum size of around 20 mm body length (25 mm total length; 10,750 µg C), the maximum size attained by *E. pacifica* (Brinton et al., 1999).

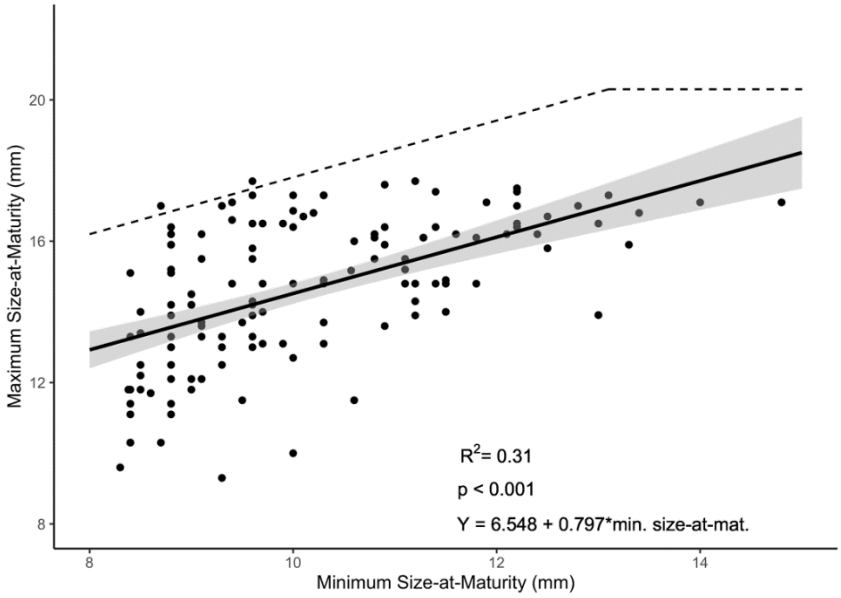

Figure 14. Maximum versus minimum size-at-maturity (BL; mm). Linear model fit to THL data (black solid line, gray = 95% confidence interval). Dashed-line indicates maximum size cap implemented in the IBM as a function of minimum size-at-maturity.

Mortality

Starvation

Starvation-induced mortality is not possible until an individual reaches the second calyptopis stage (as in Lindsey, 2013). At this stage (and subsequent stages up to the juvenile stage), an individual will die due to starvation if its weight drops below 70% of the individual's maximum weight. This starvation rule is based on the Dorman et al., (2015) IBM and is consistent with findings that indicate a 'point-of-no return' threshold of 20-35% carbon loss in crustacean larvae (Anger and Dawirs, 1981; Dawirs, 1983; Dawirs, 1987). Lower point-of-no return thresholds (~50% body carbon loss) have been observed for larval stages of *E. superba* (Meyer and Oettl, 2005). However, *E. superba*, which experience extreme variability in food abundance in the Antarctic, are likely more

resistant to starvation than *E. pacifica,* which inhabit a more food-rich environment (Quentin and Ross, 1991). Therefore, as in Dorman et al., (2015), a conservative starvation value of 30% body carbon loss was selected.

Once an individual reaches the juvenile stage, death by starvation occurs only if a juvenile or adult's weight falls below the minimum weight observed for these stages, 20 and 90 µg C, respectively. This generous starvation rule allows for considerable shrinkage (e.g., as an overwintering strategy or in response to unfavorable conditions) by accommodating adaptation to a smaller size and is consistent with observations of shrinkage in juvenile and adult krill (Marinovic and Mangel, 1999).

Lifespan

The simulation of individual growth and development is terminated once an individual reaches two years of age. This lifespan is based on estimates from observations of *E. pacifica* in the California Current (Shaw et al., 2021).

Predation

Predation mortality is not included in the IBM (e.g., as a stochastic event). Rather, predation mortality was imposed post-simulation as a size-based instantaneous mortality rate and used to weight the contribution of each cohort to the predicted size distribution at a given point in time (see 'Demographics' above).

Phase I IBM: Diagnosis

Implementation of the Phase I model brought size distributions of juvenile and adults into phase with observations, and it shifted the negative correlations between THL

observations and model output observed from the Base model to positive correlations (Figure 15). Results indicated slight improvements in the resolution of size distributions across furcilia stages but seasonal and interannual patterns were still not well resolved. Like the Base model, modeled sizes of most furcilia stages exhibited a seasonal pattern that contrasts with field observations; model size distributions were either relatively constant (e.g., F2 furcilia) or larger in winter compared to spring and summer (e.g., F7 furcilia). Correlations indicated slight improvements in F1, F3 and F4/5 furcilia but were the same for F2 furcilia and worse for F7 furcilia.

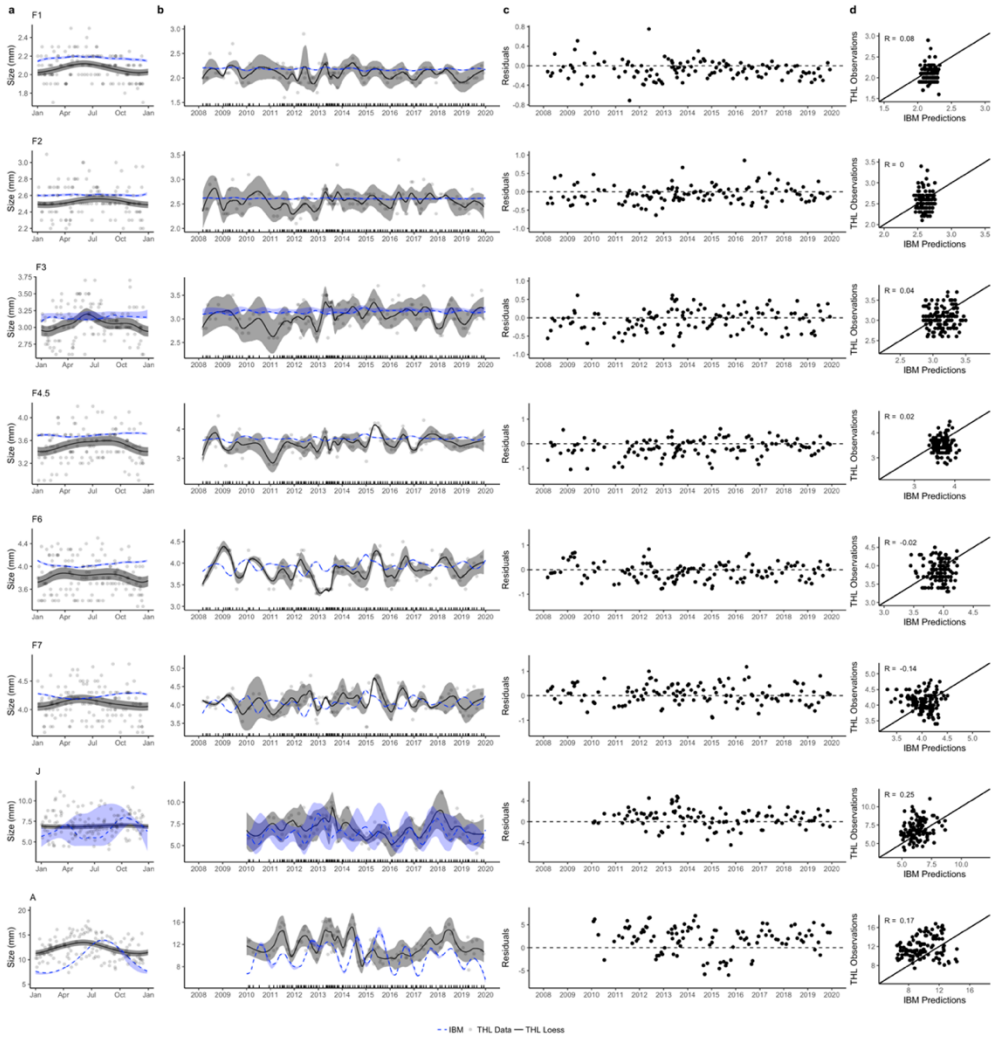

Figure 15. Stage-specific size (BL in mm; y-axis) distributions from Phase I IBM forced with a) climatologies and b) time series of temperature and chlorophyll a concentration along the THL. IBM results (blue dashed-line indicates median size; blue ribbon spans loess smooth of minimum (10^{th} quantile) and maximum (90^{th} quantile) body length) and THL data (gray points indicate median size by cruise date). THL observations in a) solid black line represents GAM fit to median size versus day-of-year, gray ribbon spans 95% confidence interval. THL observations in b) solid black line represents loess smooth of median size, gray ribbon spans ± 1 SD). c) Residuals from THL observations and IBM predictions of median size. Horizontal dashed-line at zero for reference. d) Correlation between median size of THL observations and IBM predictions. Title in top left corner of first column indicates life history stage (F1 – F7 furcilia, J = Juvenile, A = Adult) by row.

Patterns in climatological and time series scenarios indicate a major improvement in juvenile and adult size distributions. Visual inspection of patterns in size indicate model predictions are in phase with THL observations. This improvement in model-observation agreement is also reflected in correlations between observations and model predictions. However, the seasonal (spring) increase in adult size often lagged the seasonal increase observed in field data.

Phase II: Phenomenological Tuning

Following the advancements culminating in the Phase I IBM, there were no obvious mechanistic approaches likely to yield substantial improvements in model-observation agreement. Therefore, building off the Phase I model, I turned to development and evaluation of phenomenological modifications designed to explore the potential for ecosystem-based hypotheses to increase concordance between model predictions and observed patterns, with a particular focus on improving alignment at seasonal scales. Since size-at-stage reflects an integrated response to conditions over the course of an individual's life, I focused on resolving discrepancies in early life history stages prior to treatment of later life history stages.

Seasonally Variable Energetics

Individual growth rates emerge from physiological rates and exposure to environmental conditions. Published IBMs use physiological rates measured in laboratory experiments at 8 and 12 °C (Ross, 1982a; Lindsey, 2011; Dorman et al., 2015). Results from these experiments indicate that growth rate exhibits a positive relationship with

temperature. In the Dorman et al. (2015) IBM, incorporation of laboratory-based growth models generated higher growth rates during winter compared to spring and summer months. However, field observations suggest that growth rates are generally higher during spring and summer, periods typically characterized by cooler temperatures, and lower during years when delayed upwelling occurs and waters are warm (Shaw et al., 2010; Shaw et al., 2021). The cause of the discrepancy between existing growth models and field observations is not clear. At least two mechanisms might explain the observed patterns. One, enhanced nutrient concentrations and food quality during cool and productive (upwelling) seasons might enhance assimilation and growth dynamics, allowing individuals to grow more even though temperatures are relatively cool. Two, the existing bioenergetics models based on empirical data from Ross (1982a) do not account for intrinsic seasonal variability in energetics. To construct energetic expressions, Ross used data from individuals collected only in spring and summer, but noted that ingestion rates were lower in fall and winter, perhaps due to quiescent individuals (Ross, 1982b). This pattern of lower energetic rates in fall and winter months has also been observed for metabolism and ingestion of Antarctic krill, *E. superba* (Teschke et al., 2007; Piccolin et al., 2018; Höring et al., 2018). Seasonal fluctuations in euphausiid energetics have the potential to alter growth rates and size dynamics.

Implementing seasonality in euphausiid energetics has been used to advance an IBM for *E. superba* (Bahlburg et al., 2021). In the Southern Ocean, ingestion rates of Antarctic krill vary with photoperiod; during winter light conditions assimilation rates

can be as low as 36% of rates observed in summer conditions (Teschke et al., 2007). Respiration rates exhibit a similar response to photoperiod: winter light conditions correspond to significantly lower respiration rates. Bahlburg et al., (2021) accounted for seasonal variability in *E. superba* energetics by applying a day-length dependent scale factor to ingestion and metabolism submodels.

I took two approaches to incorporate variability in *E. pacifica* energetics. Both approaches are phenomenological and based on the hypothesis that euphausiid energetics vary seasonally. If this is true, accounting for seasonal variability in energetics will improve the model's ability to resolve *E. pacifica* growth and size dynamics.

Phase II IBM: Seasonal Variability in Energetics

In the Phase II approach, I generated a seasonal scale factor that is a function of day-of-year. Patterns emerging from initial attempts using a day-length-based model, as had proven useful in the Antarctic case, proved unsatisfactory, as seasonal peaks in size occurred too late in the year to align well with observations. Shifting the peak of the scale factor to better overlap with seasonal upwelling rather than day length yielded an improved fit, and is consistent with the timing of seasonal drivers of ecosystem productivity in this system (spring upwelling in the CCE v. day-length in the Antarctic). Several scale factor shapes were explored. These included factors that decreased energetic rates by 5 to 30% in winter, altered the duration of the peak in the scale factor, and lengthened the duration of the scale factor minimum in winter. I also explored unique shapes for different life history stages (e.g., F1 – F4.5 and F6 – F7 furcilia). The scale

factor presented in Figure 16 was selected because it provided a good fit between model output and observations across most life history stages (see 'Phase II IBM: Diagnosis') by resolving the timing and magnitude of seasonal fluctuations in size. The scale factor increases from January to May 1 (day-of-year = 121) and decreases from July 1 (day-of-year = 182) to December 31 (Figure 16). The peak of the scale factor falls within the window of peak climatological upwelling observed for northern California (Bograd et al., 2009). In winter, the scale factor decreases energetic rates by a maximum of 10%. Following Bahlburg et al., (2021), the energetic scale factor is applied to assimilation *and* cost components of the growth equation. Thus, the ratio between assimilation and costs remains constant. The change in growth rate reflects the balance of scaled intake and cost components in absolute, not relative, terms. This implementation is analogous to a whole-animal response; individuals are generally more active during spring and summer months and exhibit reduced activity during winter.

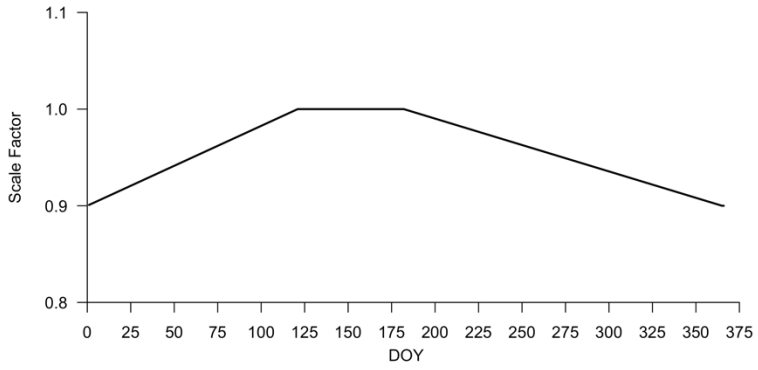

Figure 16. Day-of-year (DOY)-based scale factor applied to energetic components of feeding stage krill.

For implementation of the Phase II model, the scale factor described above was applied to energetic rates across all feeding life history stages (C1 calyptopes – adults). Growth rate of stages for which growth is calculated directly (C1 – C3 calyptopes) was scaled by applying the scale factor directly to growth rate. For F1 furcilia – adults, the scale factor was applied to assimilation and energetic costs.

Phase II IBM: Diagnosis

Scaling the energetics of feeding stages improved the match between model results and observations across furcilia stages, but degraded agreement for juvenile and adult stages (Figure 17). Specifically, the downscaling of energetic processes early in the year magnified the discrepancy between model results and observations for older stages, and especially for adults. Given the stated focus on accurately modeling adult size distributions, I retained this energetic scaling for earlier life history stages as the foundation for subsequent models, but proceeded immediately to develop models that better resolved size dynamics for juveniles and adults.

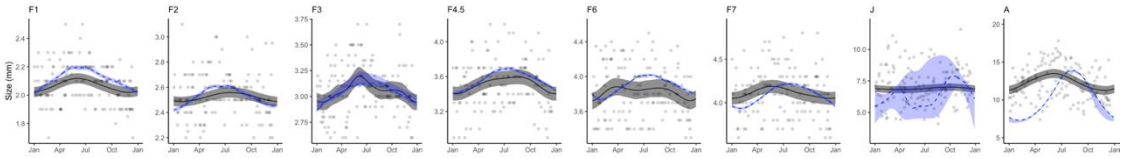

Figure 17. Size (BL in mm; y-axis) distributions from implementation of Phase II model forced with climatology of temperature and chlorophyll a concentration. IBM results (blue dashed-line indicates median size; blue ribbon spans loess smooth of minimum (10^{th} quantile) and maximum (90^{th} quantile) body length) and THL data (gray points indicate median size by cruise date; solid black line represents GAM fit to median size versus day-of-year, gray ribbon spans 95% confidence interval). Title in top left corner of each plot indicates life history stage (F1 – F7 furcilia, J = Juvenile, A = Adult).

Phase IIa IBM: (Upwelling) season-dependent energetics

To reduce the model-observation discrepancy in adult size structure during spring, I generated a second day-of-year-based scale factor to increase assimilation in adults during spring months (Figure 18). The 'spring enhancement' scale factor is based on the ecological hypothesis that assimilation is enhanced during the productive upwelling season (e.g., due to increased nutritional content of prey; Miller et al., 2017). Similar to development of the first scale factor, I explored several alternate scale factors for assimilation in adults. These included factors with a longer peak (e.g., from April to June) and a maximum value of 1.3. A scale factor that began to increase in February, peaked from April to May, and decreased until July generated a good match between model output and field observations and was consistent with the timing of physical and biogeochemical processes (e.g., upwelling, nitrate flux, phytoplankton blooms) that dominate the biological response in the CCE.

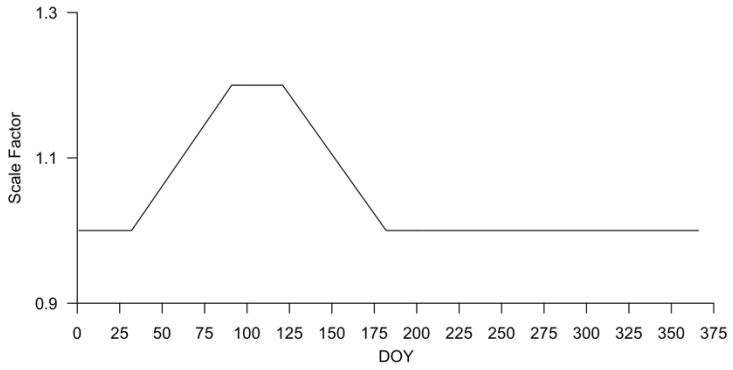

Figure 18. Day-of-year (DOY)-based, spring enhancement scale factor (y-axis) applied to assimilation rates of adults.

In the Phase IIa IBM, the first day-of-year-based scale factor (Figure 16) was applied to energetic rates in feeding stage larvae (C1 calyptopes – F7 furcilia). Since the day-of-year-based energetic scale factor did not improve resolution of juvenile size distributions in Phase II, it was not applied to juveniles in the Phase IIa model. The second 'spring enhancement' scale factor (Figure 18) was applied to assimilation in adults only.

Phase IIa IBM: Diagnosis

The Phase IIa model generates patterns in size that better match field observations (Figure 19). In general, seasonal patterns generated by the model match field observations. The model produces furcilia size distributions that are larger in spring and summer and smaller in fall and winter, in agreement with observed patterns. The increase in adult size during spring is also better resolved by the Phase IIa model. However, adult size is still underestimated in spring (Figure 20). Resolution of interannual variability improved across all life history stages. Correlations between field observations and model output improved across all life history stages. The lag in adult size during spring was apparent in several years of the time series scenario.

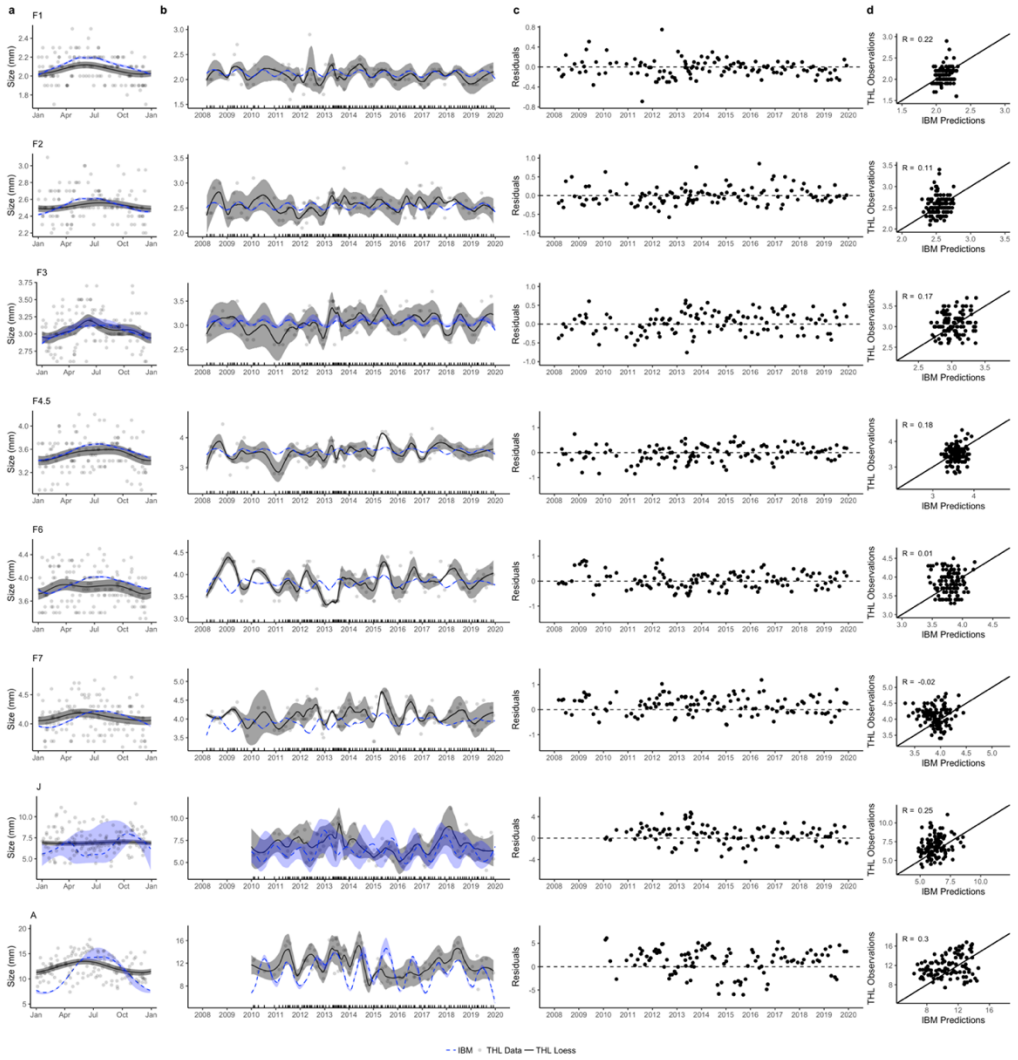

Figure 19. Stage-specific size (BL in mm; y-axis) distributions from Phase IIa IBM forced with a) climatology and b) time series of temperature and chlorophyll a concentration along the THL. IBM results (blue dashed-line indicates median size; blue ribbon spans loess smooth of minimum (10^{th} quantile) and maximum (90^{th} quantile) body length. THL observations in a) solid black line represents GAM fit to median size versus day-of-year, gray ribbon spans 95% confidence interval. THL observations in b) solid black line represents loess smooth of median size, gray ribbon spans ± 1 SD). c) Residuals from THL observations and IBM predictions of median size. Horizontal dashed-line at zero for reference. d) Correlation between median size of THL observations and IBM predictions. Title in top left corner of first column indicates life history stage (F1 – F7 furcilia, J = Juvenile, A = Adult) by row.

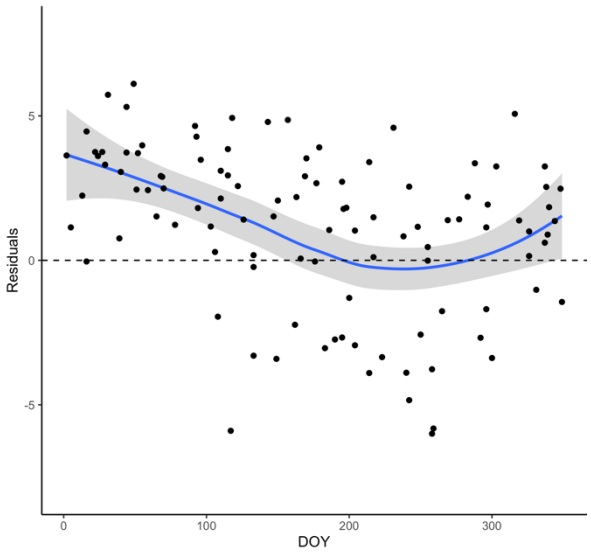

Figure 20. Residuals (y-axis) versus day-of-year (DOY; x-axis) for Phase IIa model. Loess smooth (blue line, gray ribbon spans 95% confidence interval) fit to data to highlight trend in fit between observations and model predictions.

Phase IIb IBM: Temperature-dependent adult energetics

The Phase IIb IBM incorporates a different approach to phenomenological scaling of seasonal variability in adult assimilation. Like the Phase IIa model, it builds off the core Phase II model, but instead of using a day-of-year-based scale factor nominally representative of the upwelling season, I developed a temperature-based 'upwelling' scale factor. The upwelling scale factor is a function of average temperature in the top 30 meters of the water column (Figure 21). Like the spring enhancement scale factor, this metric is a proxy for the productive upwelling season. However, the temperature-based scale factor allows for a more dynamic response by implementing enhanced assimilation during cooler conditions rather than a fixed period of time. These dynamics are consistent with greater nutrient availability and food quality during cool and productive upwelling

conditions (Miller et al., 2017). At temperatures above 12°C, the upwelling scale factor is set to one and assimilation rates are equivalent to those described above in 'Ingestion'.

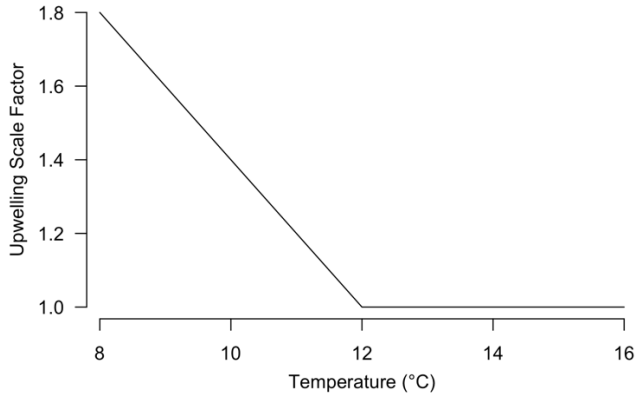

Figure 21. Temperature-dependent upwelling scale factor. Scale factor (y-axis) applied to adult assimilation rate based on average temperature in top 30 m of water.

The shape of the upwelling scale factor was based on the climatology and time series of temperature along the THL (Figure 22). Average temperature in the upper 30 meters of water tends to be coolest during the first half of the year – a period that coincides with the discrepancy in adult size. Across the time series, average temperature in the upper 30 meters spans approximately 8 to 15°C. During spring, the average temperature is typically less than 12°C. The upwelling scale factor is defined by a linear decline from a value of 1.8 to 1 over temperatures between 8 and 12°C. The resulting expression was used to obtain a temperature-dependent scale factor value (Figure 21).

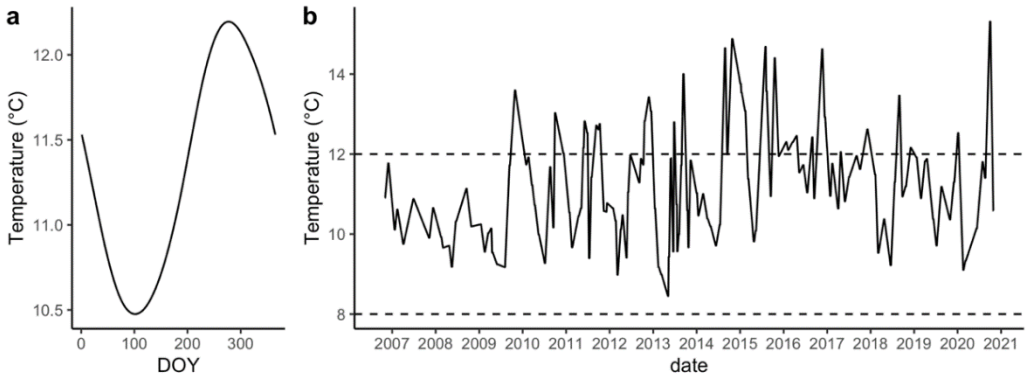

Figure 22. Temperature in the upper 30 meters at station TH04. a) Climatology (temperature versus day-of-year (DOY) and b) time series of temperature. Area between 8°C and 12°C (indicated by horizontal dashed lines) indicates range over which scale factor is not equal to one.

Since resolution of furcilia size structure was relatively well resolved in the Phase IIa model, the day-of-year-based energetic scale factor was retained for feeding larvae (C1 calyptopes – F7 furcilia). Phase I and Phase IIa models generated size distributions of juveniles that matched reasonably well with observations. The temperature-based upwelling scale factor (Figure 21) was applied to assimilation rates in adults.

Phase IIb IBM: Diagnosis

The phase IIb model does a better job at resolving seasonal and interannual variability in size distributions of adults (Figure 23). The correlation between field observations and IBM predictions of median size is substantially higher than other model versions (R = 0.48). Additionally, the RMSE for adults in the Phase IIb model is lower compared to other model versions (Table 6). Despite an improvement in predictions of adult size, size distribution still tends to be underestimated during winter and is

overestimated during a few spring/summers in the time series, most notably 2015 and 2016.

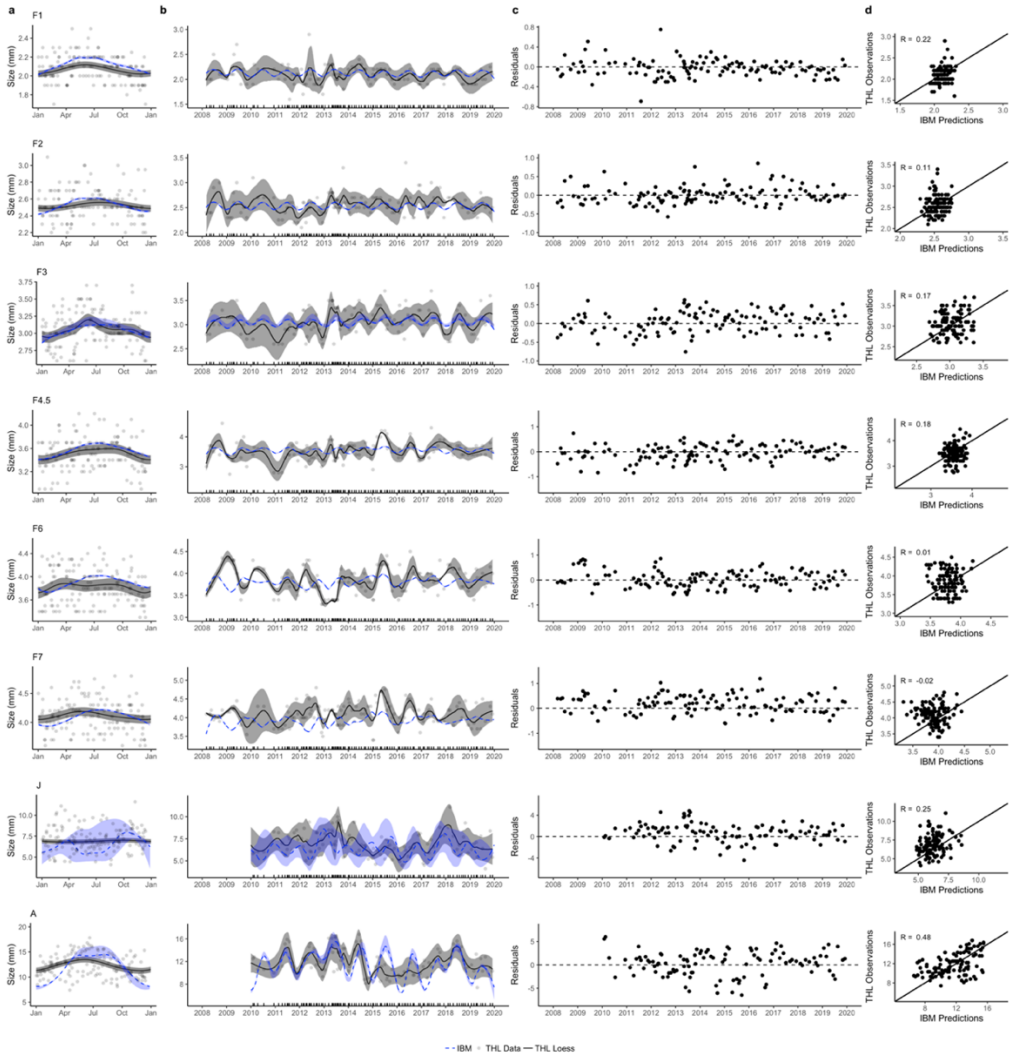

Figure 23. Stage-specific size (BL in mm; y-axis) distributions from Phase IIb IBM forced with a) climatology and b) time series of temperature and chlorophyll a concentration along the THL. IBM results (blue dashed-line indicates median size; blue ribbon spans loess smooth of minimum (10^{th} quantile) and maximum (90^{th} quantile) body length). THL observations in a) solid black line represents GAM fit to median size versus day-of-year, gray ribbon spans 95% confidence interval. THL observations in b) solid black line represents loess smooth of median size, gray ribbon spans ± 1 SD). c) Residuals from THL observations and IBM predictions of median size. Horizontal dashed-line at zero for reference. d) Correlation between median size of THL observations and IBM predictions. Title in top left corner of first column indicates life history stage (F1 – F7 furcilia, J = Juvenile, A = Adult) by row.

Table 6. Root-mean square error for select IBM versions across F1 – F7 furcilia, juvenile (Jv), and adult (Ad) life history stages.

Model Version	F1	F2	F3	F4.5	F6	F7	Jv	Ad
Base	0.265	0.278	0.319	0.440	0.482	0.370	2.327	3.309
Phase I	0.203	0.244	0.304	0.379	0.351	0.398	1.524	3.280
Phase IIa	0.181	0.234	0.286	0.322	0.333	0.408	1.544	2.778
Phase IIb	0.181	0.234	0.286	0.322	0.333	0.408	1.544	2.346

A comparison of correlations between observations and model output for adults during spring in the Phase IIa versus Phase IIb model confirms the temperature-based scale factor improved resolution of adult size distributions (Figure 24).

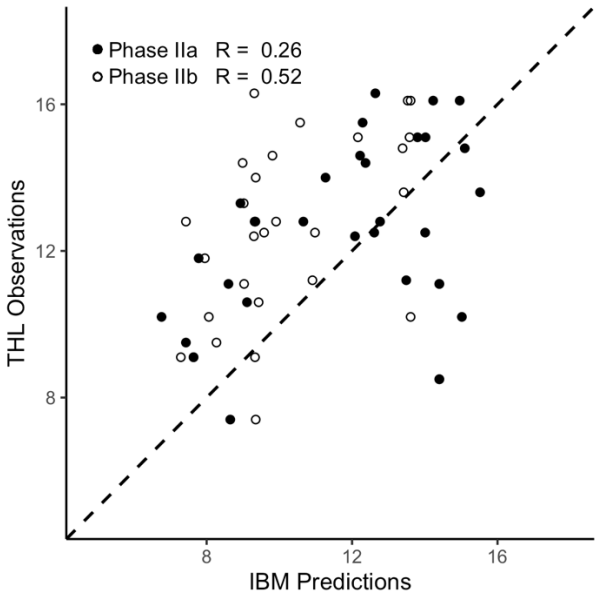

Figure 24. Comparison of correlations between observations (BL in mm; y-axis) and model output (BL in mm; x-axis) for adults during spring in the Phase IIa (closed circles) versus Phase IIb (open circles) models. Correlation (R) values noted in legend.

I also explored an alternative migration strategy that implemented migration to the depth at which maximum growth occurred. This version generated similar size dynamics and growth trajectories compared with the model that implements DVM to the maximum chlorophyll depth. Correlations between an individual's depth, temperature, and chlorophyll exposure in these two iterations of the Phase IIb model reflected similar environmental exposure throughout an individual's life (R_{depth} = 0.94, $R_{temperature}$ = 0.96, $R_{chlorophyll}$ = 0.98). The 'maximum growth' version did not improve resolution of adult size structure and was excluded from the set of models selected for presentation.

Incorporating a temperature-dependent Q_{10} for adult and juvenile ingestion resulted in a trivial improvement in model performance. Size distributions from

climatological and time series scenarios were indistinguishable between the Phase IIb model with and without this modification (not shown). The RMSE is slightly lower for juveniles and adults in the model version that incorporates a temperature-dependent Q_{10} compared to the model version that does not (1.544 versus 1.551 for juveniles and 2.346 versus 2.364 for adults). The model version that incorporates a temperature-dependent Q_{10} also produces effectively equal correlations between observed and predicted size of juveniles and adults compared to the model version that did not incorporate this modification (0.25 versus 0.24 for juveniles and 0.48 versus 0.47 for adult).

Summary of model development

Model development built upon a 'Base' version that implemented growth and development using a phenomenological approach (following Dorman et al., 2015). In the first phase of model development, existing empirical data were reanalyzed and observed relationships (i.e., the tendency for adults and juveniles to shrink at high temperatures and variability in size-at-maturity) were incorporated. In the second phase of model development, the IBM framework from Phase I was expanded by incorporating phenomenological scaling of energetics (Table 7).

Table 7. Model descriptions for select versions of the IBM created during model development. Italicized font in 'Brief Description' column indicates key change to model version.

Model Version	Brief Description	Environmental Input	day-of-year 'Energetic' Scale Factor	day-of-year 'Spring Enhancement' Scale Factor	Temperature 'Upwelling'' Scale Factor	Egg Size (µg C)	Food at Depth
Base	Directly-scaled growth following Dorman et al. (2015). Development implemented with weight thresholds (Table 1). At night, migrating stages are positioned at depth where max. chlorophyll occurs.	Egg – F2 = mean (10 m to stage specific depth) F3 - Adults = stage specific depths & DVM to maximum chl. depth	No	No	No	2.58	Chl. a at depth of individual
Phase I	Mechanistic model (growth = assimilation - metabolism - molt -reproduction). Development implemented with temperature-dependent function with extension for maturation.	As in Base	No	No	No	3.2	Chl. a at depth or 0.30*max. chl. a, whichever is greater
Phase IIa	Energetic scale factor applied to feeding larvae (C1 calyptopes- F7 furcilia). Spring enhancement scale factor applied to adults.	As in Base	Yes, feeding larvae (Figure 16)	Yes (Figure 18)	No	As in Phase I	As in Phase I
Phase IIb	Upwelling scale factor applied to adults.	As in Base	Yes, as in Phase II	No	Yes (Figure 21)	As in Phase I	As in Phase I

In general, Base and Phase I model versions do a poor job resolving realistic patterns in *E. pacifica* size distributions (Figure 7 and Figure 15). Model versions that incorporate seasonal scaling of energetics perform better and resolve realistic size distributions across most life history stages. Size distributions of F6 and F7 furcilia are poorly resolved in all model versions.

The Phase IIb model, which included an energetic scale factor for larvae, a temperature-dependent scale factor for assimilation in adults, and a temperature-dependent Q_{10} for ingestion in juveniles and adults, produced the lowest RMSE and highest correlation between observations and model predictions (Figure 23 and Table 6). This model also resolved reasonable variability in climatological and time series scenarios. As such, the Phase IIb model was selected as the 'top' model and is analyzed in subsequent sections. The top model is summarized and presented in Figure 25. A complete description of the top model, following the Overview, Design, and Details protocol for describing individual-based models can be found in Appendix D (Grimm et al., 2006; Grimm et al., 2020).

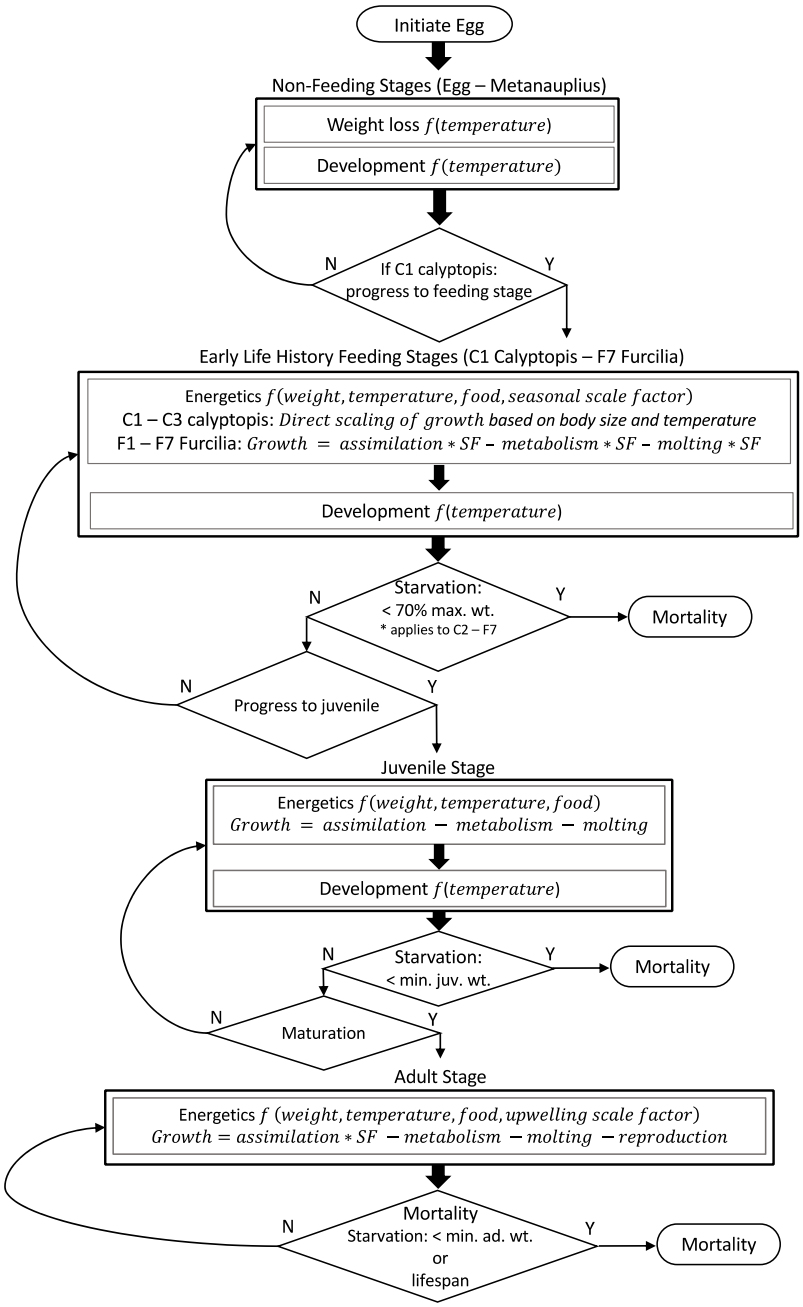

Figure 25. Flow diagram of the final model, including energetics and development submodels for non-feeding larvae, calyptopes, furcilia, juveniles, and adults. Stage transitions within composite groups (e.g., early life history stages) are subsumed in boxes for compactness. Criteria for stage transitions is determined by the temperature-dependent Bělehrádek function (see 'Development'). SF = scale factor.

Analysis of Top Model

I calculated growth, maturation, and reproductive rates for the top model and compared them to patterns observed in field. I generated daily growth rates from model output by calculating the difference between the start and end size of a particular stage on a single day. When rates did not span a full 24 hours (e.g., if transition to the next stage occurred during the 24-hour period), the growth rate was extrapolated to a full daily rate. Unless noted otherwise, growth rates are presented in mm TL d^{-1} to facilitate comparison with the literature (e.g., Shaw et al., 2010). Time to maturation represents development time (in days) from egg to the adult stage. Reproductive effort is presented as eggs per day per krill. This value was calculated by dividing the mean daily weight (in carbon) allocated to reproduction by the size of an egg (3.2 µg C). Values for minimum (10^{th} quantile), median, and maximum (90^{th} quantile) eggs per day per krill were calculated using weighted model output (as described in 'Demographics').

Growth Rates

Adult and juvenile growth rates tended to follow a seasonal pattern driven by environmental input and seasonal scale factors; lower growth rates occurred in fall or winter months and higher growth rates occurred during spring or summer months (Figure 26). The daily median adult growth rate (averaged by month for each year of the time series simulation) ranged from -0.18 (± 0.02 SD) to 0.18 (± 0.05 SD) mm TL d^{-1}. These changes translate to -1.31 to 1.39% relative to body size. Positive growth was more likely to occur during spring and summer months. Negative growth occurred 50% of the time and in all years throughout the simulation, typically during the latter half of the year. At

the individual level, minimum and maximum growth rates ranged from -0.32 mm d^{-1} to 0.42 mm d^{-1}, respectively.

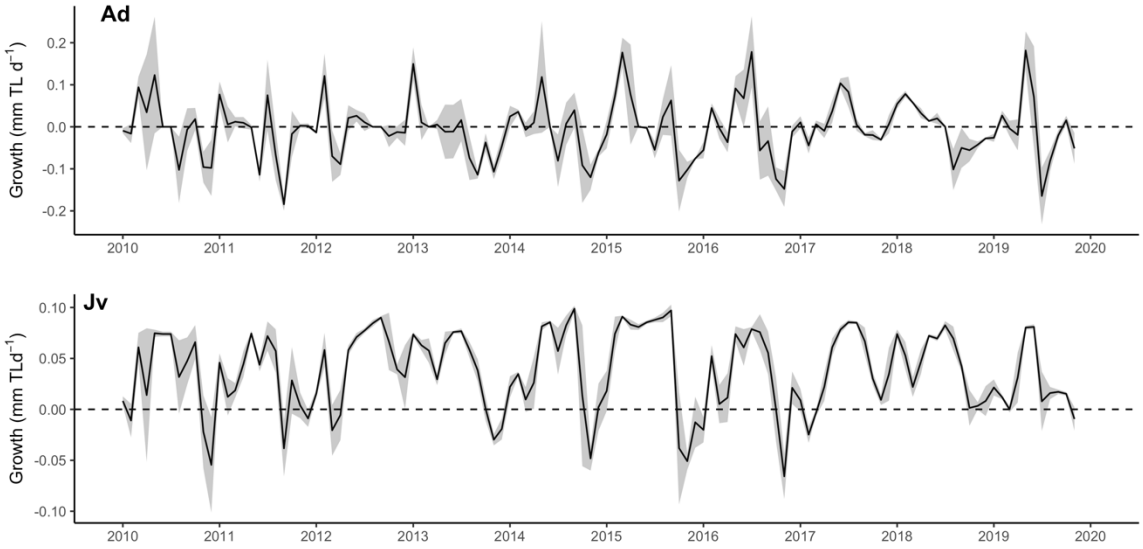

Figure 26. Daily median growth rate (y-axis; mm TL d^{-1}) averaged by month across 2010 - 2020 for adults (top) and juveniles (bottom). Gray ribbon indicates ± one standard deviation. Horizontal dashed-line at zero for reference.

Juvenile growth rates were generally lower than adults; the daily median growth rate (averaged by month for each year of the time series simulation) ranged from -0.07 (± 0.02 SD) to 0.10 (± 0.003 SD) mm TL d^{-1} (Figure 26). These changes translate to -0.72 to 1.33% relative to body size. Positive growth rates occurred throughout the year. Negative growth rates were observed less frequently than adults, occurring 9% of the time, typically during winter months. Negative growth rates did not occur during 2012, 2013, and 2018. Minimum and maximum growth rates of individuals ranged from -0.22 mm d^{-1} 0.12 mm d^{-1}, respectively.

Periods with larger adult size distributions (e.g., 2013 and 2018) tended to coincide with and follow years characterized by less severe negative growth in juvenile and adults. Similarly, larger juvenile size distribution in (e.g., in 2012/13 and 2017/18) coincided with low occurrence of negative growth.

In general, furcilia growth rates were lower than juvenile and adult growth rates (Figure 27). In contrast with juveniles and adults, growth rates tended to be highest in the fall and lowest during spring and summer. Negative growth rates (from monthly averages of median size) were not observed in F1 through F4/5 furcilia stages, but were observed in F6 – F7 Furcilia, typically during spring and summer months. At the individual level, negative growth rates were observed in F3 – F7 furcilia (Figure 27). The magnitude of negative growth increased with ontogeny.

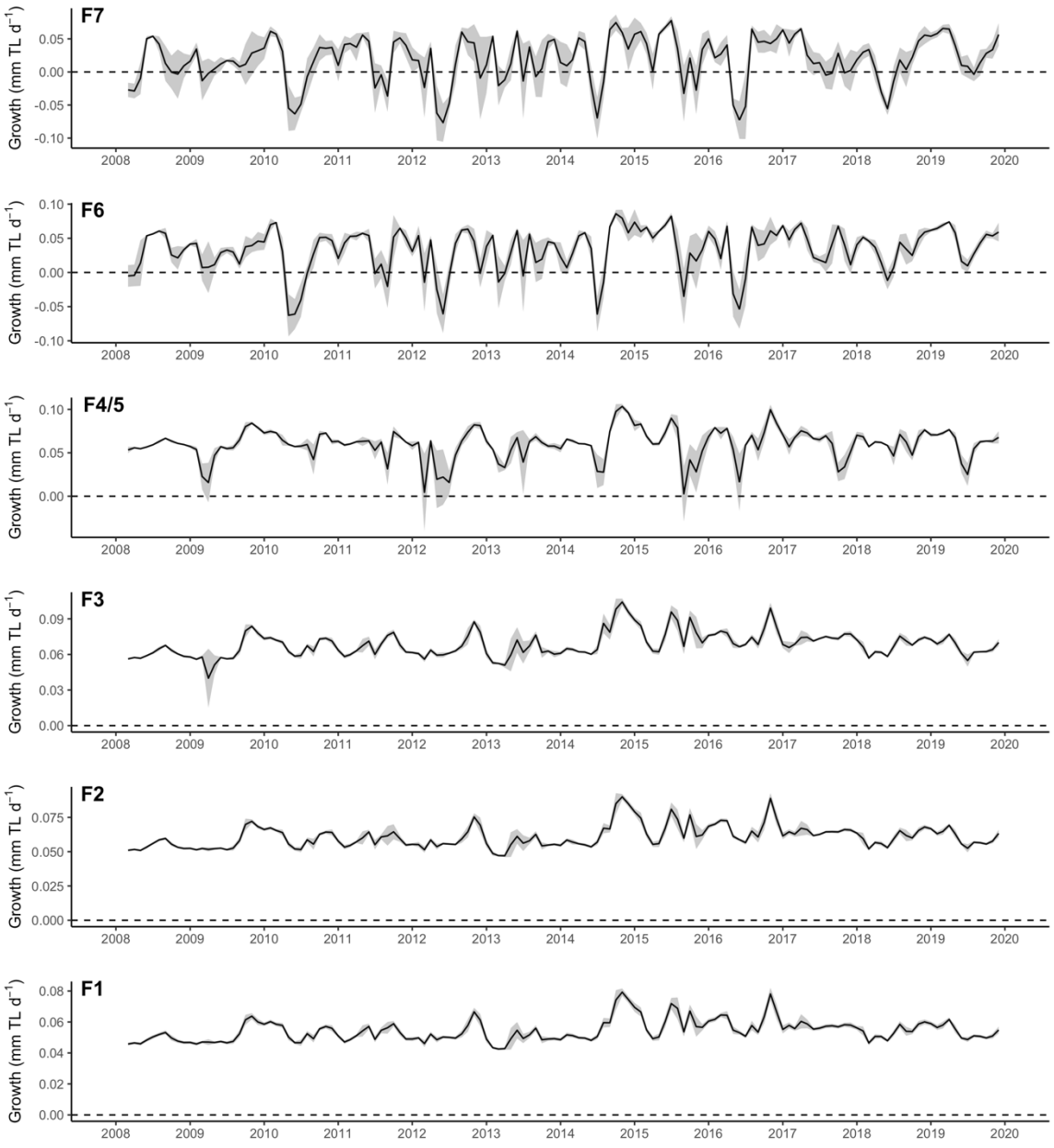

Figure 27. Daily median growth rate (y-axis; mm TL d^{-1}) averaged by month from March 2008 to January 2020 for F1 – F7 furcilia (noted in top left corner of each plot). Gray ribbon indicates ± one standard deviation. Horizontal dashed-line at zero for reference.

Table 8. Range of individual growth rates (mm TL d^{-1}) observed for F1 – F7 furcilia, juveniles, and adult stages.

Stage	Minimum	Date	Maximum	Date
F1 furcilia	0.04	06-May-2013	0.09	27-Oct-2014
F2 furcilia	0.04	08-May-2013	0.10	19-Nov-2016
F3 furcilia	-0.02	22-Apr-2009	0.11	30-Oct-2014
F4/5 furcilia	-0.07	17-Sep-2015	0.11	27-Oct-2014
F6 furcilia	-0.14	06-Mar-2012	0.11	14-Nov-2014
F7 furcilia	-0.14	20-May-2012	0.10	17-Dec-2014
Juvenile	-0.22	18-Aug-2010	0.12	15-Sep-2014
Adult	-0.32	07-Jul-2010	0.42	07-Sep-2010

Maturation and Reproduction

Development time from egg to adult ranged from 153 to 204.5 days (Figure 28a). These values fall within the range of field-based estimates (see 'Discussion'). The effect of the temperature-dependent Bělehrádek function is evident in the relationship between thermal exposure and maturation times; longer maturation times tended to correspond with cooler conditions over the lifetime of the krill while shorter maturation times corresponded to warmer conditions over the lifetime of the krill. Krill born in late September 2014 had the shortest maturation time and matured in early 2015. Krill born in early February 2013 had the longest maturation time and matured in late August 2013. As expected, body length at maturation was reduced for individuals that experienced warmer conditions (Figure 28b and d). However, individuals that experienced cooler temperatures

matured at various sizes from relatively small (~6 mm BL) to relatively large body size (~12 mm BL). Chlorophyll a exposure tended to have a positive effect on size-at-maturity; individuals exposed to low concentrations of chlorophyll a over the course of their life tended to mature at smaller sizes while larger size-at-maturation tended to correspond with exposure to greater chlorophyll a concentrations (Figure 28c and d).

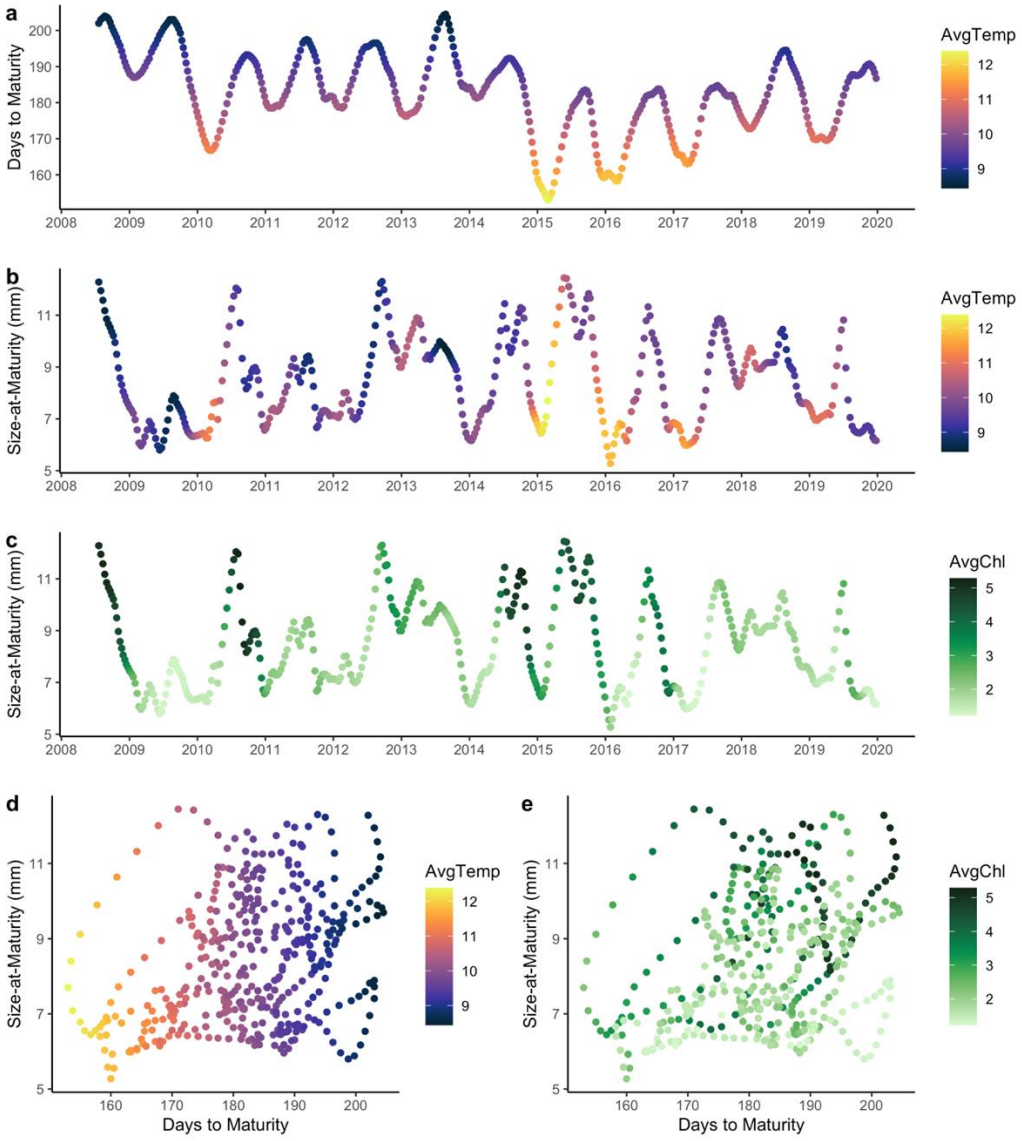

Figure 28. Maturation results from the top IBM. a) Days to maturation by date. Points are filled with the cumulative average temperature from egg to adult (see legend); b) Size-at-maturity (BL; mm) by date, point color as in a; c) Size-at-maturity by date. Points are filled with the cumulative average chlorophyll from egg to adult (see legend); d and e) Size-at maturity versus time (days) to maturity. Points filled with average temperature (d; see legend) and chlorophyll (e; see legend).

In general, the smallest individuals at maturity experienced warm conditions and low food availability (Figure 28d and e). In contrast, the largest individuals at maturity experienced cool to moderate thermal conditions and moderate to high chlorophyll a concentration. The smallest size-at-maturation (5.27 mm BL) occurred in early 2016, which corresponded with a relatively warm thermal exposure history (11.8 °C) and low chlorophyll a concentration (2.0 mg L^{-1}; Figure 28b and c). In contrast, the largest size at maturation (12.44 mm BL) occurred in May 2015 and corresponded with moderately warm thermal exposure history (10.6 °C) and higher chlorophyll a concentration (4.26 mg L^{-1}).

Field observations of size-at-maturity (indexed by 10^{th} quantile) were positively correlated with size-at-maturity in the IBM (R = 0.30; Figure 29).

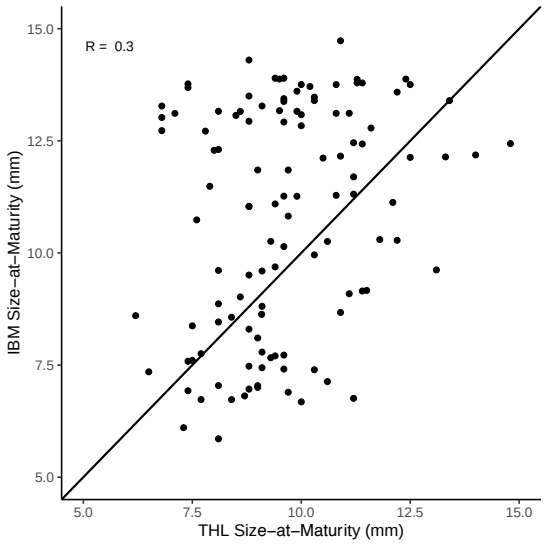

Figure 29. Size-at-maturity (BL; mm) from IBM output (y-axis) and THL observations (as indexed by the 10th quantile; x-axis). Diagonal line at 1:1 relationship for reference.

Per capita reproductive output exhibited a clear seasonal pattern. Allocation to reproduction is greatest during the summer months and declines in fall and winter months (Figure 30). Interannual variability in reproductive effort is apparent but is muted compared to seasonal fluctuations. Average reproductive output was greatest in 2013, maximum egg production peaked in March (85 eggs d^{-1} $krill^{-1}$) while median egg production peaked in August (56 egg d^{-1} $krill^{-1}$). Reproductive effort was lowest in January 2010 (1 egg d^{-1} $krill^{-1}$). The duration of reproductive "peaks" appears to have been longer from 2010 through 2015 compared to more confined peaks of reproduction during 2016, 2017, and 2019. Years with a longer period of elevated egg production (e.g., 2010-2013) tended to generate a larger number of total eggs compared to years with greater absolute production but shorter seasons (e.g., 2016).

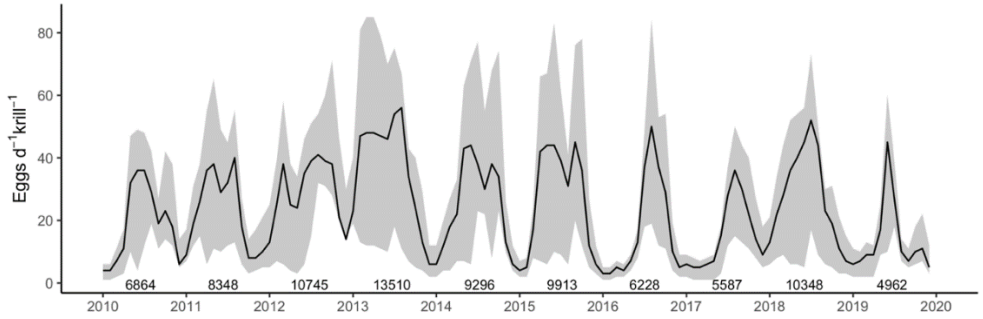

Figure 30. Reproductive effort (eggs d^{-1} $krill^{-1}$; y-axis) averaged by month from 2010 to 2020. Black line represents median reproductive effort, gray ribbon spans minimum (10th quantile) and maximum (90th quantile) reproductive effort. Numbers between year labels indicate the total of average eggs $krill^{-1}$ $year^{-1}$.

Brood size of individual krill was directly related to body size and ranged from 4 to 229 eggs $female^{-1}$ (Figure 31). The upper limit of the brood size-body size relationship

indicates exposure to optimal conditions; the spread below this limit is due to less favorable conditions. The minimum size krill producing a brood was approximately 7 mm (TL).

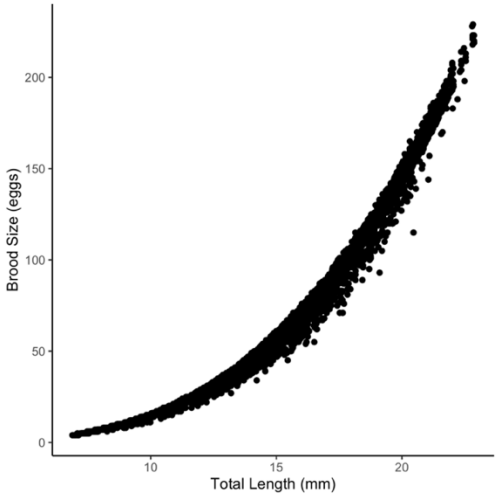

Figure 31. Brood size (eggs) versus total length (mm) of individual krill from the time series scenario of the top model.

Sensitivity Analysis

I also evaluated the sensitivity of output (i.e., size) from the top model to variation in key energetic components and environmental conditions. Rather than conduct a sensitivity analysis for each energetic parameter, I focused on sensitivity of output to variability in energetic rates. To do this, I altered ingestion, metabolism, molting, and reproductive rates by ± 10%. In each sensitivity simulation, a change to only one energetic component was implemented. Because growth is modeled as the balance of intake and costs, a change to an energetic component affected the amount of surplus energy available for growth, but did not have an immediate effect on other energetic components. For example, a 10% increase in metabolism decreased the amount of energy

(carbon) available for growth by metabolic rate*0.10. Similarly, a 10% increase in ingestion increased the amount of surplus energy available for growth.

Temperature and chlorophyll are generally correlated in upwelling systems. As context for differentiating the relative contribution of changes in temperature and food to krill size, model results were developed for a cross-factorial array of temperature (±1°C) and food offsets (± 20% chlorophyll a concentration) from seasonal climatology. Results from sensitivity analyses are presented as change in size; or the difference between body length generated by each simulation and body length generated by the un-altered climatological simulation.

Model Sensitivity: Energetics

Sensitivity analyses examining the effect of changes in key energetic components indicated diverse responses to changes in ingestion, metabolism, molt, and reproductive rates (Figure 32). Across all life history stages, changes to ingestion rate had the greatest effect on size. The magnitude of change was greatest in juvenile and adult stages, though this reflects (at least in part) a cumulative response to change in ingestion over the course of an individual's life. Changes to metabolic rate had a considerable, though smaller, effect on size. Across furcilia stages, the change in size in response to changes in ingestion and metabolism was relatively constant throughout the year. Juveniles and adults exhibited a greater response in spring and fall. Changes in molt rate were nearly inconsequential to size distributions. Similarly, changes in reproduction rate had a small effect on adult size distributions.

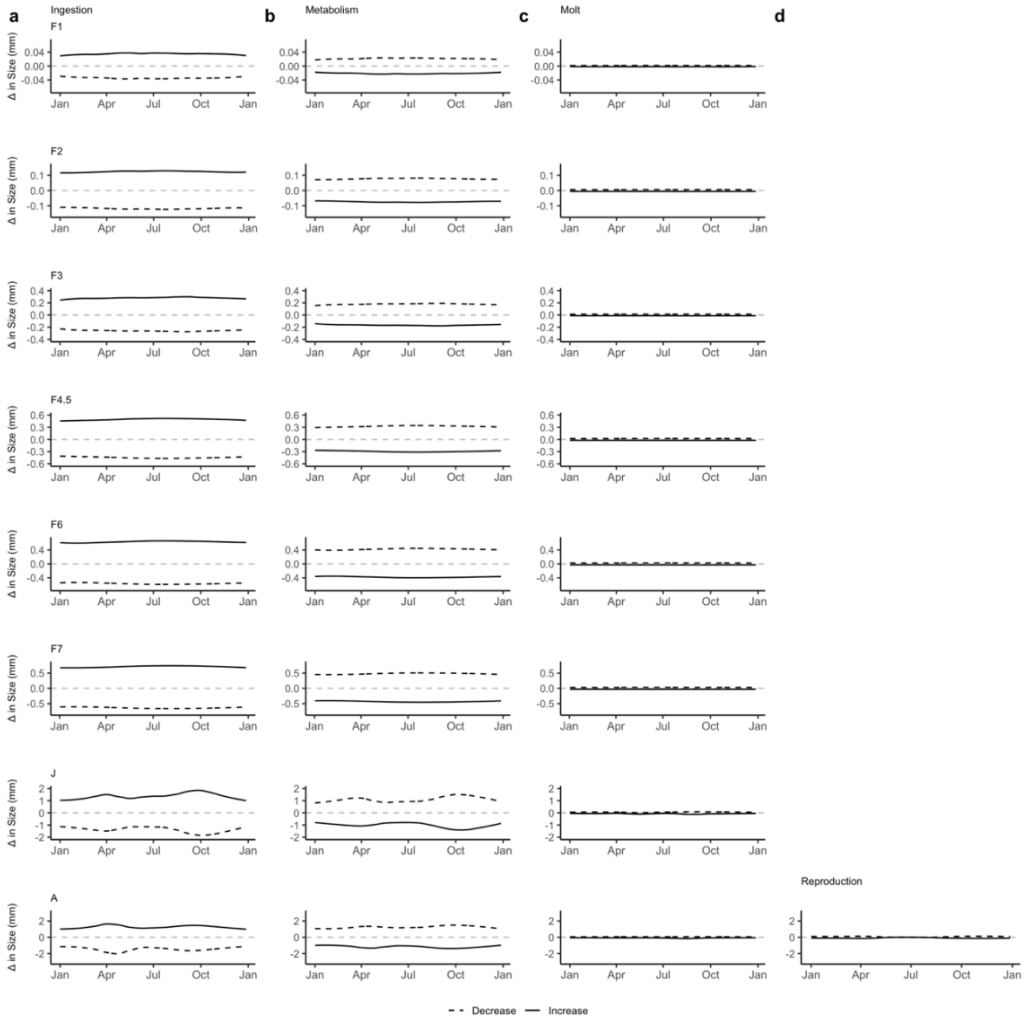

Figure 32. Results from simulations examining sensitivity of model output (size; y-axis) to changes (± 10%; see legend) in key energetic components. a) ingestion, b) metabolism, c) molt, and d) reproductive rate by stage (F1 – F7 furcilia, J = juvenile, A = adult). Note: y-axis scale varies with life history stage.

Model Sensitivity: Environmental Response

Like sensitivity analyses examining the effect of key energetic components, the effect of changes in environmental conditions represents a cumulative response over the course of an individual's life. Sensitivity to environmental conditions varied across life history stages (Figure 33). Changes in chlorophyll had little to no effect on the size of

furcilia stages (not shown). This pattern was consistent across scenarios, including those where temperature was also altered. F6 and F7 furcilia stages exhibited a weak response to variability in chlorophyll; decreased chlorophyll resulted in a slight shift to smaller size structure. In contrast, temperature had a marked effect across furcilia stages. In general, early furcilia stages exhibited a contrasting response to later furcilia stages. F1 and F2 furcilia tended to be smaller (larger) in response to increased (decreased) temperature whereas F3 – F7 furcilia tended to be larger (smaller) in response to increased (decreased) temperature.

Juvenile and adult stages exhibited a clear response to changes in chlorophyll and temperature. In general, decreased (increased) chlorophyll generated smaller (larger) size structure. Changes in chlorophyll seemed to have a greater effect on size during winter months compared to spring and summer months. Except for the scenario where temperature and chlorophyll were reduced, decreased temperature resulted in larger size structure during the spring compared to climatological results. In the case of juveniles, increased temperature resulted in larger size structure during late winter and fall, though the effect was greater when chlorophyll was also increased. Increased temperature resulted in smaller size structure during spring and winter months. In general, adult size tended to be larger (smaller) with decreased (increased) temperature. However, the magnitude of the response varied seasonally; reduced temperature generated larger size structure in adults, particularly during winter months. In contrast, increased temperature generated smaller size structure in adults, particularly during spring months.

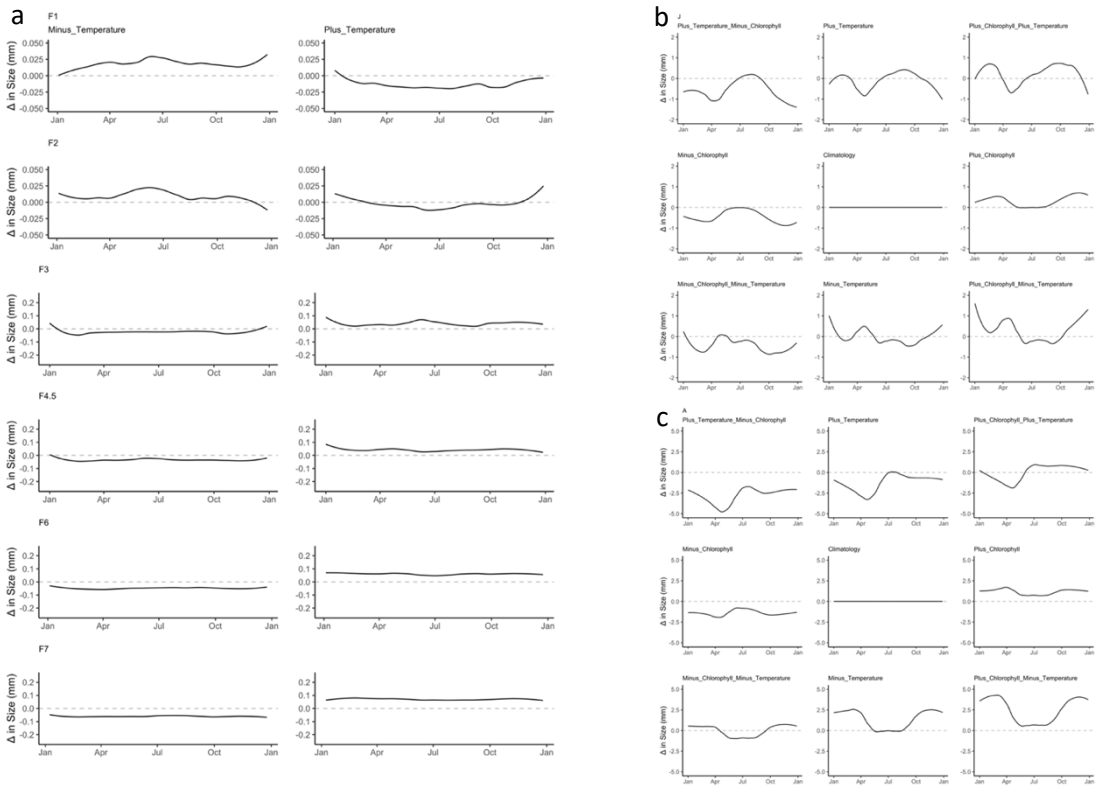

Figure 33. Results from simulations examining sensitivity to environmental input. Size of a) furcilia, b) juvenile, and c) adult stages. Title (top left plot) indicates life history stage (F1 – F7 furcilia, J = Juvenile, A = Adult). Subtitle (top left corner of each plot) indicates environmental conditions. Scenarios include combinations of temperature ± 1°C and ± 20% chlorophyll a concentration (see plot subtitles). Black lines represent the difference between body length (mm) of each model scenario versus the scenario forced with THL climatology data ($BL_{scenario}$ - $BL_{climatology}$). Dashed gray line at zero to facilitate interpretation of results.

DISCUSSION

IBMs are powerful tools for exploring how behavior and ecological interactions define individuals' fates and, in aggregate, yield emergent dynamics at the population level. However, the utility of IBMs depends on the fidelity with which the rules and mechanisms that constitute the model reflect reality. In this thesis, I use a pattern-oriented modeling approach to advance an IBM's ability to produce growth and size dynamics of *E. pacifica* in the northern California Current Ecosystem, thereby strengthening the foundation for such models to serve as tools for broader examination of ecosystem dynamics.

The model I developed incorporates three key modifications to previously published IBMs. These modifications were implemented in two phases of development. The first phase incorporated two of the modifications: improved estimates of temperature-dependent energetic parameters and extension of temperature-dependent development to maturation. The second phase incorporated the third modification—seasonal variability in energetics, including assimilation in adults. The first modification is a robust enhancement of realistic mechanisms. The second and third modifications are phenomenological extensions grounded in plausible links between environmental conditions and *E. pacifica* physiology, yet lack a detailed empirical or mechanistic basis.

Contribution of Model Revisions to Improved Realism

Overall, the iterative, pattern-oriented approach led to substantial improvement in resolution of realistic size and production dynamics. Improved agreement between model

predictions and observed size distributions was grounded in the re-analysis of available empirical data and subsequent revision of fundamental physiological submodels that make up the core of the IBM. These modifications and the extension of temperature-dependent development to adults brought model size distributions of juveniles and adults into phase with observations. Although the first phase of model development did not yield full improvement across life history stages, this step represents a major and essential advancement as it brings the IBM into agreement with observed relationships.

In the second phase of model development, remaining discrepancies between model-generated size distributions and observations were improved by tuning energetic submodels. Furcilia size distributions were brought into agreement with observations by implementing day-of-year-based seasonal variability in energetic rates. The emerging patterns are consistent with our observations indicating larger size distributions in spring and summer and smaller size distributions in fall and winter (Robertson and Bjorkstedt, 2020). Application of this scale factor to energetic rates in later life history stages did not improve discrepancies. Instead, underestimation of adult size distributions during spring was improved by implementing a scale factor for assimilation in adults. This modification was based on the hypothesis that improved prey quality or forage conditions during the productive upwelling season result in enhanced assimilation and larger size distributions and is supported by research indicating higher lipid content in phytoplankton during the cool, upwelling season and observations of greater growth rates during upwelling conditions (Shaw et al., 2010; Miller et al., 2017). The enhanced

flexibility of a temperature-based scale factor resulted in greater agreement between model output and observations compared with a day-of-year-dependent scale factor.

A similar scale factor, but based on light level, was used to implement seasonal variability in assimilation and energetic costs in an IBM for the Antarctic krill, *E. superba* (Bahlburg et al., 2021). In the Antarctic environment, *E. superba* energetics are closely tied to day length and light level. Here, day-of-year and temperature were preferred over day length because they serve as more flexible proxies for upwelling, an important driver of ecosystem responses in the CCE (Kudela et al., 2008; Bograd et al., 2009). Day-of-year was weighted to reflect climatological upwelling; the peak of the energetic scale factor coincides with a period when conditions in the CCE tend to be more productive and supportive of euphausiid growth (Kudela et al., 2008; Bograd et al., 2009; Shaw et al., 2010).

Unlike other life history stages, predictions of juvenile size distributions were not improved with implementation of a scale factor that modified energetics. The ability of the IBM to reasonably resolve juvenile size structure without implementing variability in energetics reflects the greater energetic demand of juvenile krill (compared to furcilia) and food concentrations that fluctuate from abundant in spring and summer to insufficient in fall and winter. These dynamics resulted in juvenile size distributions that generally tracked abundance of prey.

Despite marked improvements in the ability to resolve size structure for most life history stages, the final model (and all others) do a poor job resolving size structure in F6

and F7 furcilia stages. This pattern might reflect a structural element of the model; the sharp transition from a temperature-independent Q_{10} which is applied to larvae to the temperature-dependent Q_{10} applied to juveniles and adults. An alternative, though not mutually exclusive, explanation is based on the greater likelihood that individuals will skip a later furcilia stage (Feinberg et al., 2006). Skipping a stage tends to decrease development time, which has the potential to alter size dynamics, especially if increased development rates are not coupled with similar changes in growth rates. Despite the poor resolution of F6 and F7 furcilia size distributions, an improved fit between model output and field observations was restored for juvenile and adult stages. This pattern likely reflects the relatively short stage duration of F6 and F7 furcilia and low potential for growth, especially if one of these stages is skipped.

Model Analysis

In anticipation of future implementation of the IBM to simulate population dynamics, it is important to assess that the model also matches other measures of krill dynamics and to identify discrepancies as foci for future research. I consider three metrics relevant to population dynamics that are related to size, but are not specifically targeted in the pattern-matching approach: growth rates, reproduction, and maturation.

Growth Rates

Model estimates of juvenile and adult growth rates are comparable to field-based estimates of *E. pacifica* growth within the CCE. Off the coast of Oregon, growth rate estimates from instantaneous growth rate experiments (Shaw et al., 2010) and cohort

analyses (Shaw et al., 2020) ranged from approximately -0.2 to 0.5 mm TL d^{-1}. Model estimates of individual adult (-0.32 to 0.42 mm TL d^{-1}) and juvenile (-0.22 to 0.12 mm TL d^{-1}) growth rates are well within the ranges reported by Shaw et al. (2010; 2021). Furthermore, seasonal patterns in juvenile and adult growth rates are similar to field-based observations indicating greater growth in spring and summer months (Brinton, 1971; Shaw et al., 2010). This pattern was not clearly resolved by the Dorman et al. (2015) IBM and represents an improvement in model-observation agreement.

Comparable field estimates of growth rates for furcilia are sparse. Bollens et al. (1992) estimated growth rates for larval *E. pacifica* (2-5 mm) ranging from 0.04 to 0.12 mm d^{-1}. Individual (-0.14 to 0.10 mm TL d^{-1}) and monthly averages of median growth rates (-0.08 to 0.10 mm TL d^{-1}) emerging from the model for similar sized krill exhibit a wider range than field-based estimates. Additionally, Shaw et al. (2021) reported that negative growth rates were not observed for *E. pacifica* smaller than 5 mm (~3.8 mm BL). This size corresponds to approximately the F4/5 furcilia stage. IBM simulations included periods of negative growth at stages as early as F3 furcilia.

The wider range of growth rates in model predictions compared to field-based estimates and occurrence of negative growth in model krill as early as the F3 furcilia stage might be explained by biases in field-based estimates of growth rate. Furcilia experiencing poor conditions and negative growth are unlikely to be represented among survivors present in samples from the field (Taggart and Frank, 1990). Another factor possibly contributing to discrepancies between model-predictions and field-based

estimates of growth rates is that individuals in the field are not tracked, so observations of negative growth are less likely. Negative growth would have to be substantial and sustained and not be confounded with cohort transitions. Similarly, the use of modal or cohort analysis (as in Bollens et al., 1992 and Shaw et al., 2021) to estimate growth rates from field samples is less likely to result in negative growth than measurements made on individual krill. These methods generate estimates that represent average growth of the population over the time period measured. Negative growth would have to be exhibited by a substantial portion of the population to emerge in population-level estimates of growth rates.

Reproduction

Model-generated patterns in reproductive effort are consistent with field observations that indicate enhanced reproduction during spring through early fall (Smiles and Pearcy, 1971; Tanasichuk, 1998; Feinberg and Peterson, 2003). Also, the positive relationship between body length and eggs per krill is consistent with observations off southern California and Oregon (Brinton; 1976; Gómez-Gutiérrez et al., 2006). Brood size is also consistent with observations. The range (4 – 229 eggs female^{-1}) produced by the top model is well within ranges reported by Brinton (1976) for southern California (20-212 eggs female^{-}) and Gómez-Gutiérrez et al. (2006; 11-599 eggs female^{-}) and Feinberg et al. (2007; 3-804 eggs female^{-}) off Oregon. The maximum brood size predicted by the model exceeds those in Dorman et al. (max. 20 eggs female^{-1}; 2015), whose predictions tend to be lower than average brood sizes obtained from field observations.

Maturation

The effect of environmental conditions (e.g., temperature and food quality and availability) on the schedule of maturation has not been documented for *E. pacifica*. Previous IBMs implemented maturation of *E. pacifica* as an invariant weight-based threshold (Lindsey, 2013; Dorman et al., 2015). However, our research indicates size-at-maturation (as indexed by minimum size-at-maturity) is not constant and is related to thermal exposure (Robertson and Bjorkstedt, 2020). Extension of the temperature-dependent development function developed by Lindsey (2013) to juvenile stage duration yields maturation times (153 – 204 days) well within estimates obtained from field observations by Harvey et al. (90 days; 2010) and Shaw et al., (240 days; 2021).

The relationship between model size-at-maturity and temperature is generally consistent with that emerging from field-based observations of minimum adult size and concurrent temperature measurements. Like field-based observations, model individuals that have experienced higher temperatures over the course of their lifetime tend to exhibit smaller size-at-maturity (Figure 28). In comparison, model individuals exposed to cooler conditions over the course of their lifetime exhibit a wider range of size-at-maturity, including larger size-at-maturity (Figure 28). Minimum size-at-maturity within a population has not been found to correlate with chlorophyll a concentration (Robertson and Bjorkstedt, 2020). However, model results indicate krill exposed to higher levels of chlorophyll tend to be larger at maturity than those exposed to lower levels of chlorophyll (Figure 28). This discrepancy might be explained by uncertainty in field-based estimates of size-at-maturity based on the minimum size of adult distributions, as these do not

necessarily represent the range of maturation sizes exhibited across all individuals. Moreover, these metrics might be confounded by the ability for krill to shrink, yet continue to reproduce (Feinberg et al., 2007). The discrepancy might also be explained by the period over which environmental conditions were measured. IBM measurements reflect average cumulative chlorophyll exposure over the course of the individual's life whereas the relationship in THL data reflects concurrent measurements of chlorophyll a concentration.

Model Sensitivity

Model Sensitivity: Energetic Balance

Sensitivity to changes in energetic components generally reflects the portion of the energetic budget for which each component accounts. For example, size distributions are most sensitive to changes in ingestion (Figure 32). Ingestion is the only mechanism by which individuals are able to assimilate carbon; it accounts for the entire input budget and must satisfy maintenance requirements before energy is allocated to growth. As such, changes in ingestion rate have a considerable effect on size across all life history stages. A large majority of assimilated energy is allocated to metabolic demands (approximately 60 – 80%; Lasker (1966) and reanalysis developed in this study). Consequently, a change in metabolism has a marked effect on size distributions. Other energetic costs, such as molting and reproduction, represent a small portion of the energetic budget. As such, size distributions are less sensitive to changes in these processes. It is evident that accurate estimates of ingestion and metabolic rates are crucial to resolving size structure across life history stages.

Model Sensitivity: Environmental Response

Sensitivity to chlorophyll a concentration and temperature varied across life history stages (Figure 33). Size of furcilia stages was not sensitive to changes in chlorophyll a concentration. This pattern reflects a low critical concentration that is met even under reduced prey scenarios. Beyond the critical concentration threshold, ingestion (and thus growth) remains constant regardless of prey concentration. In contrast, furcilia size was sensitive to changes in temperature. This response is due to temperature-related changes in ingestion and metabolic rates; two processes that strongly effect growth and size distributions (see above and Figure 32).

Our previous analysis indicated larger size distributions of furcilia were correlated with enhanced temperature on an interannual scale (Robertson and Bjorkstedt, 2020). Except for F1 and F2 furcilia, results from sensitivity analyses are consistent with these observations (Figure 33). F1 and F2 furcilia tend to be smaller (larger) in response to increased (decreased) temperature. The discrepancy between our field observations and the F1 and F2 furcilia response in the model prompted review of the stage duration data that informed Lindsey's (2013) Bělehrádek function. It appears that development of earlier stages, particularly C3 calyptopes, may not be as sensitive to temperature as defined by the Bělehrádek function (Ross, 1981; Feinberg et al., 2006). Preliminary analysis suggests a temperature-independent stage duration during the C3 calyptopis stage generates patterns in F1 and F2 furcilia stages that are more consistent with our field observations (Figure E1). The modification to C3 calyptopis stage duration has little

effect on size dynamics of later life history stages or model performance, yet points to a new line of research and parameterization to be pursued in the future.

Juveniles and adults exhibited a clear response to changes in chlorophyll and temperature that was generally consistent with our observations; smaller (larger) size distributions tended to correspond with warmer (cooler) temperatures and increased (decreased) chlorophyll tended to generate larger (smaller) juveniles and adults. (Figure 30b and c; Robertson and Bjorkstedt, 2020).

The response to changes in environmental conditions varied by season. This pattern emerges from the combined effect of temperature on metabolic and ingestion rates, the seasonality in prey concentration, and a structural component of the IBM—implementation of a temperature-dependent Q_{10} for ingestion. Recall that due to incorporation of the temperature-dependent Q_{10}, the response of juveniles and adults to changes in temperature depends on the absolute value of temperature. For example, an increase from 9 to 10°C could generate greater growth (depending on food availability) while an increase from 14 to 15°C would generate negative growth, regardless of food availability.

Juvenile and adult size was sensitive to enhanced thermal conditions during late spring. The marked reduction in size during this period reflects enhanced metabolic demand (due to increased temperature) and reduced rates of assimilation (due in part to the temperature-dependent scale factor). This pattern, though emerging in part from implementation of a phenomenological scale factor, indicates the potential for reduced

productivity during warmer spring months and is consistent with observations indicating the importance of seasonal upwelling dynamics with respect to *E. pacifica* size (Abraham and Sydeman, 2006; Robertson and Bjorkstedt, 2020).

Size of juveniles and adults was particularly sensitive to enhanced prey availability and cooler temperatures during winter months. This response is consistent with observations that winter preconditioning, or enhanced nutrient availability and production prior to the onset of spring upwelling, plays an important role in determining production dynamics within the CCE (Schroeder et al., 2013). The strong (positive) response in size to conditions in winter also aligns with our hypothesis that seasonal trajectories of *E. pacifica* size distributions are set early in the year, and represent another facet of ecosystem preconditioning affecting higher trophic levels (Robertson and Bjorkstedt, 2020).

Juvenile and adult size structure was less sensitive to changes in chlorophyll during late spring through early fall. This pattern can be explained by assimilation rates near or equivalent to those at critical concentration; at prey concentrations exceeding this threshold, ingestion rates (and growth) are, by definition, constant.

The response of juvenile and adult size distributions to changes in temperature and chlorophyll conditions indicates the model does a reasonable job predicting size in the context of climatological variability. Our previous observations indicate that smaller size structure in juveniles and adults is related to warm-water events (e.g., El Niño), periods which are also often characterized by lower primary production (Legaard and

Thomas, 2006; Thomas et al., 2009; Kahru et al., 2018). Analogous conditions in the sensitivity analysis (i.e., +1°C and -20% chlorophyll) generated smaller size structure throughout the year for adults and for most of the year for juveniles. In contrast, conditions analogous to more productive La Niña conditions (e.g., -1°C and +20% chlorophyll) generated larger size structure in adults and juveniles.

Results from sensitivity analyses suggest *E. pacifica* populations residing in warmer, less productive regions (e.g., the offshore environment) would have smaller juvenile and adult size distributions. In contrast, populations residing in cooler, productive regions (e.g., north of the THL) would have larger juvenile and adult size distributions. These patterns are consistent with general trends in temperature-size relationships that indicate larger (smaller) body size is related to cooler (warmer) thermal exposure (e.g., Bergmann's rule, for review see Blackburn et al., 1999).

The IBM developed here represents a clear improvement in the ability to resolve realistic growth and size dynamics in *E. pacifica* populations off northern California. The ability of the IBM to resolve general trends in temperature-size relationships (see above) suggests the model might successfully capture broad changes in size dynamics when applied to regions other than Trinidad Head Line. Resolution of smaller scale size dynamics in regions outside of northern California depends on whether state-based rules (e.g., physiological rates) accurately relate the response of individuals to their environment. Physiological rates from Ross (1979) were obtained from krill collected in Puget Sound, WA. The resolution of realistic size dynamics using only these base

physiological rates (e.g., see 'Phase I' model results) suggests the IBM can be successfully applied to regions within the northern California Current Ecosystem. However, day-of-year and temperature-based scale factors used to tune the model to observations along the THL will likely need to be adjusted to resolve growth and size dynamics in regions characterized by upwelling dynamics and thermal conditions different from those off northern California. Region-specific scale factors can easily be incorporated into the existing model framework.

It is unclear whether the model I have developed can be used to resolve growth and size dynamics of other species of krill within the CCE. Diverse life history strategies (e.g., the accumulation of lipids in some krill taxa) might require species-specific physiology and behavior. Regardless, the model developed here can provide a framework into which future modifications are incorporated.

Assumptions, Uncertainties, and Opportunities for Future Research

Like other models, the IBM I have developed is a summation of hypotheses. Some of the hypotheses are well justified by data while others are more phenomenological in nature. Some hypotheses are represented by assumptions that frame the context for analysis. Here I address several assumptions and uncertainties that are relevant to the interpretation of results and that highlight issues to be addressed in future implementations of the model.

The success of the model in matching observations as well as it does is perhaps somewhat surprising given assumptions implicit in the temporal and spatial scales of the model and the underlying environmental and population data. Like cohort growth analyses, the use of population size structure to calibrate model dynamics assumes that field observations involve re-sampling of a single *E. pacifica* population. The CCE is a highly dynamic environment and transport of plankton into and out of the sampling range is almost certain to have occurred, as indicated by sharp changes in the species composition of plankton assemblages (McClatchie et al., 2016; Peterson et al., 2017; Winnacott, 2021). However, save for extreme events, the assumption that field-based samples are from a single krill population is supported by research indicating vertical migration and physical mechanisms (e.g., upwelling) contribute to retention of plankton in dynamic, nearshore environments (Peterson et al., 1979; Batchelder et al., 2002; Dorman et al., 2005; Morgan et al., 2009; Lindsey, 2013). Furthermore, the success of cohort analyses in tracking zooplankton populations over time suggests the assumption of population re-sampling is valid (Shaw et al., 2021). The most obvious potential violation of this assumption is linked to periods associated with anomalous transport (e.g., 2014-16). During periods characterized by anomalous transport (e.g., the 2014 – 2016 marine heatwave) it is possible the individuals we sampled along the THL were residents of a distinct offshore population. If this was the case, their population size distribution would reflect the integrated effect of exposure to offshore conditions and possibly diverse genetic expression and life history strategies (e.g., adaptation to warmer, less productive waters). Coupling my IBM with a coupled circulation-ecosystem model (e.g., ROMS-

NEMURO; Fiechter et al., 2018) would enable exploration of these mechanisms and might help rectify some of the size discrepancies observed during periods characterized by anomalous transport.

Environmental exposure in the model differs from *in-situ* exposure in two ways: 1) interpolation between monthly cruises produces smoothed environmental variability on a monthly scale and 2) the model is not spatially explicit in the horizontal dimension; environmental exposure history represents conditions at a fixed horizontal location (i.e., the model does not allow for horizontal transport or mixing of individuals into regions with divergent conditions). These features have the potential to contribute to discrepancies between model output and field observations. Exclusion of higher frequency variability (e.g., short duration phytoplankton blooms) from model input generates smoother growth and development trajectories than might be observed in the field, especially for life history stages with shorter stage durations, than might be observed in the field. Yet, resolution on a monthly scale is sufficient to resolve seasonal and interannual patterns and accommodates the 10-day interval between initialization of eggs. I do not expect that inclusion of higher frequency input data would significantly alter the seasonal and interannual patterns generated by the model.

The deterministic approach to implementing growth, development, and behavior is a structural assumption with implications for comparisons between model output and field-based observations. Real populations of krill are comprised of individuals that exhibit variability across a multitude of traits, such as behavior and gene expression,

which can influence how an individual responds to its environment (e.g., Valentine and Ayala, 1976; De Robertis, 2002; Tarling, 2003). Inclusion of a wider range of variability across behavioral, physiological, and morphological traits has the potential to shift patterns in population-level dynamics, including size distributions, and could reveal otherwise unresolved growth and size trajectories.

Size distributions will also be shaped by ecological interactions, such as size-based predation and shifting patterns of aversion to risk (Jørgensen et al., 2014). For example, the rules I used to implement DVM do not account for other factors affecting vertical position (e.g., such as predator distribution, size-based predation risk, energetic cost of migration, and water clarity; Bollens and Frost, 1991; Ohman and Romagnan, 2016). Incorporating migration rules that result in different environmental exposures have the potential to shift patterns in growth trajectories and size dynamics. Such additions to the current model could help rectify some of the observed discrepancies, for example by buffering the negative growth response in 2014-2016.

It is unlikely that incorporating variability in growth rates among model-individuals would have a considerable impact on model output. Krill exhibiting lower growth rates would likely experience a higher rate of attrition due to size-based mortality. Therefore, the effect of size-based mortality would limit the contribution of smaller, slower growing krill to the size distribution of the population. Incorporating variability that generates enhanced growth in individuals has the potential to shift population size distributions larger. However, this effect would be dampened by the contribution of krill

exhibiting lower growth rates. Overall, enhanced variability would likely cause more overlap among cohort size distributions, but the mean size would be roughly the same. With the goal of resolving realistic growth and size dynamics of *E. pacifica* off northern California attained, future model development should incorporate a more realistic approach and incorporate variability among individuals.

The weighting of daily cohorts' contributions to virtual samples (i.e., size distribution by date) does not appear to have compromised the fit between model output and observations. This reflects the comparison between size distributions rather than abundance, and the likelihood that the timing of egg production is relatively consistent from year to year, even if magnitude changes. Upwelling-fueled production will occur during the spring and summer and production during the winter will consistently be lower. Thus, comparisons based on weighted distributions (e.g., median size) are insensitive to whether interannual fluctuations in the magnitude of egg production are resolved or not. Moreover, by constraining population dynamics, I was able to focus on matching model output to general patterns in observations. Future 'self-renewing' generations of the IBM will likely be more successful in generating realistic population dynamics (including abundance) because processes fundamental to growth and size dynamics are better resolved. A self-renewing version of the IBM will also avoid the need for post-simulation demographic corrections.

The scale factors implemented here represent a phenomenological approach to modeling. While they help resolve realistic variability in size distributions, the ability of

an IBM to resolve realistic dynamics is likely to improve with incorporation of a more mechanistic approach. Nevertheless, these phenomenological models are grounded in well justified hypotheses, yield credible results, and point to areas where greater resolution of mechanism might be achieved. Variability in energetics might be due, at least in part, to shifts in prey quality and foraging conditions. The nutritional content of phytoplankton prey affects growth efficiencies in zooplankton (Jones et al., 2002). Upwelling-related variability in phytoplankton assemblages and biochemical composition alters prey quality, including lipid content and fatty acid composition, and affects zooplankton growth (Du and Peterson, 2014; Miller et al., 2017). Changes in prey shape, size, and toxicity can influence handling times and ingestion rates (Bargu et al., 2006). Additionally, shifts in prey density and distribution have the potential to alter feeding behavior (e.g., forage efficiency), which could drive changes in metabolic costs and energy available for surplus growth. For example, convergence of water masses at upwelling-driven fronts concentrates prey and enhances trophic interactions (Woodson and Litvin, 2015). During winter, low front activity and enhanced mixing due to storm activity might contribute to a more uniform prey distribution and lower concentrations, potentially decreasing foraging efficiency of *E. pacifica* (Farstey et al., 2002; Castelao et al., 2006; Gruber et al., 2006). One clear avenue to explore is the link between upwelling-related variability in prey and factors affecting prey, such as phytoplankton assemblage, biochemical composition, and nutrient availability. A likely and straightforward improvement to the model would be to link to outputs from coupled models or even to simple indices of upwelling-driven productivity (e.g., BEUTI; Jacox et al., 2018).

It is clear that sources of nutrition matter and information on diet may be necessary to resolve variability in growth and size structure. The model is not constructed to differentiate between sources of chlorophyll and the assumption that all chlorophyll is equal with respect to its role in growth dynamics might underpin some of the more severe discrepancies in model fit. For example, overestimation of adult size during spring and summer months in 2014 through 2016 might be explained by climate-related shifts in prey. Beginning in 2014, elevated abundance of domoic-acid producing *Pseudo-nitzschia* was observed along the THL. In 2015 and 2016, a harmful algal bloom (HAB) occurred that generated high levels of domoic acid along the West Coast, including the THL (McCabe et al., 2016; McClatchie et al., 2016; Wells et al., 2017; Trainer et al., 2020). Sustained exposure to domoic acid has been shown to suppress feeding in *E. pacifica* (Bargu et al., 2006), with obvious consequences for growth rates. Failure to account for the effects of a shift to a phytoplankton assemblage characterized by high densities of toxigenic *Pseudo-nitzschia* could readily explain the overprediction of size during this period. Since the model does not differentiate between sources of chlorophyll, the high levels of chlorophyll during spring and summer months generated larger size structure, even though phytoplankton prey might have been less nutritious or had a negative impact on assimilation rates. A shift to lower quality prey during this period is supported by concurrent measurements indicating lower lipid content in *E. pacifica* along the THL (C. Cass, unpublished data).

Similarly, underestimation of size during winter 2010, 2016, and 2017 might be explained by model structure – input data do not include alternative, non-phytoplankton prey. These periods correspond to El Niño events (2010 and 2016) and a period following the 2014-16 MHW when the THL had not yet recovered from warm water anomalies (Wells et al., 2017; Bjorkstedt and Robertson, unpublished data). El Niño reduces chlorophyll concentrations (Legaard and Thomas, 2006; Thomas et al., 2009; Kahru et al., 2018), which may force *E. pacifica* to greater reliance on other prey resources. For example, a shift to a diet with a greater proportion of ciliates might contribute to sustained growth when phytoplankton prey are less available (Fessenden and Coweles, 1994; Nakagawa et al., 2004; Okazaki et al., 2020). Since the IBM does not account for ingestion of non-phytoplankton prey during nighttime feeding (or include independent estimates of non-phytoplankton prey at-depth), growth and size distributions cannot reflect the potential for growth supported by alternate prey sources. A shift to an alternate prey source would help buffer the slow and negative growth rates, and resulting small size distributions, produced by the model.

Application of the temperature-dependent assimilation scale factor during some of the coldest conditions along the THL (Figure 2) results in the overestimation of adult size during spring and summer 2013. This discrepancy indicates the current scale factor does not accurately resolve the effect of upwelling on adult growth and size dynamics when applied at relatively low temperatures. This pattern is likely due to a non-linear relationship between upwelling-related processes and coastal production; as upwelling-

favorable winds increase beyond a threshold, productivity accessible to coastal populations declines as offshore transport outstrips the rate of bloom productivity (Botsford et al., 2003). Future model improvements could address this issue by accounting for a change in the relationship between assimilation and temperature at low temperature extremes or alternative metrics for upwelling. Linking the IBM to an ecosystem model (e.g., NEMURO) where temperature and prey composition are directly coupled could help refine the shape of the current scale factor by resolving the relationship between temperature (as a proxy for prey quality) and assimilation dynamics. Linking the IBM to this type of ecosystem model would also enable exploration of the relationship between prey composition, which might itself be a proxy for variability in prey quality (e.g., diatoms versus dinoflagellates), and growth dynamics. This could inform development of a more mechanistic scale factor based on prey composition.

Agreement between model predictions and observations of size-at-maturity might be improved by incorporating additional information relevant to maturation dynamics. For example, the IBM accounts for variability in maturation only due to temperature. Prey availability and quality might influence development rates, as has been seen in copepods (Breteler et al., 1995; Breteler et al., 2005). Accounting for the effect of prey quality and quantity, perhaps through modification of the Bělehrádek function, might yield broader agreement in size and transition dynamics throughout the life cycle.

Moreover, the maturation rule implemented in the IBM is not condition-dependent, nor does it take into account expected future conditions, both of which have

been shown to be important in analysis of life history models focused on maximizing lifetime fitness (Mangel, 2015; Reimer et al., 2019). The timing of maturation has broad fitness consequences. The benefit of early maturation (e.g., improved probability of reproduction) is balanced against smaller size, which can influence brood size and mortality (Brinton, 1976; Peterson and Wroblewski, 1984; Gómez-Gutiérrez et al., 2006). Delayed maturation can result in larger body and thus brood size, but risks reduced fitness due to mortality or shorter time at maturation. Integrating all such considerations in a comprehensive analysis with fitness measures is beyond the scope of this study. However, the model I have developed establishes a solid foundation for future fitness-based analysis of life history strategies, such as might be developed using stochastic dynamic programming or similar approaches that take an evolutionary perspective by considering the effect of current decisions in the context of future results (Mangel, 2015).

Looking forward, future research should address the assumptions and uncertainties noted above. Among these issues, information on factors that drive seasonal variability in energetics (particularly ingestion and metabolism) and prey quality (e.g., assemblage and nutritional content) is of particular importance, and should be a focus of future experimental and observational study. By resolving the drivers of dynamics currently captured as ‘scaling factors’ in the IBM, such research will provide critical, empirical grounding for replacing the phenomenological relationships proposed here with improved mechanistic resolution of growth and size dynamics. Such advances will support efforts to generalize the IBM so it can be applied to regions outside northern

California, incorporated into larger-scale ecosystem models (e.g., NEMURO), and used to complement analyses focused on spatial distributions of krill (e.g., Santora et al., 2011) Explicit resolution of size structure within ecosystem models will contribute to improved estimates of krill production and resolution of predator-prey dynamics. Similarly, information on the size structure of krill populations can complement spatial analyses of krill by providing information on the condition of an important forage component within the CCE.

CONCLUSION

Patterns and trends in size distributions of *E. pacifica* (as documented in Robertson and Bjorkstedt, 2020) motivated development of an IBM capable of producing realistic variability in size across life history stages. The model I have developed generates variability in *E. pacifica* size, growth, and development that is generally consistent with observations. Long-term, high-frequency field observations enabled a pattern-oriented modeling approach that helped rectify discrepancies between model output and field-based observations. By incorporating a few key modifications, the IBM I have developed represents an advancement toward obtaining more accurate predictions of *E. pacifica* dynamics.

Improved predictions of *E. pacifica* development, growth, and size distributions have implications across a broad range of issues, including estimates of forage biomass and research focused on life history strategies and population dynamics. Resolution of adult size distributions is particularly important for obtaining accurate estimates of production – size-dependent metrics such as brood size and mortality affect estimates of fecundity and production (Peters, 1983; Kiørboe, 2008). Similarly, accounting for variability in development time and size-at-maturation can contribute to better estimates of production by more accurately resolving the reproductive state of individuals within a population. Since adults account for the majority of *E. pacifica* biomass, accurate prediction of adult size is especially important for estimates of forage biomass (Robertson and Bjorkstedt, 2020).

In addition to the improved resolution of *E. pacifica* size dynamics, the IBM I have developed provides a useful framework for incorporating additional model advancements. The parsing of growth into specific energetic processes enables future modifications to physiological rates (e.g., metabolism) to accommodate our growing understanding of how *E. pacifica* respond to ongoing change in environmental conditions, such as ocean acidification, deoxygenation, and harmful algal blooms (McLaskey et al., 2016, Bargu et al, 2006).

The model I have developed can be applied to a broad range of research. For example, at the individual and population level, the IBM can be used to investigate potential responses to climate-variability. Size and biomass predictions can provide important information on the (future) state of forage within the CCE. This type of information has the potential to contribute to ecosystem-based management of fisheries dependent on or affected by forage resources within the CCE. The IBM can also be incorporated into larger-scale ecosystem models to provide detailed estimates of *E. pacifica* biomass and improved estimates of forage resources within the CCE.

It is evident the response of *E. pacifica* to its environment is complex. Because of their importance and high connectivity in the CCE, efforts that help resolve and predict the response of this critical forage species are worthwhile. Among these efforts are detailed, high-frequency, and long-term field observations, the value of which is highlighted here. Without the time series of observations, important information from a real-system would not have been available. This information was crucial for developing

an IBM for *E. pacifica* that resolves realistic variability in growth and size dynamics. The enhanced capabilities of the model I have developed strengthen the ability of the IBM to serve as a tool for deepening our understanding of a crucial forage species and how dynamics at the individual and population-level are translated to broader ecosystem-level dynamics.

REFERENCES

Abraham, C.L. and Sydeman, W.J., 2004. Ocean climate, euphausiids and auklet nesting: inter-annual trends and variation in phenology, diet and growth of a planktivorous seabird, *Ptychoramphus aleuticus*. *Marine Ecology Progress Series*, *274*, pp.235-250.

Abraham, C.L. and Sydeman, W.J., 2006. Prey-switching by Cassin's auklet Ptychoramphus aleuticus reveals seasonal climate-related cycles of *Euphausia pacifica* and Thysanoessa spinifera. *Marine Ecology Progress Series*, *313*, pp.271-283.

Alcaraz, M., Felipe, J., Grote, U., Arashkevich, E. and Nikishina, A., 2014. Life in a warming ocean: thermal thresholds and metabolic balance of arctic zooplankton. *Journal of Plankton Research*, *36*(1), pp.3-10.

Andrello, M., Mouillot, D., Somot, S., Thuiller, W. and Manel, S., 2015. Additive effects of climate change on connectivity between marine protected areas and larval supply to fished areas. *Diversity and Distributions*, *21*(2), pp.139-150.

Anger, K. and Dawirs, R.R., 1981. Influence of starvation on the larval development of *Hyas araneus* (Decapoda, Majidae). *Helgoländer Meeresuntersuchungen*, *34*(3), pp.287-311.

Bahlburg, D., Meyer, B. and Berger, U., 2021. The impact of seasonal regulation of metabolism on the life history of Antarctic krill. *Ecological Modelling*, *442*, p.109427.

Bargu, S., Lefebvre, K. and Silver, M.W., 2006. Effect of dissolved domoic acid on the grazing rate of krill *Euphausia pacifica*. *Marine Ecology Progress Series*, *312*, pp.169-175.

Barth, J.A., Menge, B.A., Lubchenco, J., Chan, F., Bane, J.M., Kirincich, A.R., McManus, M.A., Nielsen, K.J., Pierce, S.D. and Washburn, L., 2007. Delayed upwelling alters nearshore coastal ocean ecosystems in the northern California current. *Proceedings of the National Academy of Sciences*, *104*(10), pp.3719-3724.

Batchelder, H.P. and Miller, C.B., 1989. Life history and population dynamics of *Metridia pacifica*: results from simulation modelling. *Ecological Modelling*, *48*(1-2), pp.113-136.

Batchelder, H.P., Edwards, C.A. and Powell, T.M., 2002. Individual-based models of copepod populations in coastal upwelling regions: implications of physiologically

and environmentally influenced diel vertical migration on demographic success and nearshore retention. *Progress in Oceanography*, *53*(2-4), pp.307-333.

Becker, B.H., Peery, M.Z. and Beissinger, S.R., 2007. Ocean climate and prey availability affect the trophic level and reproductive success of the marbled murrelet, an endangered seabird. *Marine Ecology Progress Series*, *329*, pp.267-279.

Bělehrádek, J., 1930. Temperature coefficients in biology. *Biological Reviews*, *5*(1), pp.30-58.

Bi, H., Peterson, W.T. and Strub, P.T., 2011. Transport and coastal zooplankton communities in the northern California Current system. *Geophysical Research Letters*, *38*(12).

Bivand, R. and Lewin-Koh, N. (2021). maptools: Tools for Handling Spatial Objects. R package version 1.1-1. https://CRAN.R-project.org/package=maptools

Blackburn, T.M., Gaston, K.J. and Loder, N., 1999. Geographic gradients in body size: a clarification of Bergmann's rule. *Diversity and distributions*, *5*(4), pp.165-174.

Blechschmidt, J., Wittmann, M.J. and Blüml, C., 2020. Climate change and green sea turtle sex ratio—preventing possible extinction. *Genes*, *11*(5), p.588.

Boden, B.P., 1950. The post-naupliar stages of the crustacean *Euphausia pacifica*. *Transactions of the American Microscopical Society*, *69*(4), pp.373-386.

Bograd, S.J., Schroeder, I., Sarkar, N., Qiu, X., Sydeman, W.J. and Schwing, F.B., 2009. Phenology of coastal upwelling in the California Current. *Geophysical Research Letters*, *36*(1).

Bollens, S.M. and Frost, B.W., 1991. Diel vertical migration in zooplankton: rapid individual response to predators. *Journal of Plankton Research*, *13*(6), pp.1359-1365.

Bollens, S.M., Frost, B.W. and Lin, T.S., 1992. Recruitment, growth, and diel vertical migration of *Euphausia pacifica* in a temperate fjord. *Marine Biology*, *114*(2), pp.219-228.

Bosley, K.L., Miller, T.W., Brodeur, R.D., Bosley, K.M., Van Gaest, A. and Elz, A., 2014. Feeding ecology of juvenile rockfishes off Oregon and Washington based on stomach content and stable isotope analyses. *Marine biology*, *161*(10), pp.2381-2393.

Botsford, L.W., Lawrence, C.A., Dever, E.P., Hastings, A. and Largier, J., 2003. Wind strength and biological productivity in upwelling systems: an idealized study. *Fisheries Oceanography*, *12*(4-5), pp.245-259.

Breteler, K., 1995. Development of *Pseudocalanus elongatus* (Copepoda, Calanoida) cultured at different temperature and food conditions. *Marine Ecology Progress Series*, *119*, pp.99-110.

Breteler, W.K., Schogt, N. and Rampen, S., 2005. Effect of diatom nutrient limitation on copepod development: role of essential lipids. *Marine Ecology Progress Series*, *291*, pp.125-133.

Brinton, E., 1976. Population biology of *Euphausia pacifica* off southern California. *Fishery Bulletin*, *74*(4), pp.733-762.

Brinton, E., Ohman, M.D., Townsend, A.W. and Knight, M.D., 1999. Euphausiids of the World Ocean, CD-ROM edn.

Brinton, E. and Townsend, A., 2003. Decadal variability in abundances of the dominant euphausiid species in southern sectors of the California Current. *Deep Sea Research Part II: Topical Studies in Oceanography*, *50*(14-16), pp.2449-2472.

Brodeur, R.D., Pearcy, W.G., 1992, Effects of environmental variability on trophic interactions and food web structure in a pelagic upwelling ecosystem, *Mar. Ecol. Prog. Ser.*, 101-119.

Brodeur, R.D., Suchman, C.L., Reese, D.C., Miller, T.W. and Daly, E.A., 2008. Spatial overlap and trophic interactions between pelagic fish and large jellyfish in the northern California Current. *Marine Biology*, *154*(4), pp.649-659.

Castelao, R.M., Mavor, T.P., Barth, J.A. and Breaker, L.C., 2006. Sea surface temperature fronts in the California Current System from geostationary satellite observations. *Journal of Geophysical Research: Oceans*, *111*(C9).

Chao, Y., Farrara, J.D., Bjorkstedt, E., Chai, F., Chavez, F., Rudnick, D.L., Enright, W., Fisher, J.L., Peterson, W.T., Welch, G.F. and Davis, C.O., 2017. The origins of the anomalous warming in the California coastal ocean and San Francisco Bay during 2014–2016. *Journal of Geophysical Research: Oceans*, *122*(9), pp.7537-7557.

Chavez, F.P. and Messié, M., 2009. A comparison of eastern boundary upwelling ecosystems. *Progress in Oceanography*, *83*(1-4), pp.80-96.

Checkley Jr, D.M. and Barth, J.A., 2009. Patterns and processes in the California Current System. *Progress in Oceanography*, *83*(1-4), pp.49-64.

Chenillat, F., Rivière, P., Capet, X., Di Lorenzo, E. and Blanke, B., 2012. North Pacific Gyre Oscillation modulates seasonal timing and ecosystem functioning in the California Current upwelling system. *Geophysical Research Letters*, *39*(1).

Cossins, A.R. and Bowler, K., 1987. Rate compensations and capacity adaptations. In *Temperature biology of animals* (pp. 155-203). Springer, Dordrecht.

Dagg, M.J., 1976. Complete carbon and nitrogen budgets for the carnivorous amphipod, *Calliopius laeviusculus* (Krøyer). *Internationale Revue der gesamten Hydrobiologie und Hydrographie*, *61*(3), pp.297-357.

Dawirs, R.R., 1983. Respiration, energy balance and development during growth and starvation of *Carcinus maenas* L. larvae (Decapoda: Portunidae). *Journal of Experimental Marine Biology and Ecology*, *69*(2), pp.105-128.

Dawirs, R.R., 1987. Influence of limited starvation periods on growth and elemental composition (C, N, H) of *Carcinus maenas* (Decapoda: Portunidae) larvae reared in the laboratory. *Marine Biology*, *93*(4), pp.543-549.

DeAngelis, D.L. and Mooij, W.M., 2005. Individual-based modeling of ecological and evolutionary processes. *Annu. Rev. Ecol. Evol. Syst.*, *36*, pp.147-168.

DeAngelis, D.L. and Grimm, V., 2014. Individual-based models in ecology after four decades. *F1000prime reports*, *6*.

DeAngelis, D.L., 2018. Individual-based models and approaches in ecology: populations, communities and ecosystems. CRC Press.

De Robertis, A., 2002. Size-dependent visual predation risk and the timing of vertical migration: An optimization model. *Limnology and Oceanography*, *47*(4), pp.925-933.

Di Lorenzo, E., Mountain, D., Batchelder, H.P., Bond, N. and Hofmann, E.E., 2013. Advances in marine ecosystem dynamics from US GLOBEC: The horizontal-advection bottom-up forcing paradigm. *Oceanography*, *26*(4), pp.22-33.

Dilling, L., Wilson, J., Steinberg, D. and Alldredge, A., 1998. Feeding by the euphausiid *Euphausia pacifica* and the copepod *Calanus pacificus* on marine snow. *Marine Ecology Progress Series*, *170*, pp.189-201.

Dorman, J.G., Powell, T.M., Sydeman, W.J. and Bograd, S.J., 2011. Advection and starvation cause krill (*Euphausia pacifica*) decreases in 2005 Northern California coastal populations: Implications from a model study. *Geophysical Research Letters*, *38*(4).

Dorman, J.G., Sydeman, W.J., Bograd, S.J. and Powell, T.M., 2015. An individual-based model of the krill *Euphausia pacifica* in the California Current. *Progress in Oceanography*, *138*, pp.504-520.

Du, X. and Peterson, W.T., 2014. Seasonal cycle of phytoplankton community composition in the coastal upwelling system off central Oregon in 2009. *Estuaries and coasts*, *37*(2), pp.299-311.

Ege, R. and Krogh, A., 1914. On the relation between the temperature and the respiratory exchange in fishes. *Internationale Revue der gesamten Hydrobiologie und Hydrographie*, *7*(1), pp.48-55.

Farstey, V., Lazar, B. and Genin, A., 2002. Expansion and homogeneity of the vertical distribution of zooplankton in a very deep mixed layer. *Marine Ecology Progress Series*, *238*, pp.91-100.

Feinberg, L.R. and Peterson, W.T., 2003. Variability in duration and intensity of euphausiid spawning off central Oregon, 1996–2001. *Progress in Oceanography*, *57*(3-4), pp.363-379.

Feinberg, L.R., Shaw, C.T. and Peterson, W.T., 2006. Larval development of *Euphausia pacifica* in the laboratory: variability in developmental pathways. *Marine Ecology Progress Series*, *316*, pp.127-137.

Feinberg, L.R., Shaw, C.T. and Peterson, W.T., 2007. Long-term laboratory observations of *Euphausia pacifica* fecundity: comparison of two geographic regions. *Marine Ecology Progress Series*, *341*, pp.141-152.

Feinberg, L.R., Peterson, W.T. and Shaw, C.T., 2010. The timing and location of spawning for the Euphausiid *Thysanoessa spinifera* off the Oregon coast, USA. *Deep Sea Research Part II: Topical Studies in Oceanography*, *57*(7-8), pp.572-583.

Fessenden, L. and Cowles, T.J., 1994. Copepod predation on phagotrophic ciliates in Oregon coastal waters. *Marine Ecology-Progress Series*, *107*, pp.103-103.

Fiechter, J., Edwards, C.A., Moore, A.M. 2018. Wind, circulation, and topographic effects on alongshore phytoplankton variability in the California Current. Geophysical Research Letters, 45(7), 3238-3245.

Forster, J. and Hirst, A.G., 2012. The temperature-size rule emerges from ontogenetic differences between growth and development rates. *Functional Ecology*, *26*(2), pp.483-492.

Gómez-Gutiérrez, J., 2003. Comparative study of the population dynamics, secondary productivity, and reproductive ecology of the euphausiids *Euphausia pacifica* and *Thysanoessa spinifera* in the Oregon upwelling region.

Gómez-Gutiérrez, J., Peterson, W.T., Miller C.B., 2005, Cross-shelf life-stage segregation and community structure of the euphausiids off central Oregon, *Deep Sea Res. Pt II*, 52(1), 289-315, https://doi.org/10.1016/j.dsr2.2004.09.023.

Gómez-Gutiérrez, J., Feinberg, L.R., Shaw, T. and Peterson, W.T., 2006. Variability in brood size and female length of *Euphausia pacifica* among three populations in the North Pacific. *Marine Ecology Progress Series*, *323*, pp.185-194.

Grimm, V., Revilla, E., Berger, U., Jeltsch, F., Mooij, W.M., Railsback, S.F., Thulke, H.H., Weiner, J., Wiegand, T. and DeAngelis, D.L., 2005. Pattern-oriented modeling of agent-based complex systems: lessons from ecology. *science*, *310*(5750), pp.987-991.

Grimm, V., Berger, U., Bastiansen, F., Eliassen, S., Ginot, V., Giske, J., Goss-Custard, J., Grand, T., Heinz, S.K., Huse, G. and Huth, A., 2006. A standard protocol for describing individual-based and agent-based models. *Ecological modelling*, *198*(1-2), pp.115-126.

Grimm, V. and Railsback, S.F., 2013. *Individual-based modeling and ecology*. Princeton university press.

Grimm, V., Railsback, S.F., Vincenot, C.E., Berger, U., Gallagher, C., DeAngelis, D.L., Edmonds, B., Ge, J., Giske, J., Groeneveld, J. and Johnston, A.S., 2020. The ODD protocol for describing agent-based and other simulation models: A second update to improve clarity, replication, and structural realism. *Journal of Artificial Societies and Social Simulation*, *23*(2).

Grote, U., Pasternak, A., Arashkevich, E., Halvorsen, E. and Nikishina, A., 2015. Thermal response of ingestion and egestion rates in the Arctic copepod *Calanus glacialis* and possible metabolic consequences in a warming ocean. *Polar Biology*, *38*(7), pp.1025-1033.

Gruber, N., Frenzel, H., Doney, S.C., Marchesiello, P., McWilliams, J.C., Moisan, J.R., Oram, J.J., Plattner, G.K. and Stolzenbach, K.D., 2006. Eddy-resolving simulation of plankton ecosystem dynamics in the California Current System. *Deep Sea Research Part I: Oceanographic Research Papers*, *53*(9), pp.1483-1516.Gruber, N., Frenzel, H., Doney, S.C., Marchesiello, P., McWilliams, J.C., Moisan, J.R., Oram, J.J., Plattner, G.K. and Stolzenbach, K.D., 2006. Eddy-resolving simulation of plankton ecosystem dynamics in the

California Current System. *Deep Sea Research Part I: Oceanographic Research Papers*, *53*(9), pp.1483-1516.

Hamner, B. and Frasco, M. (2018). Metrics: Evaluation Metrics for Machine Learning. Rpackage version 0.1.4. https://CRAN.R-project.org/package=Metrics

Harvey, H.R., Ju, S.J., Son, S.K., Feinberg, L.R., Shaw, C.T. and Peterson, W.T., 2010. The biochemical estimation of age in Euphausiids: Laboratory calibration and field comparisons. *Deep Sea Research Part II: Topical Studies in Oceanography*, *57*(7-8), pp.663-671.

Hickey, B.M. and Banas, N.S., 2008. Why is the northern end of the California Current System so productive?. *Oceanography*, *21*(4), pp.90-107.

Höring, F., Teschke, M., Suberg, L., Kawaguchi, S. and Meyer, B., 2018. Light regime affects the seasonal cycle of Antarctic krill (*Euphausia superba*): impacts on growth, feeding, lipid metabolism, and maturity. *Canadian Journal of Zoology*, *96*(11), pp.1203-1213.

Hunt, S.L., Mulligan, T.J. and Komori, K., 1999. Oceanic feeding habits of Chinook salmon, *Oncorhynchus tshawytscha*, off northern California. *FISHERY BULLETIN-NATIONAL OCEANIC AND ATMOSPHERIC ADMINISTRATION*, *97*, pp.717-721.

Iguchi, N. and Ikeda, T., 1994. Experimental study on brood size, egg hatchability and early development of a euphausiid *Euphausia pacifica* from Toyama Bay, southern Japan Sea. *Bull Jpn Sea Natl Fish Res Inst*, *44*, pp.49-57.

Im, D.H. and Suh, H.L., 2016. Ontogenetic feeding migration of the euphausiid *Euphausia pacifica* in the East Sea (Japan Sea) in autumn: a stable isotope approach. *Journal of Plankton Research*, *38*(4), pp.904-914.

Jacox, M.G., Fiechter, J., Moore, A.M. and Edwards, C.A., 2015. ENSO and the California Current coastal upwelling response. *Journal of Geophysical Research: Oceans*, *120*(3), pp.1691-1702.

Jacox, M.G., Edwards, C.A., Hazen, E.L. and Bograd, S.J., 2018. Coastal upwelling revisited: Ekman, Bakun, and improved upwelling indices for the US West Coast. *Journal of Geophysical Research: Oceans*, *123*(10), pp.7332-7350.

Jones, R.H., Flynn, K.J. and Anderson, T.R., 2002. Effect of food quality on carbon and nitrogen growth efficiency in the copepod *Acartia tonsa*. *Marine Ecology Progress Series*, *235*, pp.147-156.

Jones, T., Parrish, J.K., Peterson, W.T., Bjorkstedt, E.P., Bond, N.A., Ballance, L.T., Bowes, V., Hipfner, J.M., Burgess, H.K., Dolliver, J.E., Lindquist, K., Lindsey, J., Nevins H.M., Robertson, R.R., Roletto, J., Wilson, L., Joyce, T., and Harvey, J. 2018. Massive mortality of a planktivorous seabird in response to a marine heatwave. *Geophysical Research Letters*, *45*(7), pp.3193-3202.

Jørgensen, C., Opdal, A.F., Fiksen, Ø. 2014. Can behavioural ecology unite hypotheses for fish recruitment?. ICES Journal of Marine Science, 71(4), 909-917.

Kahru, M., Jacox, M.G. and Ohman, M.D., 2018. CCE1: Decrease in the frequency of oceanic fronts and surface chlorophyll concentration in the California Current System during the 2014–2016 northeast Pacific warm anomalies. *Deep Sea Research Part I: Oceanographic Research Papers*, *140*, pp.4-13.

Kingsolver, J.G. and Woods, H.A., 1997. Thermal sensitivity of growth and feeding in *Manduca sexta* caterpillars. *Physiological Zoology*, *70*(6), pp.631-638.

Kiørboe, T., 2008. *A mechanistic approach to plankton ecology*. Princeton University Press.

Kishi, M.J., Kashiwai, M., Ware, D.M., Megrey, B.A., Eslinger, D.L., Werner, F.E., Noguchi-Aita, M., Azumaya, T., Fujii, M., Hashimoto, S. and Huang, D., 2007. NEMURO—a lower trophic level model for the North Pacific marine ecosystem. *Ecological Modelling*, *202*(1-2), pp.12-25.

Kudela, R.M., Banas, N.S., Barth, J.A., Frame, E.R., Jay, D.A., Largier, J.L., Lessard, E.J., Peterson, T.D. and Vander Woude, A.J., 2008. New insights into the controls and mechanisms of plankton productivity in coastal upwelling waters of the northern California Current System. *Oceanography*, *21*(4), pp.46-59.

Lasker, R., 1966. Feeding, growth, respiration, and carbon utilization of a euphausiid crustacean. *Journal of the Fisheries Board of Canada*, *23*(9), pp.1291-1317.

Legaard, K.R. and Thomas, A.C., 2006. Spatial patterns in seasonal and interannual variability of chlorophyll and sea surface temperature in the California Current. *Journal of Geophysical Research: Oceans*, *111*(C6).

Leising, A.W., 2001. Copepod foraging in patchy habitats and thin layers using a 2-D individual-based model. *Marine Ecology Progress Series*, *216*, pp.167-179.

Lemoine, N.P. and Burkepile, D.E., 2012. Temperature-induced mismatches between consumption and metabolism reduce consumer fitness. *Ecology*, *93*(11), pp.2483-2489.

Lenarz, W.H., Ven Tresca, D.A., Graham, W.M., Schwing, F.B. and Chavez, F., 1995. Explorations of El Niño Events and Associated Biological Population Dynamics off Central California. *California Cooperative Oceanic Fisheries Investigations Report*, pp.106-119.

Lilly, L.E. and Ohman, M.D., 2018. CCE IV: El Niño-related zooplankton variability in the southern California Current System. *Deep Sea Research Part I: Oceanographic Research Papers*, *140*, pp.36-51.

Lindsey, B.J., 2013. Bioenergetics and behavior of the krill *Euphausia pacifica* in the California Current System off the Oregon coast.

Liu, H.L. and Sun, S., 2010. Diel vertical distribution and migration of a euphausiid *Euphausia pacifica* in the Southern Yellow Sea. *Deep Sea Research Part II: Topical Studies in Oceanography*, *57*(7-8), pp.594-605.

Mangel, M., 2015. Stochastic dynamic programming illuminates the link between environment, physiology, and evolution. *Bulletin of Mathematical Biology*, *77*(5), pp.857-877.

Marinovic, B., Mangel, M., 1999. Krill can shrink as an ecological adaptation to temporarily unfavorable environments. *Ecol. Lett.*, *2*, pp.338-343.

Marinovic, B.B., Croll, D.A., Gong, N., Benson, S.R. and Chavez, F.P., 2002. Effects of the 1997–1999 El Niño and La Niña events on zooplankton abundance and euphausiid community composition within the Monterey Bay coastal upwelling system. *Progress in Oceanography*, *54*(1-4), pp.265-277.

Meynecke, J.O. and Richards, R.G., 2014. A full life cycle and spatially explicit individual-based model for the giant mud crab (*Scylla serrata*): a case study from a marine protected area. *ICES Journal of Marine Science*, *71*(3), pp.484-498.

McCabe, R.M., Hickey, B.M., Kudela, R.M., Lefebvre, K.A., Adams, N.G., Bill, B.D., Gulland, F.M., Thomson, R.E., Cochlan, W.P. and Trainer, V.L., 2016. An unprecedented coastwide toxic algal bloom linked to anomalous ocean conditions. *Geophysical Research Letters*, *43*(19), pp.10-366.

McClatchie, S., Goericke, R., Leising, A., Auth, T.D., Bjorkstedt, E., Robertson, R.R., Brodeur, R.D., Du, X., Daly, E.A., Morgan, C.A., Chavez, F.P., Debich, A.J., Hildebrand, J., Field, J., Sakuma, K., Jacox, M.G., Kahru, M., Kudela, R., Andserson, C., Largier, J., Lavaniegos, B.E., Gomez-Valdes, J., Jimenez-Rosenberg, S.P.A., McCabe, R., Melin, S.R., Ohman, M.D., Sala, L.M., Peterson, B., Fisher, J., Shroeder, I.D., Bograd, S.J., Hazen, E.L., Schneider, S.R., Golightly, R.T., Suryan, R.M., Gladics, A.J., Loredo, S., Porquez, J.M., Thompson, A.R., Weber, E.D., Watson, W., Trainer, V., Warzybok, P., Bradley,

R., Jahncke, J., 2016. State of the California Current 2015–16: Comparisons with the 1997–98 El Ni.o. Calif. Coop. Oceanic Fish. Invest. Rep. 57, 5–61.

McLaskey, A.K., Keister, J.E., McElhany, P., Olson, M.B., Busch, D.S., Maher, M. and Winans, A.K., 2016. Development of *Euphausia pacifica* (krill) larvae is impaired under pCO2 levels currently observed in the Northeast Pacific. *Marine Ecology Progress Series*, *555*, pp.65-78.

Meyer, B. and Oettl, B., 2005. Effects of short-term starvation on composition and metabolism of larval Antarctic krill *Euphausia superba*. *Marine Ecology Progress Series*, *292*, pp.263-270.

Miller, T.W. and Brodeur, R.D., 2007. Diets of and trophic relationships among dominant marine nekton within the northern California Current ecosystem. *Fishery Bulletin*, *105*(4), pp.548-559.

Miller, T.W., Brodeur, R.D., Rau, G. and Omori, K., 2010. Prey dominance shapes trophic structure of the northern California Current pelagic food web: evidence from stable isotopes and diet analysis. *Marine Ecology Progress Series*, *420*, pp.15-26.

Miller, J.A., Peterson, W.T., Copeman, L.A., Du, X., Morgan, C.A. and Litz, M.N., 2017. Temporal variation in the biochemical ecology of lower trophic levels in the Northern California Current. *Progress in Oceanography*, *155*, pp.1-12.

Morgan, S.G., Fisher, J.L., Miller, S.H., McAfee, S.T. and Largier, J.L., 2009. Nearshore larval retention in a region of strong upwelling and recruitment limitation. *Ecology*, *90*(12), pp.3489-3502.

Nakagawa, Y., Endo, Y. and Sugisaki, H., 2003. Feeding rhythm and vertical migration of the euphausiid *Euphausia pacifica* in coastal waters of north-eastern Japan during fall. *Journal of plankton research*, *25*(6), pp.633-644.

Nakagawa, Y., Ota, T., Endo, Y., Taki, K. and Sugisaki, H., 2004. Importance of ciliates as prey of the euphausiid *Euphausia pacifica* in the NW North Pacific. *Marine Ecology Progress Series*, *271*, pp.261-266.

Ohman, M.D., 1984. Omnivory by *Euphausia pacifica*: The role of copepod prey. *Marine ecology progress series. Oldendorf*, *19*(1), pp.125-131.

Ohman, M.D. and Romagnan, J.B., 2016. Nonlinear effects of body size and optical attenuation on diel vertical migration by zooplankton. *Limnology and Oceanography*, *61*(2), pp.765-770.

Okazaki, Y., Takahashi, K., Nishibe, Y. and Ichinomiya, M., 2020. Post-spring-bloom feeding rates of krill *Euphausia pacifica* (Euphausiacea) in the Oyashio region, western North Pacific. *Progress in Oceanography*, *181*, p.102245.

Ospina-Alvarez, A., Parada, C. and Palomera, I., 2012. Vertical migration effects on the dispersion and recruitment of European anchovy larvae: from spawning to nursery areas. *Ecological Modelling*, *231*, pp.65-79.

Park, J.I., Kang, C.K. and Suh, H.L., 2011. Ontogenetic diet shift in the euphausiid *Euphausia pacifica* quantified using stable isotope analysis. *Marine Ecology Progress Series*, *429*, pp.103-109.

Peck, M.A. and Hufnagl, M., 2012. Can IBMs tell us why most larvae die in the sea? Model sensitivities and scenarios reveal research needs. *Journal of Marine Systems*, *93*, pp.77-93.

Peters, R.H., 1983. *The ecological implications of body size* (Vol. 2). Cambridge university press.

Peterson, I. and Wroblewski, J.S., 1984. Mortality rate of fishes in the pelagic ecosystem. *Canadian Journal of Fisheries and Aquatic Sciences*, *41*(7), pp.1117-1120.

Peterson, W.T., Miller, C.B. and Hutchinson, A., 1979. Zonation and maintenance of copepod populations in the Oregon upwelling zone. *Deep Sea Research Part A. Oceanographic Research Papers*, *26*(5), pp.467-494.

Peterson, W.T., Fisher, J.L., Strub, P.T., Du, X., Risien, C., Peterson, J. and Shaw, C.T., 2017. The pelagic ecosystem in the Northern California Current off Oregon during the 2014–2016 warm anomalies within the context of the past 20 years. *Journal of Geophysical Research: Oceans*, *122*(9), pp.7267-7290.

Piccolin, F., Suberg, L., King, R., Kawaguchi, S., Meyer, B. and Teschke, M., 2018. The seasonal metabolic activity cycle of Antarctic krill (*Euphausia superba*): evidence for a role of photoperiod in the regulation of endogenous rhythmicity. *Frontiers in physiology*, *9*, p.1715.

Politikos, D., Somarakis, S., Tsiaras, K.P., Giannoulaki, M., Petihakis, G., Machias, A. and Triantafyllou, G., 2015. Simulating anchovy's full life cycle in the northern Aegean Sea (eastern Mediterranean): A coupled hydro-biogeochemical–IBM model. *Progress in Oceanography*, *138*, pp.399-416.

Quetin, L.B. and Ross, R.M., 1991. Behavioral and physiological characteristics of the Antarctic krill, *Euphausia superba*. *American Zoologist*, *31*(1), pp.49-63.

Rademacher, C., Neuert, C., Grundmann, V., Wissel, C. and Grimm, V., 2004. Reconstructing spatiotemporal dynamics of Central European natural beech forests: the rule-based forest model BEFORE. *Forest Ecology and Management*, *194*(1-3), pp.349-368.

Railsback, S.F., Harvey, B.C., Lamberson, R.H., Lee, D.E., Claasen, N.J. and Yoshihara, S., 2002. Population-level analysis and validation of an individual-based cutthroat trout model. *Natural Resource Modeling*, *15*(1), pp.83-110.

Rall, B.C., Vucic-Pestic, O., Ehnes, R.B., Emmerson, M. and Brose, U., 2010. Temperature, predator-prey interaction strength and population stability. *Global Change Biology*, *16*(8), pp.2145-2157.

R Core Team, 2021. R: A language and environment for statistical computing. R Foundation for Statistical Computing, Vienna, Austria. URL https://www.R-project.org/.

Reilly, C.A., Echeverria, T.W. and Ralston, S., 1992. Interannual variation and overlap in the diets of pelagic juvenile rockfish(genus: *Sebastes*) off Central California. *Fishery Bulletin*, *90*(3), pp.505-515.

Reimer, J.R., Mangel, M., Derocher, A.E. and Lewis, M.A., 2019. Modeling optimal responses and fitness consequences in a changing Arctic. *Global change biology*, *25*(10), pp.3450-3461.

Robertson, R.R. and Bjorkstedt, E.P., 2020. Climate-driven variability in *Euphausia pacifica* size distributions off northern California. *Progress in Oceanography*, *188*, p.102412.

Ross, R.M., 1979. Carbon and nitrogen budgets over the life of *Euphausia pacifica*, PhD. Thesis, University of Washington, Seattle, WA.

Ross, R.M., 1981. Laboratory culture and development of *Euphausia pacifica*. *Limnology and Oceanography*, *26*(2), pp.235-246.

Ross, R.M., 1982a. Energetics of *Euphausia pacifica*. I. Effects of body carbon and nitrogen and temperature on measured and predicted production. *Marine Biology*, *68*(1), pp.1-13.

Ross, R.M., 1982b. Energetics of *Euphausia pacifica*. II. Complete carbon and nitrogen budgets at 8 and 12 C throughout the life span. *Marine Biology*, *68*(1), pp.15-23.

Ruzicka, J.J., Brodeur, R.D., Emmett, R.L., Steele, J.H., Zamon, J.E., Morgan, C.A., Thomas, A.C. and Wainwright, T.C., 2012. Interannual variability in the Northern California Current food web structure: changes in energy flow pathways and the

role of forage fish, euphausiids, and jellyfish. *Progress in Oceanography*, *102*, pp.19-41.

Santora, J.A., Sydeman, W.J., Schroeder, I.D., Wells, B.K. and Field, J.C., 2011. Mesoscale structure and oceanographic determinants of krill hotspots in the California Current: Implications for trophic transfer and conservation. *Progress in Oceanography*, *91*(4), pp.397-409.

Sato, M., Dower, J.F., Kunze, E. and Dewey, R., 2013. Second-order seasonal variability in diel vertical migration timing of euphausiids in a coastal inlet. *Marine Ecology Progress Series*, *480*, pp.39-56.

Schoenherr, J.R., 1991. Blue whales feeding on high concentrations of euphausiids around Monterey Submarine Canyon, *Can. J. of Zool.*, 69(3), 583-594, https://doi.org/10.1139/z91-088.

Shaw, C.T., Peterson, W.T. and Feinberg, L.R., 2010. Growth of *Euphausia pacifica* in the upwelling zone off the Oregon coast. *Deep Sea Research Part II: Topical Studies in Oceanography*, *57*(7-8), pp.584-593.

Shaw, C.T., Bi, H., Feinberg, L.R. and Peterson, W.T., 2021. Cohort analysis of *Euphausia pacifica* from the Northeast Pacific population using a Gaussian mixture model. *Progress in Oceanography*, *191*, https://doi.org/10.1016/j.pocean.2020.102495.

Schroeder, I.D., Black, B.A., Sydeman, W.J., Bograd, S.J., Hazen, E.L., Santora, J.A. and Wells, B.K., 2013. The North Pacific High and wintertime pre-conditioning of California current productivity. *Geophysical Research Letters*, *40*(3), pp.541-546.

Smiles, M.C., Pearcy, W.G., 1971. Size structure and growth rate of *Euphausia pacifica* off the Oregon coast, *Fish. Bull.*, 69(1) 79-86.

Smith, P., 1985. A case history of an anti-El Niño to El Niño transition on plankton and nekton distribution and abundances. In: Wooster WS, Fluharty DL (Eds.), El Niño North: Niño effects in the eastern subarctic Pacifica Ocean, Washington Sea Grant Program, Seattle, 121-142.

Sydeman, W.J., Bradley, R.W., Warzybok, P., Abraham, C.L., Jahncke, J., Hyrenbach, K.D., Kousky, V., Hipfner, J.M. and Ohman, M.D., 2006. Planktivorous auklet *Ptychoramphus aleuticus* responses to ocean climate, 2005: Unusual atmospheric blocking?. *Geophysical Research Letters*, *33*(22).

Taggart, C. T., and K. F. Frank. 1990. Perspectives on larval fish ecology and recruitment processes: probing the scales of relationships. In: K. Sherman and L. M.

Alexander (Eds.), Patterns, processes, and yields of large marine ecosystems (pp. 151-164). *AAAS Selected Symposium Series*

Tanasichuk, R.W., 1998. Interannual variations in the population biology and productivity of *Euphausia pacifica* in Barkley Sound, Canada, with special reference to the 1992 and 1993 warm ocean years. *Marine Ecology Progress Series*, *173*, pp.163-180.

Tarling, G.A., 2003. Sex-dependent diel vertical migration in northern krill *Meganyctiphanes norvegica* and its consequences for population dynamics. *Marine Ecology Progress Series*, *260*, pp.173-188.

Teschke, M., Kawaguchi, S. and Meyer, B., 2007. Simulated light regimes affect feeding and metabolism of Antarctic krill, *Euphausia superba*. *Limnology and oceanography*, *52*(3), pp.1046-1054.

Theilacker, G.H., Kimball, A.S. and Trimmer, J.S., 1986. Use of an ELISPOT immunoassay to detect euphausiid predation on larval anchovy. *Mar. Ecol. Prog. Ser*, *30*, pp.127-131.

Thomas, A.C., Brickley, P. and Weatherbee, R., 2009. Interannual variability in chlorophyll concentrations in the Humboldt and California Current Systems. *Progress in Oceanography*, *83*(1-4), pp.386-392.

Trainer, V.L., Kudela, R.M., Hunter, M.V., Adams, N.G. and McCabe, R.M., 2020. Climate extreme seeds a new domoic acid hotspot on the US west coast. *Frontiers in Climate*, *2*, p.23.

Valentine, J.W. and Ayala, F.J., 1976. Genetic variability in krill. *Proceedings of the National Academy of Sciences*, *73*(2), pp.658-660.

Van Winkle, W., Rose, K.A., Winemiller, K.O., Deangelis, D.L., Christensen, S.W., Otto, R.G. and Shuter, B.J., 1993. Linking life history theory, environmental setting, and individual-based modeling to compare responses of different fish species to environmental change. *Transactions of the American Fisheries Society*, *122*(3), pp.459-466.

Vance, P.M. Keister, J.E., and Peterson, W.T., 2003. Seasonal and annual variation in the population composition and depth distributions of the euphausiid, *Euphausia pacifica*. EOS Trans, American Geophysical Union. Honolulu, HI, 84(52) OS21B-19.

Ware, D.M. and Thomson, R.E., 2005. Bottom-up ecosystem trophic dynamics determine fish production in the Northeast Pacific. *science*, *308*(5726), pp.1280-1284.

Wells, B.K., Schroeder, I.D., Bograd, S.J., Hazen, E.L., Jacox, M.G., Leising, A., Mantua, N., Santora, J.A., Fisher, J., Peterson, W.T., Bjorkstedt, E., Robertson, R.R., Chavez, F.P., Goericke, R., Kudela, R., Anderson, C., Lavaniegos, B.E., Gomez-Valdes, J., Brodeur, R.D., Daly, E.A., Morgan, C.A., Auth, T.D., Field, J.C., Sakuma, K., McClatchie, S., Thompson, A.R., Weber, E.D., Watson, W., Suryan, R.M., Parrish, J., Dolliver, J., Loredo, S., Porquez, J.M., Zamon, J.E., Schneider, S.R., Golightly, R.T., Warzybok, P., Bradley, R., Jahncke, J., Sydeman, W., Melin, S.R., Hildebrand, J., Debich, A.J., Thayre, B., 2017. State of the California Current 2016–2017: Still anything but "normal" in the North. *California Cooperative Oceanic Fisheries Investigations Reports, 58*, pp.1-55.

Winnacott, B. 2021. Response of Coastal Ichthyoplankton Assemblages off Northern California to Seasonal Oceanographic and Climate Variability. Master's Thesis. Humboldt State University.

Wood, S.N., 2017. Generalized Additive Models: an Introduction with R. Chapman and Hall/CRC.

Woodson, C.B. and Litvin, S.Y., 2015. Ocean fronts drive marine fishery production and biogeochemical cycling. *Proceedings of the National Academy of Sciences, 112*(6), pp.1710-1715.

APPENDIX A

Hydrographic data from THL station TH04 (41°03.50 N, 124°26.00 W; ~450 m water depth) were interpolated between (roughly) monthly cruises to provide daily values of temperature and chlorophyll at 1-meter bins from the surface to 200 m (Figure 2).

For the early part of the THL record, hydrographic data are limited to the upper 150 m of the water column, thus requiring extrapolation to 200 m to span the migration range of krill. Based on comparisons to cases for which full (420 m) temperature profiles were available, direct linear extrapolation based on, e.g., the change in temperature with depth from 120 m to 150 m yielded unacceptably low temperatures at depth, as the rate of change of temperature with depth declines with depth. Therefore, an iterative method was developed to generate more realistic extrapolations of temperatures below 150 m, and implemented using hydrographic data for station TH04.

For each cruise lacking deep temperature data, (1) the temperature at 400 m (T_{400}) was predicted from a linear relationship between temperature at 140 m and at 400 m estimated from data from cruises for full (> 400 m) temperature profiles, and (2) a cruise-specific linear relationship between temperature and depth at the base of the hydrographic cast (depths between 120 and 150 m) was fit and the slope of this relationship designated as S_{base}. The extrapolation then proceeds iteratively for each successively deeper 1-m depth bin as follows. First, the change in temperature over depth between the (current) deepest temperature (T_D; observation or previous extrapolation) and

temperature at 400 m is calculated as ($T_{400} - T_D$)/(*400 - D*), where *D* is the current depth; this slope is designated as S_{anchor}. Second, the rate of change in temperature with depth over the next 1 m is calculated following equation A1:

$$S_{new} = w * S_{base} + (1 - w) * S_{anchor} \quad \text{(A1)}$$

where the relative contribution of S_{base} (i.e., the rate of change with temperature with depth at the base of the observed temperature profile) declines with depth per $w = 1 - D/200$. Temperature at the next deeper 1-m depth bin is calculated from the current deepest temperature and S_{new}. The algorithm is iterated to extrapolate the temperature profile to a depth of 200 m. Application of this algorithm yields a temperature profile that maintains continuity with the change in temperature with depth observed at the bottom of the hydrographic cast, yet is tuned towards more gradual changes in temperature with increasing depth. Comparisons between observed and extrapolated temperature profiles for cruises with full hydrographic profiles confirm that this approach generates realistic temperature profiles between 150 m and 200 m.

Chlorophyll data were extrapolated by extending the last observed value (typically a value close to zero) throughout the remainder of the water column below the depth at which the last value was observed. Note that this extrapolation has little or no impact on model results due to non-phytoplankton prey at depth that are assumed to scale with maximum chlorophyll concentration.

APPENDIX B

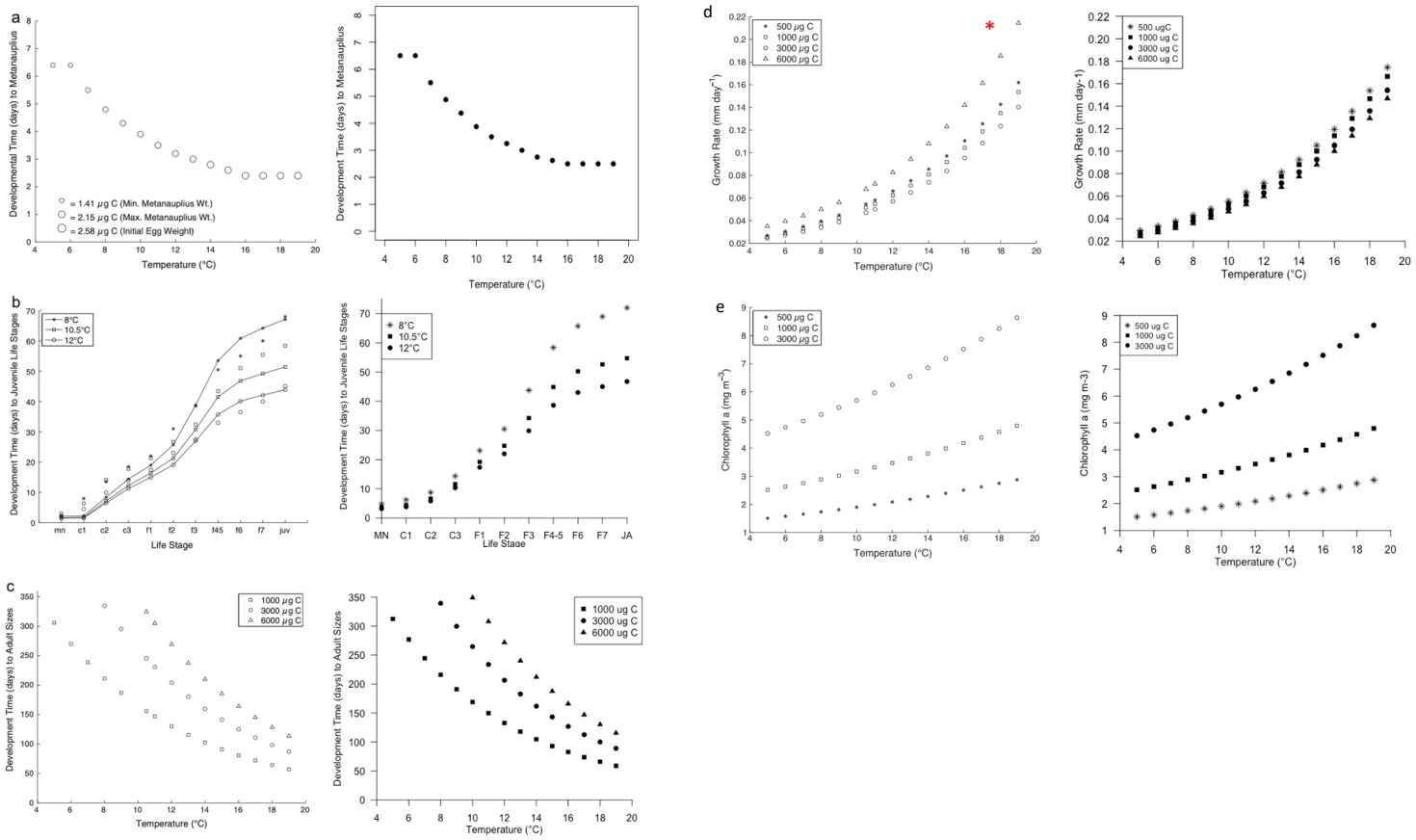

Figure B1. Results from Dorman et al. IBM (2015; plots with open symbols) and after porting the energetic submodels from Dorman et al. (2015) into R (plots with closed symbols). a) Development time to metanauplius versus temperature; b) Development time to juvenile life stages at 8, 10.5, and 12 °C (see legend); c) Development time to 1000, 3000, and 6000 µg C adults (see legend) versus temperature; d) Growth rate for various weights (see legend) under maximum food conditions, red asterisk indicates errata for growth rate of 6000 µg C individual (J. Dorman, personal communication, 8 January 2020); e) Chlorophyll concentration needed for maximum growth at various weights (see legend).

APPENDIX C

Table C1. Coefficients for the temperature-dependent Bělehrádek function ($Duration_i = a_{Dur,i}(T + B)^{c_{Dur}}$) . Coefficients for the egg through F7 furcilia stages are from Lindsey (2013). Coefficients for the juvenile stage were estimated in this study.

Stage *(i)*	$a_{Dur,i}$	B
Egg	1217	15.052
Nauplius N1	599	15.052
Nauplius N2	1423	15.052
Metanauplius	2547	15.052
Calyptopis C1	5767	15.052
Calyptopis C2	2771	15.052
Calyptopis C3	2621	15.052
Furcilia F1	4045	15.052
Furcilia F2	4269	15.052
Furcilia F3	8239	15.052
Furcilia F4/5	5693	15.052
Furcilia F6	3296	15.052
Furcilia F7	2247	15.052
Juvenile	$9.0*10^4$	8

APPENDIX D

The model I have developed is described below following the Overview, Design, and Details (ODD) protocol for describing individual-based models (Grimm et al., 2006; Grimm et al., 2020). The format specified by this protocol consists of three blocks (ODD) comprised of seven elements: purpose, state variables and scales, process overview and scheduling, design concepts, initialization, input, and submodels.

Overview

Purpose

The purpose of the individual-based model is to predict realistic size, growth, and maturation dynamics of *Euphausia pacifica* off northern California.

State variables and scales

The model I developed is based on published IBMs for *E. pacifica* (Lindsey, 2013; Dorman et al., 2015). Like those models, the IBM versions developed herein build upon the POPCYCLE framework. POPCYCLE was initially developed to implement species-specific physiology and behavior at the individual-level for copepods (Batchelder and Miller, 1989). Bioenergetic rates (e.g., growth and assimilation rates) are calculated in carbon per unit of time (e.g., μg C d^{-1}) and are a function of life history stage, body size (μg C), and environmental exposure (temperature and food concentrations). Migration behavior (i.e., vertical position) is dependent upon life history stage and time of day. Model development, data analysis, and simulations were conducted in R (4.0.4; R Core Team, 2021).

The IBM is comprised of two levels: individuals and their environment. Individuals are characterized by their size (weight in µg of carbon) and life history stage. The IBM includes 15 life history stages: egg, nauplius 1 and 2, metanauplius, calyptopis C1 - C3, furcilia F1 - F7 (furcilia F4/5 are combined), juvenile, and adult. Life history stage determines behavior (e.g., feeding, vertical position) as well as how growth is modeled (directly or indirectly; Table D1). The environment is characterized by water temperature (°C) and food availability (µg C). Date is included for use in seasonal scale factors (functions that allow seasonal tuning of energetics) and as an index for environmental input.

Table D1. Feeding behavior and type of growth submodel for *E. pacifica* life history stages in the Phase I IBM. 'Direct' growth model indicates growth is calculated by scaling expressions that relate growth rate to body size and temperature. In contrast 'Mechanistic' growth model indicates growth is calculated from the remainder of assimilated energy following allocation to metabolism, molting, and in the case of adults, reproduction.

Stage #	Stage	Feeding	Growth Model
1	Egg	No	Direct
2	Nauplius N1	No	Direct
3	Nauplius N2	No	Direct
4	Metanauplius	No	Direct
5	Calyptopis C1	Yes	Direct
6	Calyptopis C2	Yes	Direct
7	Calyptopis C3	Yes	Direct
8	Furcilia F1	Yes	Mechanistic: (Assimilation – Costs)
9	Furcilia F2	Yes	Mechanistic: (Assimilation – Costs)
10	Furcilia F3	Yes	Mechanistic: (Assimilation – Costs)
11	Furcilia F4/5	Yes	Mechanistic: (Assimilation – Costs)
12	Furcilia F6	Yes	Mechanistic: (Assimilation – Costs)
13	Furcilia F7	Yes	Mechanistic: (Assimilation – Costs)
14	Juvenile	Yes	Mechanistic: (Assimilation – Costs)
15	Adult	Yes	Mechanistic: (Assimilation – Costs)

Hydrographic data collected at THL station TH04 (Figure D1; 41°03.50 N, 124°26.00 W; ~450 m water depth) were interpolated between (roughly) monthly cruises

to provide daily values of environmental conditions at 1-meter bins from the surface to 200 m (Figure D2). In cases where hydrographic data were only available in the top 150 m, data were extrapolated from the last observed depth to 200 m (see Appendix A for methods).

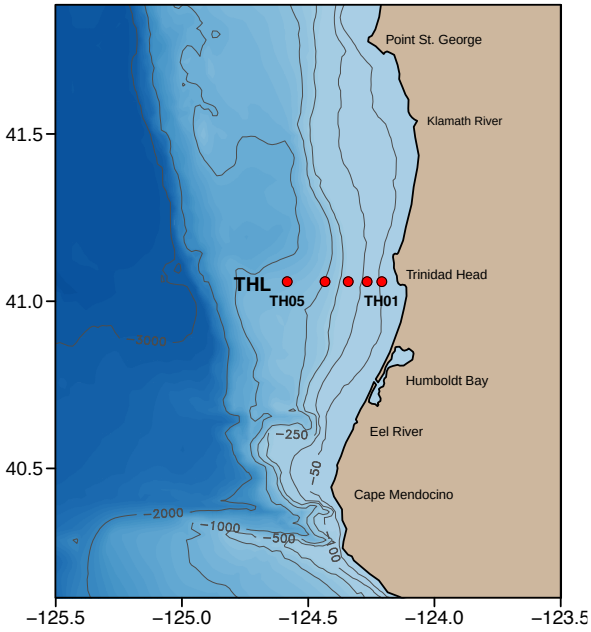

Figure D1. Bathymetric map of sampling location; Trinidad Head Line (THL; 41°03.50 N) off Trinidad, CA. Nearshore station (TH01) and offshore station (TH05) are labeled for reference. Bottom-depth is labeled in meters.

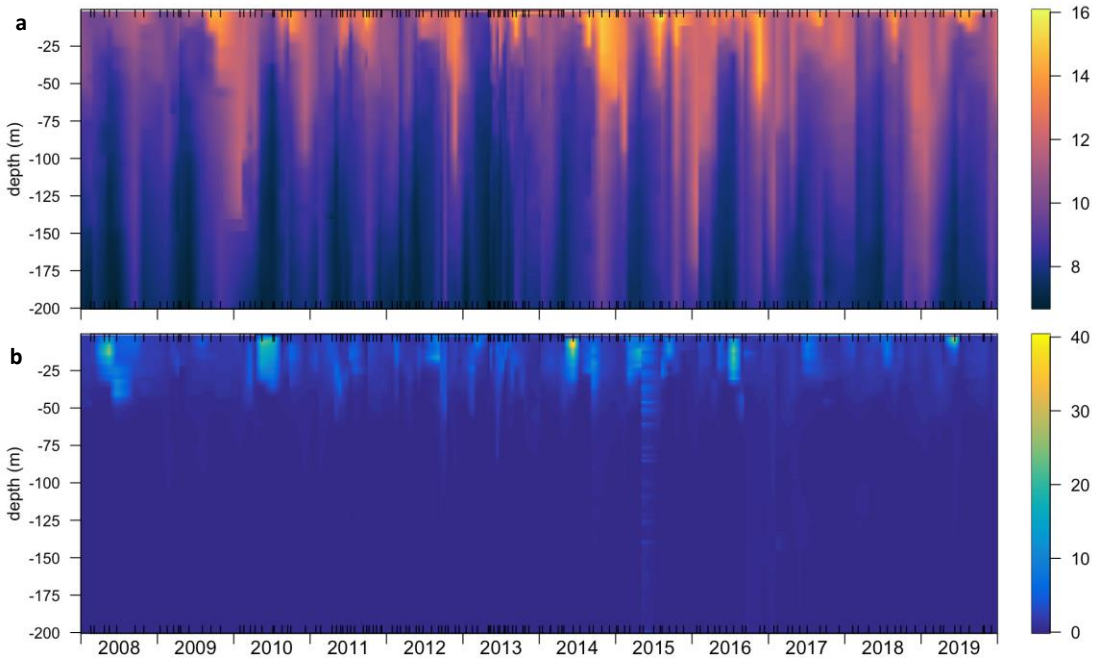

Figure D2. Time series (x-axis) of hydrographic data by depth (y-axis) at THL station TH04. a) Interpolated temperature (°C); b) Interpolated chlorophyll a concentration (mg L^{-1}). Rug indicates date of cruise and measurement.

Process overview and scheduling

A 30-minute timestep is used to calculate growth and development throughout the period of interest. The length of this timestep enables realistic implementation of vertical migration and provides frequent updates to individual stage variables (e.g., size).

At each timestep, vertical position, temperature, and food availability are determined (Figure D3). Energetic components (e.g., growth) are calculated based on environmental conditions and the state of the individual. If reproductive requirements have been met, adults reproduce. Following calculation of physiological rates, development is calculated. The individual is then evaluated for mortality, due either to starvation or end of lifespan.

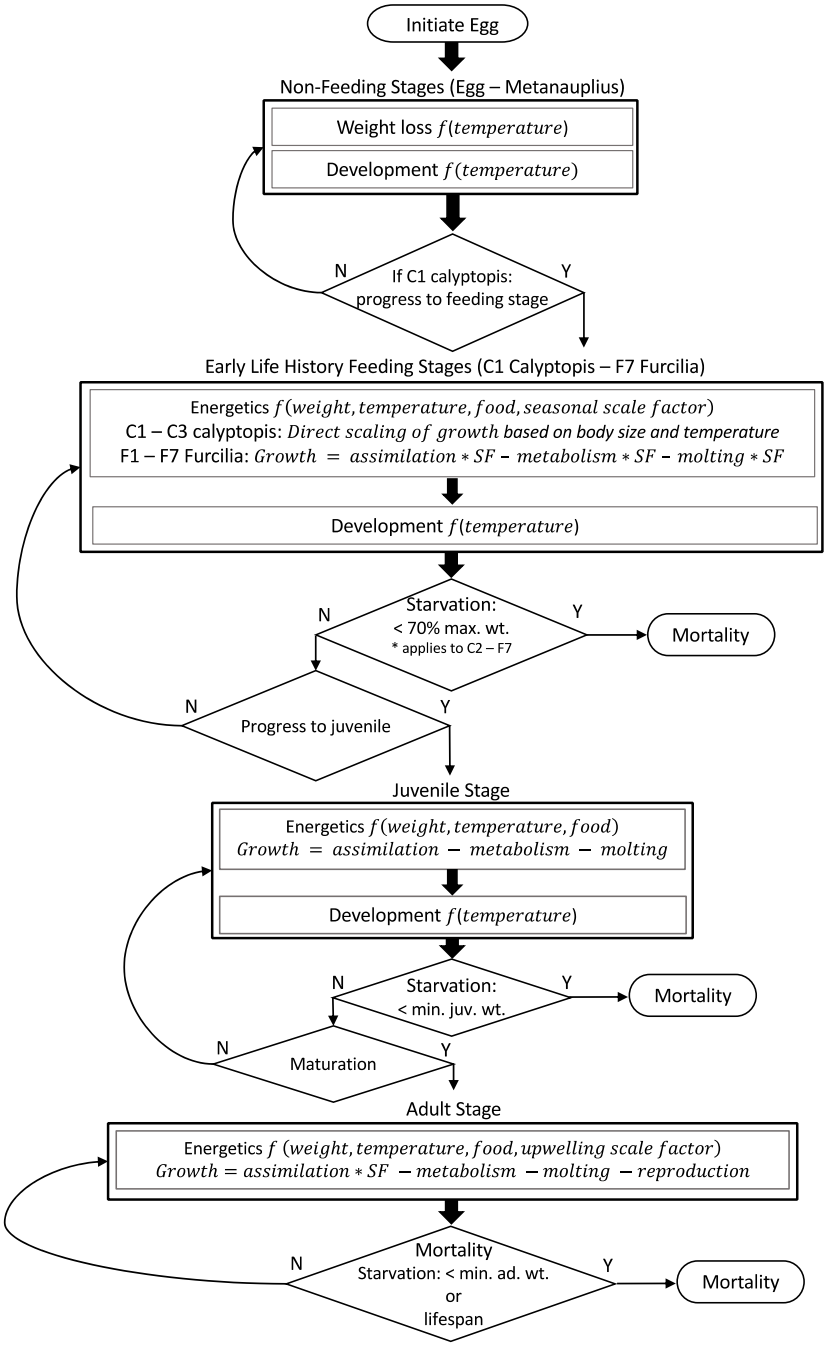

Figure D3. Flow diagram of the final model, including energetics and development submodels for non-feeding larvae, calyptopes, furcilia, juveniles, and adults. Stage transitions within composite groups (e.g., early life history stages) are subsumed in boxes for compactness. Criteria for stage transitions is determined by the temperature-dependent Bělehrádek function (see 'Development'). SF = scale factor.

Design concepts

Emergence: Growth and development emerge from an individual's physiology and exposure to environmental conditions. An individual's environmental exposure is determined by its vertical position, which is a function of stage and time of day. At night, vertically migrating krill are distributed to maximum chlorophyll depth. Adaptation and fitness are not modeled explicitly.

Sensing: Individuals are omniscient; it is assumed the individual knows their stage and environment throughout the water column so they are able to migrate without error according to stage-specific depth rules.

Stochasticity: Bioenergetics and behavior of an individual is deterministic and based on empirical relationships and observations.

Observation: IBM data are recorded at six-hour intervals. These data include: date, depth, environmental conditions, energetic components, and individual characteristics (e.g., size, stage, age, and mortality status).

Initialization: Eggs are initiated two years prior to start dates of interest. This allows for development and growth of krill prior to dates of interest and is based on the expected life span of two years.

Input: The IBM is driven by hydrographic data (temperature and chlorophyll a concentration) and a date-specific schedule of sunrise and sunset (for implementation of DVM).

Details

Vertical Position and Migration Behavior

In the IBM, daytime depth is stage-dependent and based on *in-situ* observations (Vance et al., 2003; Im and Suh, 2016; Table D2). To simulate mixing of non-migrating krill, egg – F2 furcilia stages are exposed to the mean of temperature and chlorophyll a concentration over a stage-specific depth range. Vertical migration is implemented once krill reach the F3 furcilia stage, the first stage at which swimming legs are fully developed (Boden, 1950). At the onset of dusk, individuals are moved from their stage-specific daytime depth to the depth (below 10 m) at which maximum chlorophyll concentration occurs. Individuals return to their corresponding daytime depth with the onset of dawn. Civil twilight, the time at which the sun is 6° below the horizon, is used to mark the onset of dawn and dusk, which translates to a minimum of 7.75 (summer) and maximum of 13.75 (winter) hours spent in shallower waters. The timing of civil twilight is date-specific and determined using 'crepuscule' in 'maptools' (Bivand and Lewin-Koh;

Table D2. Diel vertical migration (DVM) behavior of krill in IBMs. Stages with day and night depth ranges (e.g., 10 to 100 m) are exposed to the mean temperature and chlorophyll a concentration across the noted depth range. Horizontal dashed-lines indicate transition to new behavior or depth (also indicated with text).

Table D2. Diel vertical migration (DVM) behavior of krill in IBMs. Non-migrating stages (Egg – F2 furcilia) are exposed to the mean temperature and chlorophyll a concentration across the noted depth range (e.g.,10 to 100 m). Krill performing DVM migrate at night to the depth at which maximum chlorophyll occurs and return to their stage-specific day depth during daylight hours.

Stage	DVM	Day Depth (m)	Night Depth (m)
Egg	No	10 to 100	10 to 100
Nauplius N1	No	10 to 100	10 to 100
Nauplius N2	No	10 to 100	10 to 100
Metanauplius	No	10 to 50	10 to 50
Calyptopis C1	No	10 to 50	10 to 50
Calyptopis C2	No	10 to 50	10 to 50
Calyptopis C3	No	10 to 50	10 to 50
Furcilia F1	No	10 to 50	10 to 50
Furcilia F2	No	10 to 50	10 to 50
Furcilia F3	Yes	25	Maximum Chlorophyll Depth
Furcilia F4/5	Yes	35	Maximum Chlorophyll Depth
Furcilia F6	Yes	45	Maximum Chlorophyll Depth
Furcilia F7	Yes	50	Maximum Chlorophyll Depth
Juvenile	Yes	150	Maximum Chlorophyll Depth
Adult	Yes	200	Maximum Chlorophyll Depth

Body Size

Published IBMs and those developed here express individual state in units of carbon weight (W; µg C). However, our field-based observations of *E. pacifica* body size and published information on growth rates (e.g., Shaw et al., 2010) record body size as a length measurement. To facilitate comparisons between model output and field observations, body weight (W) was converted to dry weight (DW; mg), total length (TL; mm), and body length (BL; mm) per the following equations (D1-D3):

$$DW = \frac{\frac{W+1.985}{0.401}}{1000} \quad \text{(D1)}$$

$$TL = \frac{DW}{0.795}^{1/3.239} \quad \text{(D2)}$$

$$BL = \frac{TL-0.2807}{1.218} \quad \text{(D3)}$$

following (Shaw et al., 2010; Feinberg et al., 2007, and Ross, 1982a).

Body length, which represents the distance from the back of the eye to the base of the telson (Shaw et al., 2010), is used for comparison to length measurements along the THL. Total length, which represents the distance from the back of the eye to the tip of the telson (Gómez-Gutiérrez et al., 2006), is used for comparison to published growth rates, which Preliminary versions of the model revealed biased estimates for F1 and F2 furcilia.

Rather than modify energetics, which would impact growth and body size of subsequent life history stages, I modified the weight-to-length conversion for F1 and F2 furcilia as follows (equations D4 and D5):

$$F1\ Furcilia\ TL = DW^{1/3.239} \quad \text{(D4)}$$

$$F2\ Furcilia\ TL = \frac{DW}{0.900}^{1/3.239} \quad \text{(D5)}$$

This modification is justified by the difference in body form between F1 and F2 furcilia and later life history stages, especially the broader telson and wider carapace. This modification has no impact on weight-based processes in the model and is consistent with the POM approach.

Demographics

The IBM developed here are not implemented to simulate population dynamics, they track a single individual representative of a cohort. However, field observations are a composite of individual growth trajectories (size-at-age) that arise from variable egg production over time and mortality due to predation. Therefore, it is necessary to weight the contribution of each simulated cohort (i.e., size-age trajectory) to the size distribution existing on each day for fair comparison to field observations. To do so, I weight the initial value of each cohort by climatological egg production and apply cumulative size-

dependent mortality over the course of that cohort's lifetime. Production and size-based mortality rates are applied to model output post-simulation. Note that other sources of mortality (i.e., starvation or end of lifespan) are implemented in the IBM (see 'Generic Model Process' above and 'Mortality' below).

Egg production (eggs d^{-1}) was estimated by fitting a GAM to *E. pacifica* egg density (from THL vertical ring-net data collected at station TH02 from 2009 – 2016) as a function of day-of-year (Figure D3). Observations of egg densities greater than two standard deviations from the mean were removed prior to fitting the model. The GAM was based on a cubic-cyclic spline to ensure continuity across the start and end of the seasonal cycle. Effective degrees of freedom were fixed (edf = 8) to resolve early and late seasonal peaks in egg production. To implement egg production as a discrete value, egg densities predicted by the GAM were scaled to a maximum of 1000 eggs d^{-1} and rounded to the nearest integer for weighting of IBM output data.

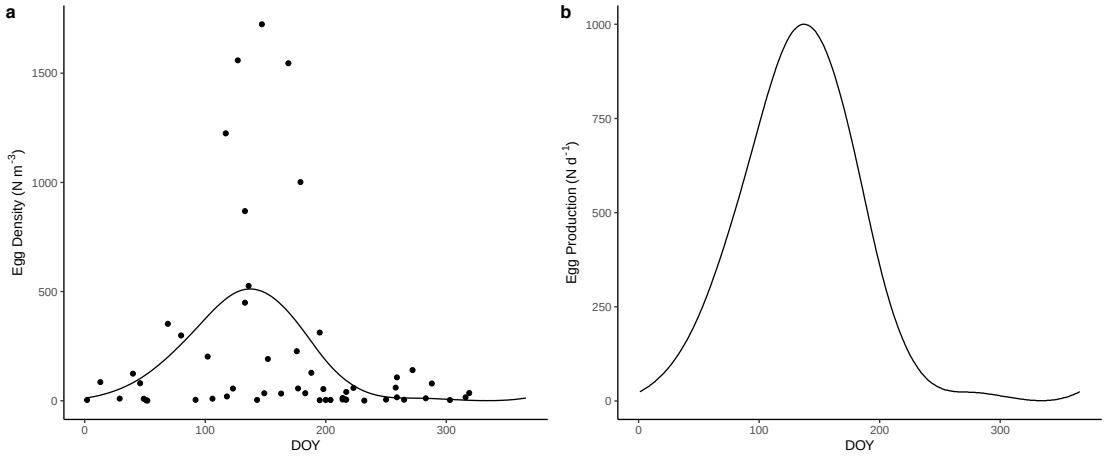

Figure D3. Observed and predicted egg density. a) GAM (line) fit to THL observations (points) of egg density by day-of-year (x-axis) at THL station TH02 from 2009 – 2016; b) Scaled egg production values by day-of-year.

Size-based (predation) mortality was calculated following Peterson-Wroblewski (1984) who estimated weight-based instantaneous mortality as (equation D6):

$$Mortality = (5.26 * 10^{-3}) * DW^{-0.25} \quad \text{(D6)}$$

where $Mortality$ is instantaneous mortality (day^{-1}) and DW is dry weight (g). Body weight (µg C) was converted to dry weight (g) following equation 1. The size-specific instantaneous mortality rate was applied to the daily mean size of the individual.

Resulting densities by date and stage were used to generate population size distributions (e.g., median body length) over time. Stage-specific minimum (10th

quantile), median (50th quantile), and maximum (90th quantile) size was calculated for life history stages for which THL observations exist (F1 furcilia – adults).

Energetic Submodels

Energetic submodels (physiological rates) are defined in text as daily rates of carbon allocation (μg C d^{-1}). In the IBM, daily rates are scaled to 1/48 of the daily rate to reflect the 30-minute time step at which they are applied.

Growth

Growth dynamics over the life history of *E. pacifica* are described in detail below, but share a common characteristic of being dependent on temperature. To capture this dependence, Q_{10} relationships were used to scale physiological rates by temperature using equation D7:

$$Rate_2 = Rate_1 * Q_{10}^{(T_2 - T_1)/10°C} \quad \text{(D7)}$$

where $Rate_2$ is the projected physiological rate at temperature T_2 (expressed in °C), $Rate_1$ is a known physiological rate at temperature T_1, and Q_{10} is the factor by which the physiological rate increases per 10°C rise in temperature. In this study, Q_{10} coefficients were established for each physiological process (i.e., ingestion, metabolism, molting, and

reproduction) based on information in Ross (1979). Q_{10} values were calculated using the complete expression relating each physiological rate to weight at 8 and 12°C (Table D3). This method differs from that utilized by Ross (1982a) by including the intercept and weight-specific coefficient regardless of whether they were significantly different at 8 and 12°C.

Table D3. Expressions for physiological rates from Ross (1979 and 1982a) and from my re-analysis of Ross's data. Intercept (a) and weight-specific coefficients (b) for allometric equations describing the relationship between physiological rate (µg C d^{-1}) and body weight (µg C), where physiological rate = $a * W^b$. A = Adults, J = Juveniles, F = furcilia, FJA = furcilia, juvenile, and adults. Note that growth of early life history feeding stages (ELHF) follows a linear equation where growth = $a + W * b$. Q_{10} coefficients in this study are calculated using complete allometric expressions (versus only using intercepts if weight specific coefficients were not significantly different, as in Ross, 1979 and 1982a).

Source	Physiological rate (Stage)	Q_{10}	T (°C)	*a*	*b*
Ross (1979, 1982a)	Ingestion (FJA)	3.35	8	0.249	0.910
			12	0.404	0.910
Ross (1979, 1982a)	Metabolism (A)	1.9	8	0.154	0.810
			12	0.200	0.810
Ross (1979, 1982a)	Metabolism (J)	1.9	8	0.154	0.810
			12	0.200	0.810
Ross (1979, 1982a)	Metabolism (F)	2	8	0.171	0.839
			12	0.266	0.839
Ross (1979, 1982a)	Reproduction (A)	3.6	8	0.006	1.035
			12	0.010	1.035
Ross (1979, 1982a)	Molting (FJA)	2.46[a]	8	0.011	0.853
			12	0.021	0.805

Source	Physiological rate (Stage)	Q_{10}	T (°C)	*a*	*b*
Ross (1979, 1982a)	Growth (ELHF)		8	-0.057	0.124
			12	-0.315	0.198
This study	$Ingestion_{Max}$ (FJA)	3.35	8	0.249	0.910
			12	0.404	0.910
This study	Metabolism (A)	3.37	8	0.139	0.930
			12	0.224	0.932
This study	Metabolism (J)	3.35	8	0.121	0.964
			12	0.192	0.968
This study	Metabolism (F)	3.25	8	0.103	0.996
			12	0.162	1.001
This study	Reproduction (A)	3.61	8	0.006	1.035
			12	0.010	1.035
This study	Molting (FJA)	$5.08*weight^{-0.12}$	8	0.011	0.853
			12	0.021	0.805
This study	Growth (ELHF)	1.74	8	-0.057	0.124
			12	-0.315	0.198

a: Average Q_{10} for all weights, range is 3.37 (30 ug C) to 1.93 (3,000 ug C).

Growth of non-feeding stages

Following Lindsey (2013), initial egg weight is set at 3.2 µg C (versus 2.58 in the Dorman et al. (2015) IBM), based on observations of *E. pacifica* egg size off Oregon (Gómez-Gutiérrez et al., 2003).

By definition, non-feeding stages lose weight. Estimates from Ross (1979) indicate greater rates of weight loss in non-feeding stages at 8°C compared to 12°C. This pattern contradicts general rate-temperature relationships, in which metabolic rate tends to increase with temperature, at least over range of temperatures typically experienced by an organism (Cossins and Bowler, 1987). Since alternative rates for non-feeding stages were not available, I selected a rate to implement weight loss (-0.145 µg C d^{-1}) within the range of Ross's observations that generated realistic sizes of early life history stages. The rate of weight loss in non-feeding stages was scaled with temperature using a generic Q_{10} of 2.0.

Growth of feeding stages

Growth of feeding stages (calyptopis C1 through adult) is dependent upon temperature and food concentration. Food concentration in µg C is estimated from chlorophyll a concentration following a 1 µg chlorophyll a: 60 µg C conversion (as in Dorman et al., 2015).

Growth rates of furcilia, juvenile, and adult stages are calculated as a function of explicit input and output variables following the expression for a carbon-only crustacean energy budget (equation D8; Dagg 1976):

$$Growth = Assimilation - Metabolism - Molting - Reproduction \quad \text{(D8)}$$

Specific definitions are developed below, but components of this model can generally be described in the following terms. Assimilation is calculated as the product of ingestion and assimilation efficiency, the amount of carbon ingested that is retained and available for energetic processes. Metabolism represents the energy required for catabolic and anabolic processes. As in Ross (1982a) metabolic rate estimates account for leakage, or the amount of dissolved organic carbon released from the individual. Molt rate is calculated as the loss of carbon at each ecdysis (molt event) divided by the molt interval in days. Allocation to reproduction was estimated by Ross (1982a) and is based on the total amount of carbon allocated to broods over an individual's lifetime following maturation.

Growth rates of early life history feeding stages (ELHF; calyptopis C1 – C3) are modeled directly using the empirical relationship between growth rate (µg C d^{-1}) and body weight (W, µg C) (Ross, 1982a; equation D9).

$$Growth \text{ (derived at 12°C)} = -0.315 + 0.198\,W \quad \text{(D9)}$$

Growth of ELHF stages is scaled with temperature using a Q_{10} of 1.74 (Table D3).

The ELHF growth expression (equation D9) was derived under maximal food resources. As such, it represents maximum growth rate for ELHF stages. To account for

variability in food resources, growth rates of ELHF stages were scaled by the ratio of available food concentration to critical concentration, the food concentration at which maximal growth is achieved (see 'Assimilation' below for how critical concentration is calculated).

Growth: Assimilation

Ingestion is dependent on size, temperature (Ross, 1982a), and food concentration (Ohman, 1984; Kiørboe, 2008). Q_{10} coefficients are used to scale ingestion rates with temperature. To account for the effects of body weight and food concentration, I developed an ingestion rate function of the Type III form identified by Ohman (1984; Equation D10):

$$Ingestion\ Rate_{Food\ Concentration} = \frac{a_{FoodConc.} * Food\ Concentration^2}{1 + a_{FoodConc.} * T_h * Food\ Concentration^2} \quad \text{(D10)}$$

where $a_{FoodConc.}$ is the capture efficiency or attack rate and T_h is the handling time and scale this equation with body weight.

To determine weight-dependent critical concentration, which is defined as the food concentration at which maximal growth is achieved, I fit an allometric model to critical concentration data from Ross (1979) and Ohman (1984; Table D4 and Figure D4; *critical concentration = 16.48*W$^{0.35}$*). An allometric model was preferred over an

asymptotic model on the basis of greater biological relevance; as body size increases, the amount food required to maintain a larger size and grow is expected to increase, not to plateau, thus requiring more food to achieve maximum growth. Ingestion rates were then predicted as a function of weight and food density using a Type III functional response model scaled so that ingestion is 90% of maximum ingestion ($Ingestion_{Max}$; TableD3) at critical concentration across all sizes (Figure D4). Ingestion is capped so that it does not exceed ingestion at critical concentration (as in Dorman et al., 2015).

Table D4. Critical concentration (CC; µg C l^{-1}) for various sizes of *E. pacifica* krill at 8 and 12°C. Data from Ross (1979) and Ohman (1984). NA indicates field does not apply to data source.

Source	Size class (µg C)	Avg. weight in size class	CC at 8°C	CC at 12°C
Ross (1979)	< 750	273	100	125
Ross (1979)	750-1650	1205	190	225
Ross (1979)	1650	2564	320	375
Ohman (1984)	NA	4700	290	NA

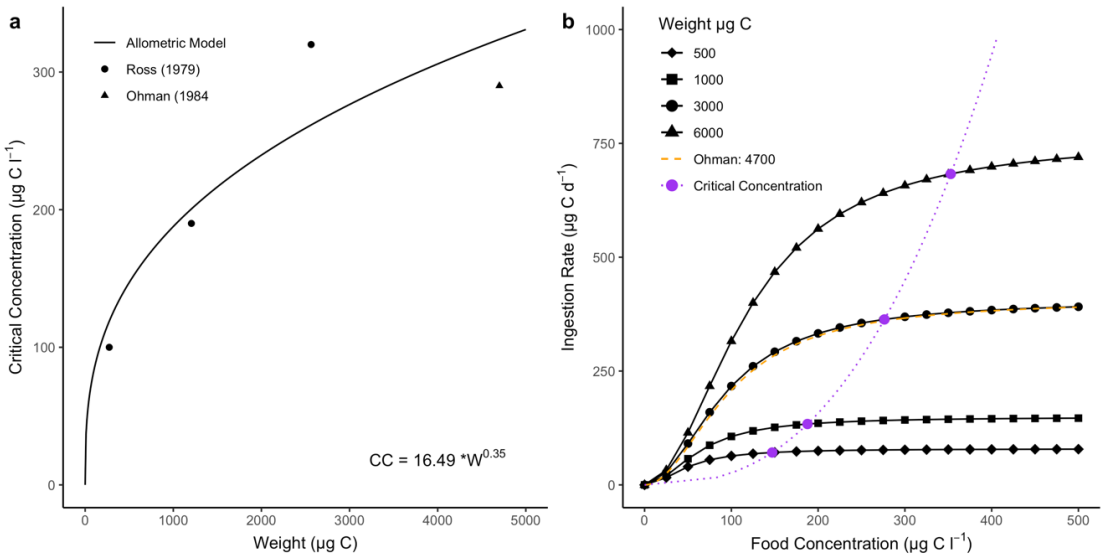

Figure D4. a) Allometric model (line) fit to critical concentration (µg C l^{-1}; y-axis) and weight data (x-axis) at 8°C from Ross (1979; points) and Ohman (1984; triangle); b) Predicted ingestion rates for various sizes of krill using weight- and food concentration-dependent function (at 8°C to match experimental temperature in Ohman, 1984). Closed purple circles and purple dotted-line indicate critical concentration at various body sizes (see legend). Orange dashed-line represents the Type III functional response for the average krill size (4700 µg C) in Ohman's (1984) study.

Existing IBMs scale energetics using Q_{10} values determined by Ross (1979). In the Dorman et al. (2015) IBM, growth rate is scaled directly with the Q_{10} for growth. In the Lindsey (2013) IBM, ingestion and respiration are scaled with corresponding Q_{10} values from Ross (1979), who calculated a greater Q_{10} for ingestion than metabolism (i.e., ingestion increases faster than metabolism as temperature increases). The result in both IBMs is that growth rate exhibits a positive relationship with temperature and is not constrained at higher temperatures. A monotonic increase in growth with temperature, however, contradicts observations that juvenile and adult *E. pacifica* growth rates are negatively related to temperature above 14°C, even when food is not limiting (Marinovic and Mangel, 1999). Furthermore, a rise-and-fall pattern in growth rate with respect to

temperature is observed across a wide range of taxa and can reflect a consumption-metabolism mismatch, whereby energetic costs exceed assimilation (Rall et al., 2010; Lemoine and Burkepile, 2012 and references therein; Alcaraz et al., 2014; Grote et al., 2015).

To resolve disparities between growth predictions from existing IBMs and observations, I refined the energetics component of the IBM to allow for shrinking as reported in Marinovic and Mangel (1999) by modifying the Q_{10} value used for scaling of ingestion rates in juvenile and adult stages. This modification is supported by observations that indicate Q_{10} values tend to decrease with increasing temperature (Ege and Krogh, 1914; Alcaraz et al., 2014). At intermediate and high temperatures, the relationship between ingestion rate and temperature is strongly correlated with that of growth rate and temperature, more so than the thermal sensitivity of other energetic components (Kingsolver and Woods, 1997). Based on the strong correlation between thermal sensitivity of ingestion and growth, I chose to modify ingestion (as opposed to other energetic components).

In my IBM, transition to a temperature-dependent Q_{10} begins once an individual reaches the juvenile stage. Dependency on the temperature-dependent Q_{10} scales linearly with juvenile weight, such that for krill exceeding 266 µg C (~8 mm TL, the minimum size of krill in Marinovic and Mangel, 1999), the Q_{10} is defined by a sigmoidal relationship with temperature (Figure D5). The sigmoidal model was anchored by the Q_{10} value for ingestion (3.35) estimated by Ross (1982a) at temperatures between 8 and 12

°C and tuned by manipulation of Q_{10} values at higher temperatures to generate negative growth rates consistent with rates reported by Marinovic and Mangel (1999). The resulting Q_{10} values are within a typical range for biological rates (Cossins and Bowler, 1987).

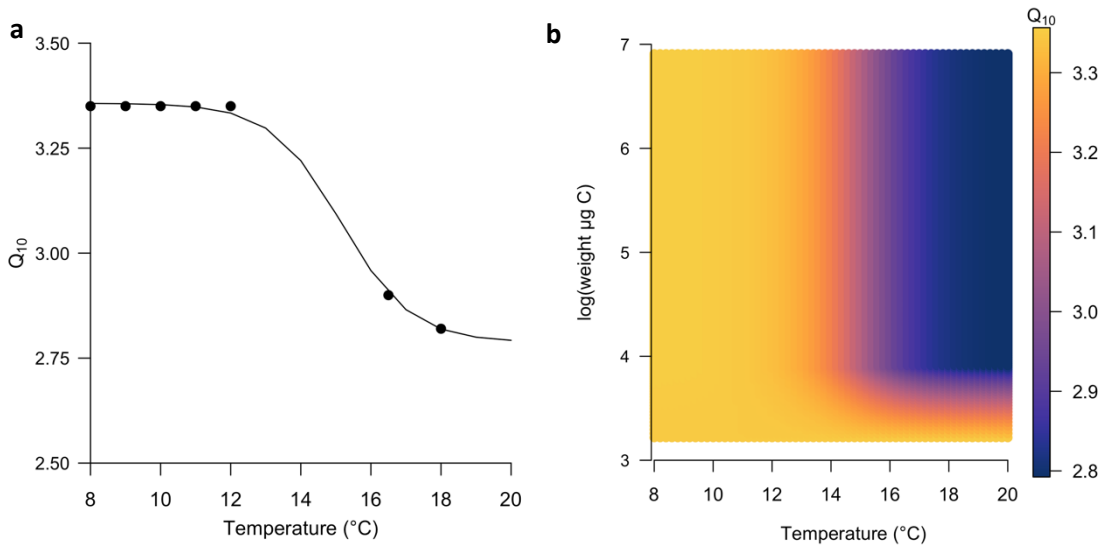

Figure D5. Q_{10} values for ingestion. a) Predicted Q_{10} values for ingestion generated from sigmoidal model (black line) fit to empirical (upper asymptote) and simulated (lower asymptote) Q_{10} data; b) Q_{10} ingestion values (see color legend) for various log-scaled weights of krill (y-axis) and temperatures (x-axis).

Preliminary IBM simulations with realistic environmental conditions indicated that individuals in stages with substantial vertical migrations (i.e., juvenile and adult) frequently exhibit negative growth during the daytime when they are deeper in the water column. The magnitude of negative growth generated unrealistic growth dynamics as a consequence of inadequate food resources at depth. The IBM accounts only for phytoplankton food. However, krill are also capable of feeding on alternate food sources (e.g., marine snow and zooplankton) that are more broadly distributed and available at

depth (Dilling et al., 1998; Nakagawa et al., 2003; Park and Suh, 2011; Im and Suh, 2016). To account for food at depth, I modified the environment so food concentration for juvenile and adult stages is 30% of what was available at the daily maximum chlorophyll depth. This modification is only implemented if food at depth is below 30% of what was available at the maximum chlorophyll depth. This modification is supported by evidence indicating *E. pacifica* feed on alternate prey sources (e.g., tintinnids and copepods) while at depth during the daytime (Nakagawa et al., 2003). I also decreased metabolic demand during daylight hours by 30% for adults and 20% for juveniles. This modification reflects observations that indicate decreased feeding activity during the day at depth (Nakagawa et al., 2003).

Growth: Metabolism

Ross's direct measurement of growth was greater than the difference between assimilation and energetic costs. Ross attributed the discrepancy in the energy budget to possible measurement errors (Ross 1982b). Metabolic rate was suspected to have been underestimated, possibly as a consequence of suppressed activity due to confinement of krill in a small vial during respiration experiments and errors in leakage estimates.

Under the assumption that empirical estimates of metabolism were the sole source of imbalance in Ross's (1982a) energy budget, I re-calculated metabolic rates for furcilia, juvenile, and adult stages using Ross's data and expressions for assimilation, growth, molting, and reproduction. I rearranged equation D8 to generate a new estimate of metabolic rate (equation D11, Figure D6, and Table D3):

$$Metabolism = Assimilation - Growth - Molting - Reproduction \quad \text{(D11)}$$

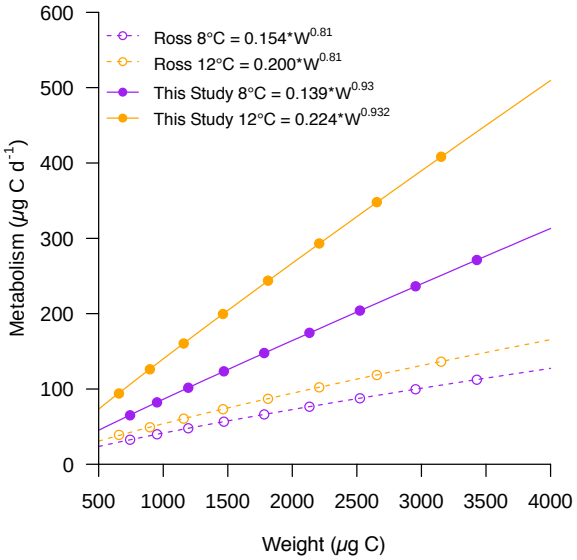

Figure D6. Adult metabolic rate at 8 (purple) and 12°C (orange) versus body weight. Expressions are from Ross (1982a; dashed-lines) and this study (solid-lines). Open circles represent original data from Ross (1979), filled circles represent metabolic rates calculated in this study. New allometric equation for metabolic rate assumes underestimation in original estimate by Ross (1982a).

Growth: Molting

I retained the allometric equation for molt rate determined by Ross (1982a; Table D3). The Q_{10} for molt rate exhibits a clear inverse relationship with body weight (Ross, 1979). To account for this pattern, I fit an allometric model to data from Ross (1979). The resulting model expresses the temperature sensitivity of molt rate ($Q_{10\,Molt}$; equation D12) as a function of body weight (W; Figure D7) and is defined as:

$$Q_{10\,Molt} = 5.08 * W^{-0.12} \quad \text{(D12)}$$

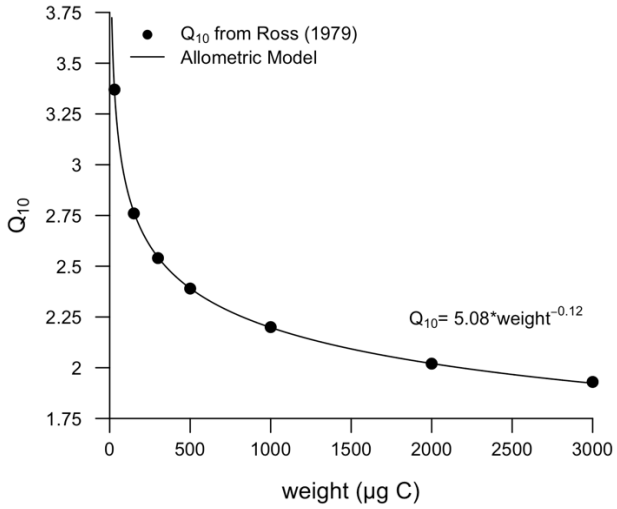

Figure D7. Allometric model (line) fit to Q_{10} values (points) for molt production and weight data from Ross (1979).

Growth: Reproduction

Allocation of energy to reproduction commences once an individual reaches maturity. Allocation to reproduction follows the relationship defined in Ross (1979; equation D13):

$$Reproductive\ Weight\ Allocation\ (RWA) = 0.010(W + 1.98)^{1.035} \quad \text{(D13)}$$

Where allocation to stored reproductive weight (RWA; µg C) at each timestep is predicted as a function of body weight (W; µg C). Allocation of energy to reproductive stores is independent of whether there is sufficient food to maintain costs of living. This

allows an individual to shrink but still reproduce, as has been observed in the field and laboratory (e.g., Shaw et al., 2010).

Release of eggs is based on rules from the Dorman et al. (2015) IBM. Release of eggs occurs only at night and is dependent upon interbrood period (the time between release of eggs) and the ratio of stored reproductive weight (RW) to body weight (BW). Interbrood period is set to 10 days. Individuals release eggs every 10 days if RW:BW is between 2.5 and 7.5%. If the RW:BW ratio is greater than 7.5%, eggs are released independent of interbrood period. The number of eggs released is equal to the reproductive weight divided by egg weight (3.2 µg C). If any reproductive weight is leftover after egg release, it is conserved as reproductive weight for subsequent timesteps.

Application of Mechanistic Submodels for Growth

Results from the Phase I model indicate that growth rates for furcilia stages are similar to those predicted by the Base IBM (Figure D8a). Growth rates for juvenile and adult stages closely match growth rates from the Base IBM up to 12°C, at which point they reflect the modification that generates negative growth above 17.28°C (Figure D8 b - e).

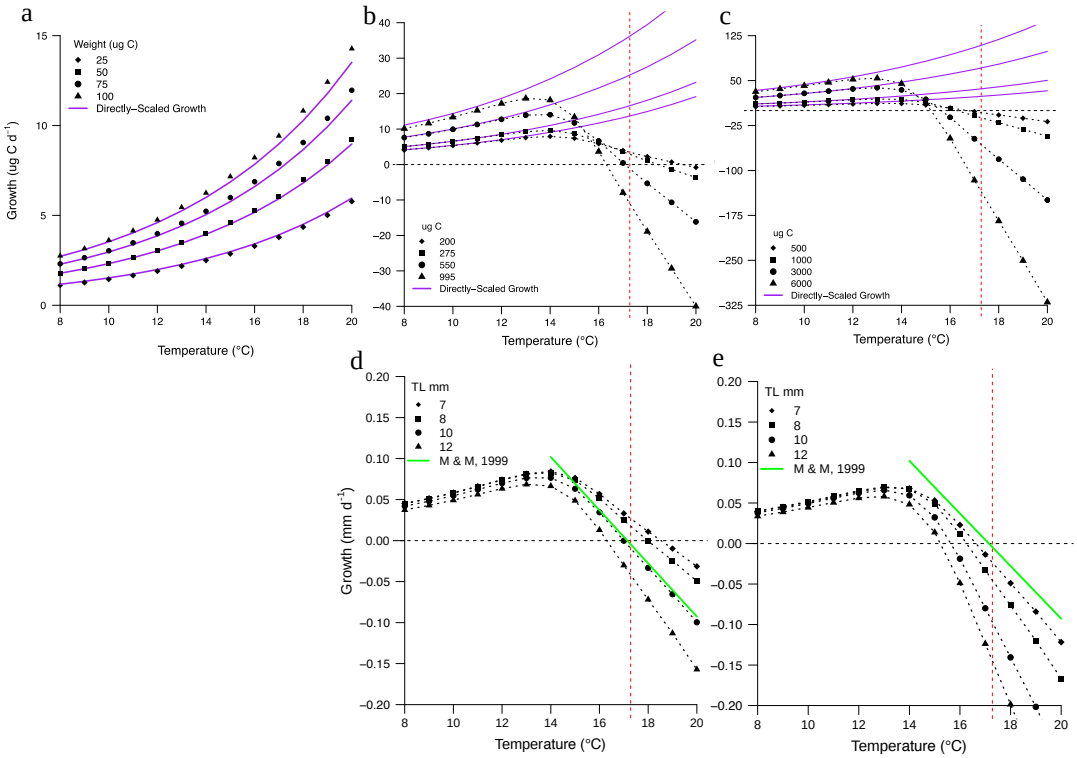

Figure D8. Growth rates (top row: µg C d^{-1}; bottom row: mm d^{-1} TL) for various sizes (see legend) of a) furcilia, b and d) juvenile, and c and e) adult life history stages based on the Base IBM (purple lines in top row) and Phase I IBM (black dashed-lines with symbols; see legend). Purple lines in top row represent empirically estimated growth rates based on measurements of growth at 8 and 12°C (Ross, 1982b; Dorman et al., 2015). Solid green line in bottom row represents estimate of negative growth rates for the average size krill (10 mm) used in Marinovic and Mangel, 1999. Vertical red-dashed line indicates observed transition to negative growth at 17.28°C (Marinovic and Mangel, 1999). Horizontal dashed-line at zero for reference.

Development

Immature stages

Development of immature stages is defined by a Bělehrádek function developed by Lindsey (2013) for *E. pacifica*. The Bělehrádek model predicts stage duration as a function of temperature (Bělehrádek, 1930). The Bělehrádek model Lindsey (2013) developed is based on empirical data of *E. pacifica* development rates from Ross (1981)

and Feinberg et al. (2006) (Figure D9). Progression to the subsequent life history stage is determined by equation D14:

$$Duration_i = a_{Dur,i}(T + B)^{c_{Dur}} \quad \text{(D14)}$$

where $Duration_i$ is the duration of stage i in days, $a_{Dur,i}$ is an empirically determined stage-specific constant which defines the initial functional slope (day °C^{-1}; Table C1), T is temperature in °C, B is a stage-independent temperature shift specific to *E. pacifica* (15.052°C), and c_{Dur} is an empirically derived constant that determines curvature (here, c_{Dur} = -2.05).

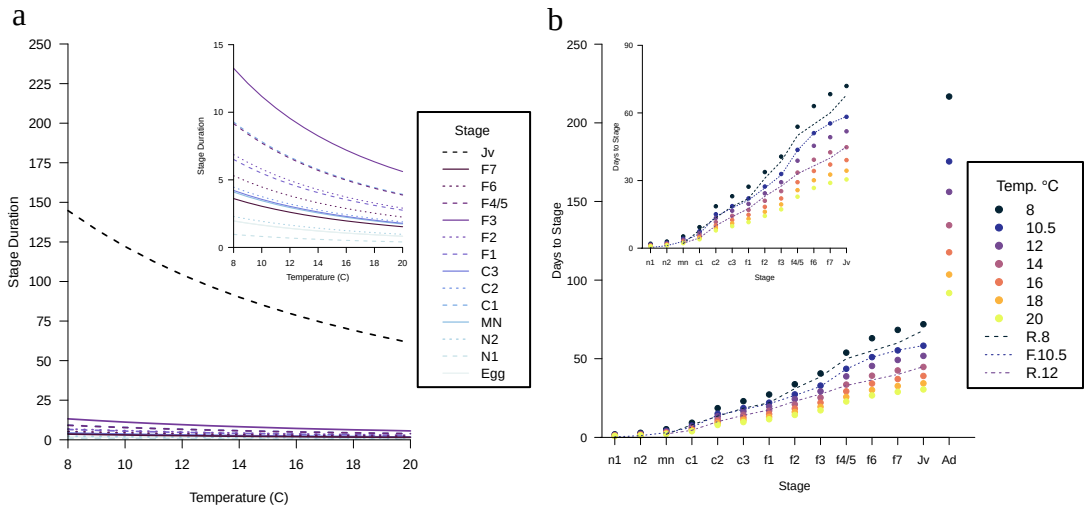

Figure D9. Bělehrádek function for development of *E. pacifica* (development to juvenile stage was reproduced using Lindsey's (2013) Bělehrádek function). a) Stage duration (days) versus temperature. Inset depicts stage duration of eggs through F7 furcilia. b) Days to stage (development time) versus stage at various

temperatures (see legend). R.8 and R.12 indicate empirical observations at 8 and 12°C, respectively (Ross, 1981; Ross, 1982b). F.10.5 indicates empirical observation at 10.5°C (Feinberg et al., 2006). Inset depicts development time for n1 nauplii through juveniles.

Maturation

Both Lindsey (2013) and Dorman et al. (2015) implement maturation using invariant weight-based maturation rules (e.g., maturity occurs once an individual reaches 1500 µg C). To accommodate variability in size-at-maturation (as was observed in Robertson and Bjorkstedt, 2020), I defined a schedule of maturation by extending the Bělehrádek function developed by Lindsey (2013). To include an estimate for juvenile stage duration, and thus a temperature-dependent schedule for maturation, I estimated juvenile stage duration from data in Ross (1982b) and field observations (Harvey et al., 2010; Shaw et al., 2021). I retained the value for the curvature coefficient used by Lindsey (2013) but generated new estimates for $B_{juvenile}$ and $a_{Dur,}$juvenile. The coefficients for juvenile stage duration ($a_{Dur,juvenile}$ = 9.0*10^4, $B_{juvenile}$ = 8, c = -2.05) generate a schedule of development within the range of estimates from laboratory and field-based experiments (Figure D9; Ross; 1982b; Harvey et al., 2010; Shaw et al., 2021).

Maximum Size

Rather than implement an invariant weight limit on maximum adult size (as in Dorman et al., 2015), maximum weight of adults was constrained using a linear model that predicted maximum size as a function of minimum size-at-maturity. A linear model was fit to minimum size-at-maturity (10^{th} quantile) data from THL samples collected at station TH03 – TH05 from 2008 to 2020 (Figure D10; for comprehensive sampling and processing methods see Robertson and Bjorkstedt, 2020). Model individuals were

allowed to exceed the predicted size by 50% up to a maximum size of around 20 mm body length (25 mm total length; 10,750 µg C), the maximum size attained by *E. pacifica* (Brinton et al., 1999).

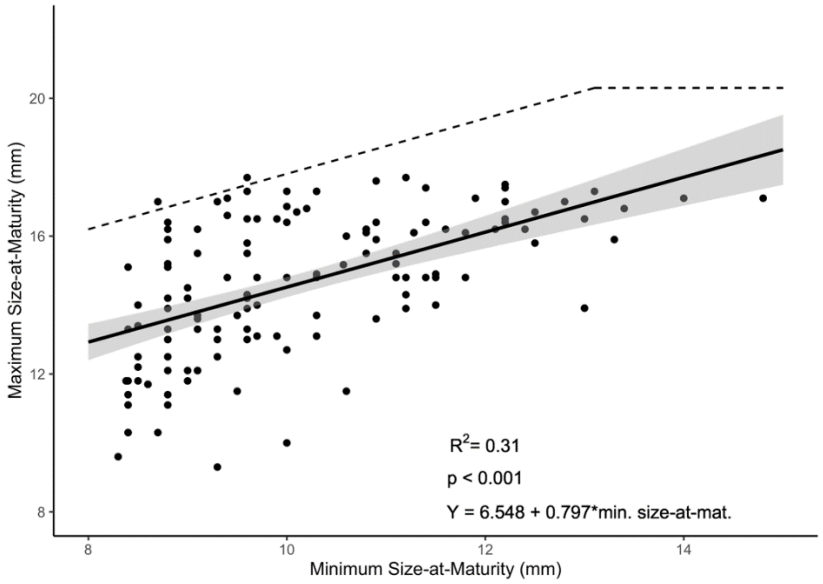

Figure D10. Maximum versus minimum size-at-maturity (BL mm). Linear model fit to THL data (black solid line, gray = 95% confidence interval). Dashed-line indicates maximum size cap implemented in the IBM as a function of minimum size-at-maturity.

Mortality

Starvation

Starvation-induced mortality is not possible until an individual reaches the second calyptopis stage (as in Lindsey, 2013). At this stage (and subsequent stages up to the juvenile stage), an individual will die due to starvation if its weight drops below 70% of the individual's maximum weight. This starvation rule is based on the Dorman et al., (2015) IBM and is consistent with findings that indicate a 'point-of-no return' threshold of 20-35% carbon loss in crustacean larvae (Anger and Dawirs, 1981; Dawirs, 1983;

Dawirs, 1987). Lower point-of-no return thresholds (~50% body carbon loss) have been observed for larval stages of *E. superba* (Meyer and Oettl, 2005). However, *E. superba*, which experience extreme variability in food abundance in the Antarctic, are likely more resistant to starvation than *E. pacifica*, which inhabit a more food-rich environment (Quentin and Ross, 1991). Therefore, as in Dorman et al., (2015), a conservative starvation value of 30% body carbon loss was selected.

Once an individual reaches the juvenile stage, death by starvation occurs only if a juvenile or adult's weight falls below the minimum weight observed for these stages, 20 and 90 µg C, respectively. This generous starvation rule allows for considerable shrinkage (e.g., as an overwintering strategy or in response to unfavorable conditions) by accommodating adaptation to a smaller size and is consistent with observations of shrinkage in juvenile and adult krill (Marinovic and Mangel, 1999).

Lifespan

The simulation of individual growth and development is terminated once an individual reaches two years of age. This lifespan is based on estimates from observations of *E. pacifica* in the California Current (Shaw et al., 2021).

Predation

Predation mortality is not included in the IBM (e.g., as a stochastic event). Rather, predation mortality was imposed post-simulation as a size-based instantaneous mortality rate and used to weight the contribution of each cohort to the predicted size distribution at a given point in time (see 'Demographics' above).

Energetic Scale Factors

Individual growth rates emerge from physiological rates and exposure to environmental conditions. Published IBMs use physiological rates measured in laboratory experiments at 8 and 12 °C (Ross, 1982a; Lindsey, 2011; Dorman et al., 2015). Results from these experiments indicate that growth rate exhibits a positive relationship with temperature. In the Dorman et al. (2015) IBM, incorporation of laboratory-based growth models generated higher growth rates during winter compared to spring and summer months. However, field observations suggest that growth rates are generally higher during spring and summer, periods typically characterized by cooler temperatures, and lower during years when delayed upwelling occurs and waters are warm (Shaw et al., 2010; Shaw et al., 2021). The cause of the discrepancy between existing growth models and field observations is not clear. At least two mechanisms might explain the observed patterns. One, enhanced nutrient concentrations and food quality during cool and productive (upwelling) seasons might enhance assimilation and growth dynamics, allowing individuals to grow more even though temperatures are relatively cool. Two, the existing bioenergetics models based on empirical data from Ross (1982a) do not account for intrinsic seasonal variability in energetics. To construct energetic expressions, Ross used data from individuals collected only in spring and summer, but noted that ingestion rates were lower in fall and winter, perhaps due to quiescent individuals (Ross, 1982b). This pattern of lower energetic rates in fall and winter months has also been observed for metabolism and ingestion of Antarctic krill, *E. superba* (Teschke et al., 2007; Piccolin et

al., 2018; Höring et al., 2018). Seasonal fluctuations in euphausiid energetics have the potential to alter growth rates and size dynamics.

Implementing seasonality in euphausiid energetics has been used to advance an IBM for *E. superba* (Bahlburg et al., 2021). In the Southern Ocean, ingestion rates of Antarctic krill vary with photoperiod; during winter light conditions assimilation rates can be as low as 36% of rates observed in summer conditions (Teschke et al., 2007). Respiration rates exhibit a similar response to photoperiod: winter light conditions correspond to significantly lower respiration rates. Bahlburg et al., (2021) accounted for seasonal variability in *E. superba* energetics by applying a day-length dependent scale factor to ingestion and metabolism submodels.

I generated similar scale factors to implement seasonal variability in *E. pacifica* energetics. Rather than day length, the scale factors are a function of day-of-year and temperature. These metrics were preferred over day length because they enable coupling of energetics to a proxy for physical and biogeochemical processes (e.g., upwelling, nitrate flux, phytoplankton blooms) that dominate the biological response in the California Current Ecosystem.

Energetics of early life history feeding stages (calyptopis C1 - F7 furcilia) were scaled using the day-of-year-based scale factor (Figure D11). Growth rate of stages for which growth is calculated directly (calyptopis C1 - C3) is scaled by applying the scale factor directly to growth rate. For F1 – F7 furcilia, the scale factor is applied to metabolism, ingestion, molting, and reproduction. Growth (for calyptopis C1 – C3),

metabolism, ingestion, and molting rates of early life history stages were decreased by a maximum of 10% in winter. The energetic scale factor increases linearly from January 1 to May 1 (day-of-year = 121) and decreases linearly from July 1 (day-of-year 182) to January. Scaling of early life history stage energetics reflects the hypothesis that assimilation and energetic costs are reduced in winter months. The peak of the scale factor falls within the window of peak climatological upwelling observed for northern California (Bograd et al., 2009). In winter, the scale factor decreases energetic rates by a maximum of 10%. Following Bahlburg et al., (2021), the energetic scale factor is applied to assimilation *and* cost components of the growth equation. Thus, the ratio between assimilation and costs remains constant. The change in growth rate reflects the balance of scaled intake and cost components in absolute, not relative, terms. This implementation is analogous to a whole-animal response; individuals are generally more active during spring and summer months and exhibit reduced activity during winter.

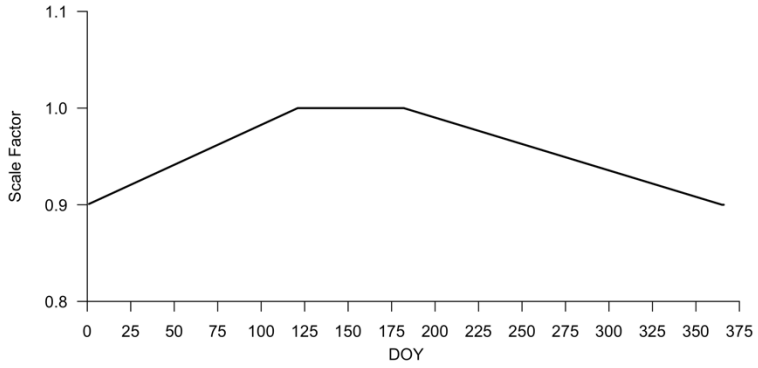

Figure D11. Day-of-year (DOY)-based scale factor applied to energetic components of feeding stage krill.

Analyses during model development indicated a persistent discrepancy between model predictions and observations of adult size in spring. From approximately March

through June, adult size was underestimated by the IBM. To improve model predictions, a temperature-dependent scale factor is applied to adult assimilation rates. The 'Upwelling Scale Factor' is a multiplicative scale factor that is a function of average temperature in the top 30 meters of the water column. The upwelling scale factor enhances assimilation during cooler conditions, a pattern that is consistent with greater nutrient availability and food quality during cool and productive upwelling conditions (Figure D12; Miller et al., 2017). At temperatures above 12°C, the upwelling scale factor is set to one and assimilation rates are equivalent to those described in 'Ingestion'.

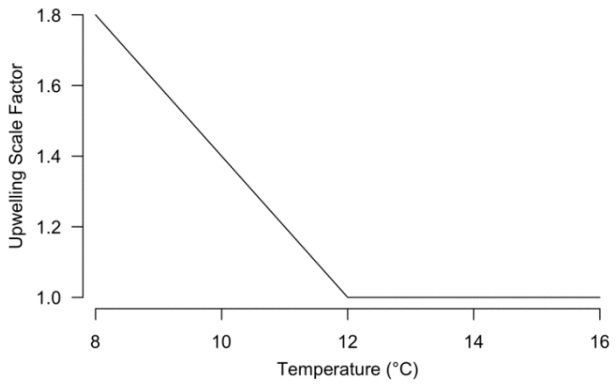

Figure D12. Upwelling scale factor. Temperature-dependent factor (y-axis) applied to adult assimilation rate based on average temperature in the top 30 m of water.

APPENDIX E

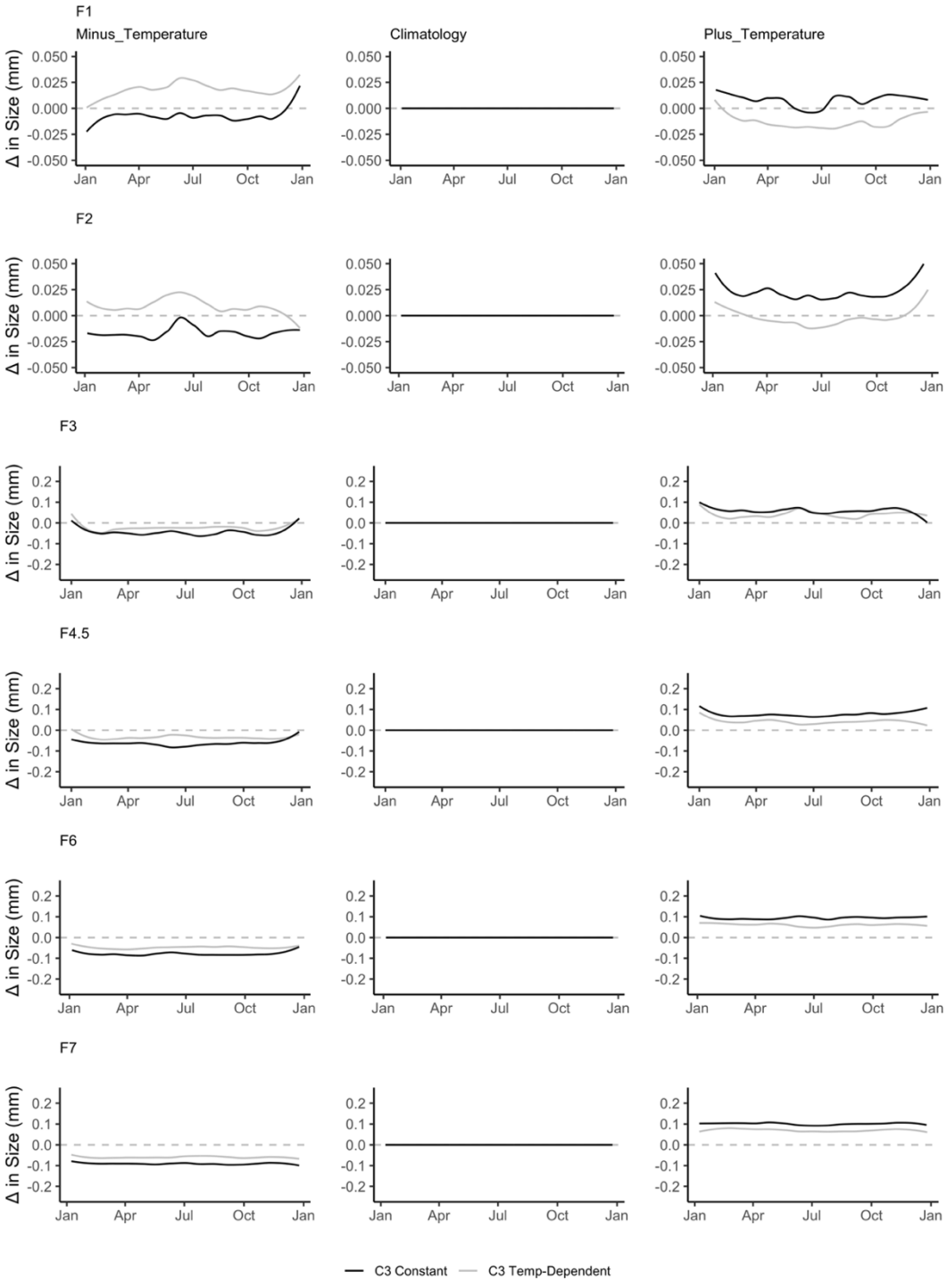
F1
Minus_Temperature
Climatology
Plus_Temperature
F2
F3
F4.5
F6
F7
Δ in Size (mm)
0.050
0.025
0.000
-0.025
-0.050
0.2
0.1
0.0
-0.1
-0.2
Jan
Apr
Jul
Oct
Jan
C3 Constant
C3 Temp-Dependent

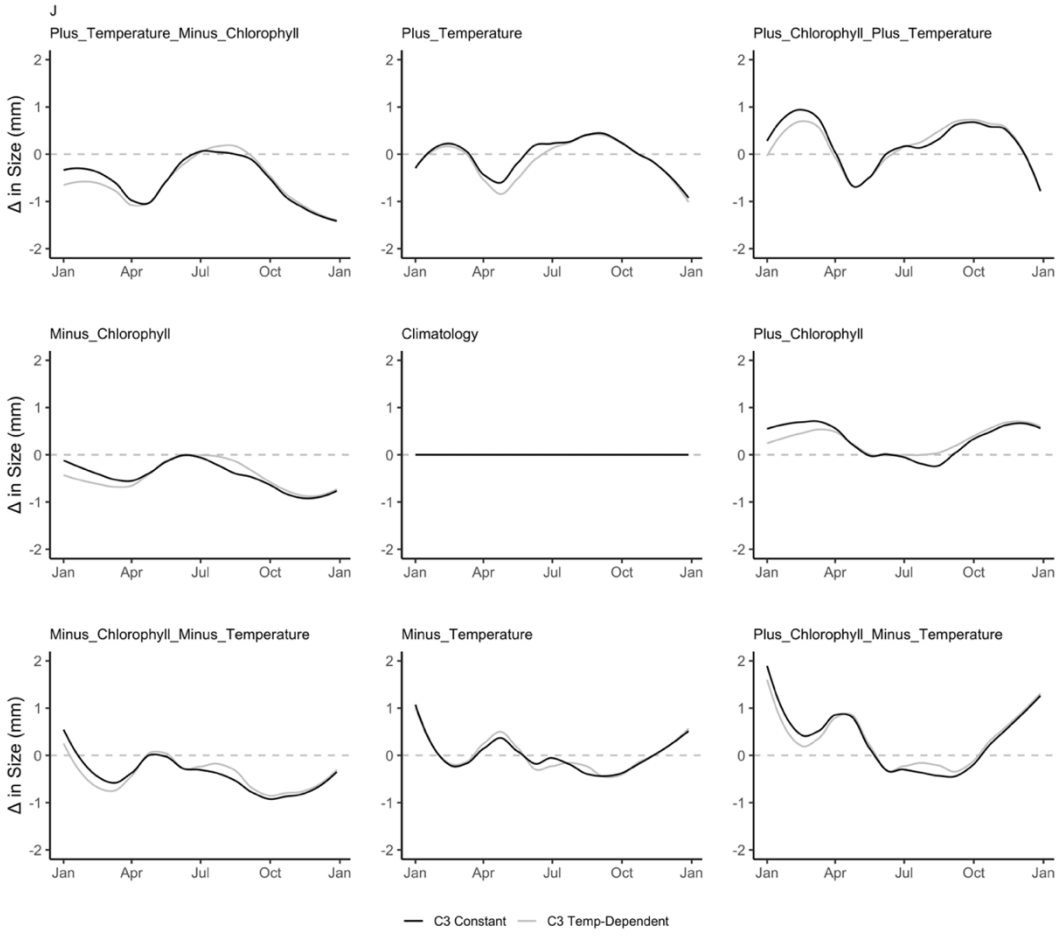
J
Plus_Temperature_Minus_Chlorophyll
Plus_Temperature
Plus_Chlorophyll_Plus_Temperature
Minus_Chlorophyll
Climatology
Plus_Chlorophyll
Minus_Chlorophyll_Minus_Temperature
Minus_Temperature
Plus_Chlorophyll_Minus_Temperature
Δ in Size (mm)
2
1
0
-1
-2
Jan
Apr
Jul
Oct
Jan
C3 Constant
C3 Temp-Dependent

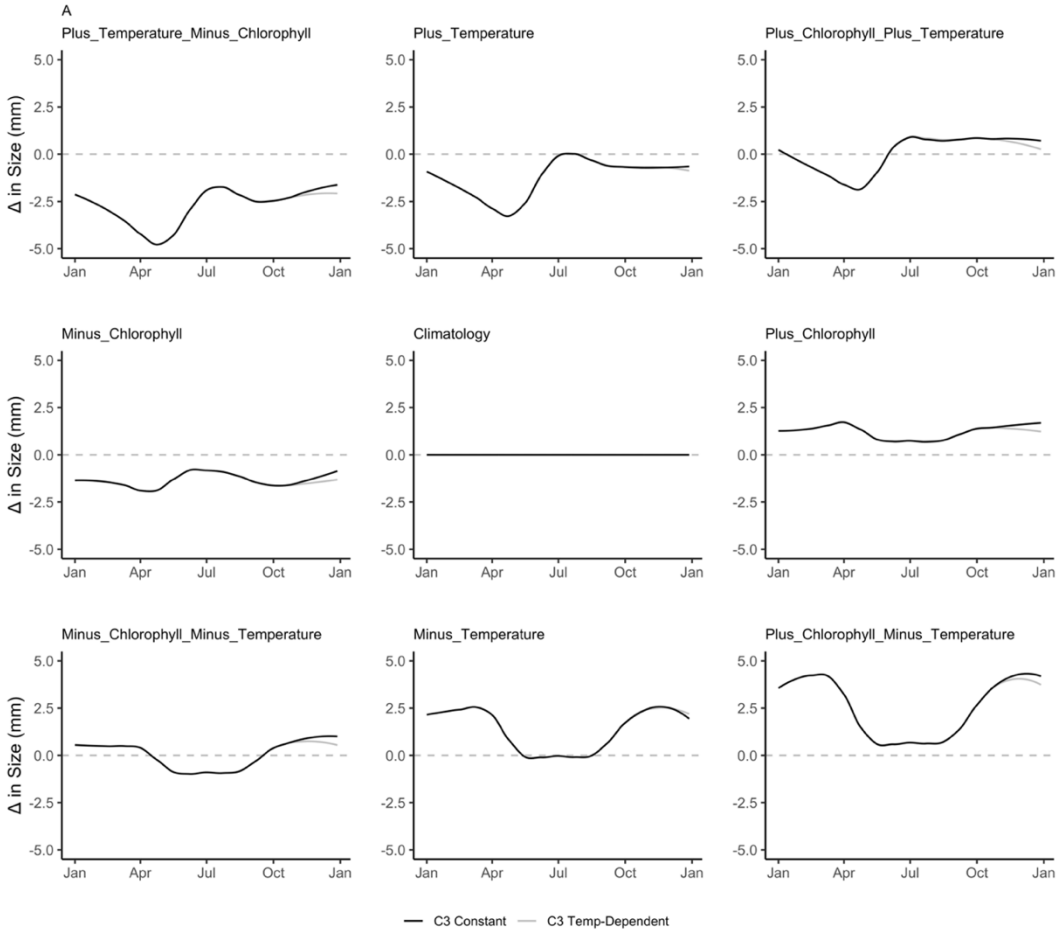

Figure E1. Results from sensitivity analysis examining the response in size to environmental variability for furcilia (top), juvenile (middle), and adult stages (bottom). Title (top left plot) indicates life history stage (F1 – F7 furcilia, J = Juvenile, A = Adult). Subtitle (top left corner of each plot) indicates environmental conditions. Scenarios include THL climatology and combinations of temperature ± 1°C and ± 20% chlorophyll a concentration (see plot subtitles). Gray line represents the difference between body length (mm) of each model scenario versus the scenario forced with THL climatology data ($BL_{scenario}$ - $BL_{climatology}$). Black line represents results from a modified model with constant, temperature-independent stage duration for the C3 calyptopis stage (3.5 days). Dashed gray line at zero to facilitate interpretation of results.